Resonant state expansion for non-relativistic quantum mechanics in one dimension

Abdullahi Tanimu

A Thesis submitted to

Cardiff University

for the degree of

Doctor of Philosophy

July 2018

Declaration

This work has not been submitted in substance for any other degree or award at this or any other university or place of learning, nor is being submitted concurrently in candidature for any degree or other award.

Signed: _____
Candidate

Date: _____

Statement 1

This thesis is being submitted in partial fulfillment of the requirements for the degree of Doctor of Philosophy.

Signed: _____
Candidate

Date: _____

Statement 2

This thesis is the result of my own independent work/ investigation, except where otherwise stated. Other sources are acknowledged by giving explicit references. The views expressed are my own.

Signed: _____
Candidate

Date: _____

Statement 3

I hereby give consent for my thesis, if accepted, to be available for photocopying and for inter-library loan, and for the title and summary to be made available to outside organisations.

Signed: _____
Candidate

Date: _____

Acknowledgments

I wish to express my gratitude to my supervisor, Dr Egor Muljarov, for all the teaching, guidance, kind patience and support received during my studies. I have benefited greatly from Dr Egor Muljarov's willingness to share his new ideas and notes with me. Dr. Egor Muljarov has shown a great deal of patience and support to all students under his supervision. I have been very fortunate to be supervised by such dedicated scholer.

I would like to thank Dr Francesco Masia and Dr Joe Wilkes for the discussion about my coding. I would like to thank my office mates, Hame, Chaitanya, Amy, Sergey, Tom and Sam for the discussions about the RSE and for their wealth of knowledge about the resources available in the Cardiff University Physics department.

I would like to thank also the management of Umaru Musa Yar'adua University, Katsina for the full funding of my PhD studies.

Finally, I would like to thank my family. My parents, for the

support and love they have shown to me. I could not have taken this opportunity if they had not helped me through the early stages of education with patience and encouragement. Most of all, thanks to my wife, Saadiya, and my children Khadija, Ahmad and Hafsa for their love, and kind patience over the last three years.

Abstract

This thesis presents my work that I have done together with my supervisor, Dr Egor Muljarov. It is based on the resonant state expansion (RSE), a rigorous perturbation theory, recently developed in electrodynamics. Here, the RSE is applied to non-relativistic quantum mechanical systems in one dimension. To facilitate the analytics, the model of Dirac delta functions for describing quantum potentials was employed. The resonant states (RSs) of a symmetric double quantum well structure modeled by delta functions was first calculated. The full set of these RSs is investigated. This includes bound, anti-bound and normal resonant states which are all eigenstates solutions of Schrödingers equation with boundary conditions of outgoing waves. These RSs are then taken as an unperturbed basis state, for the quantum mechanical (QM) analogue of the RSE (QM-RSE). The transformation of the RSs and their transitions between different subgroups as well as the role of each subgroup in observables, such as the quantum transmission, is also analysed.

The resonant state expansion is first verified for a triple

quantum well systems, showing convergence to the available analytic solution as the number of resonant states in the basis increases. The method is then applied to multiple quantum well and barrier structures, including finite periodic systems. Results are compared with the eigenstates in triple quantum wells and infinite periodic potentials described by the famous Kronig-Penney model, revealing the nature of the resonant states in the studied systems.

Publications

A. Tanimu, E. A. Muljarov. Resonant states in double and triple quantum wells. arXiv:1802.09855v1 (Submitted to European Physical Journal B).

A. Tanimu, E. A. Muljarov. Resonant state expansion applied to one-dimensional quantum systems (Submitted to Phys. Rev. A).

Presentations

A. Tanimu and E. A. Muljarov. Resonant states of the one-dimensional Schrödinger equation. *Postgraduate Conference*, Cardiff, UK, (September 2016).

A. Tanimu and E. A. Muljarov. Resonant state expansion for one-dimensional Schrödinger problems. *Annual Early Career Researcher Poster Competition*, Cardiff, UK, (June 2017).

A. Tanimu and E. A. Muljarov. Resonant state expansion in quantum mechanics: Application to multiple quantum well structures. *Theoretical group talk*, Cardiff, UK, (February 2018).

A. Tanimu and E. A. Muljarov. Resonant state expansion applied to multiple quantum well structures . *Speaking of science conference*, Cardiff, UK, (May 2018).

Contents

Chapter 1

Introduction

This thesis present the work I have done with my supervisor Dr Egor Muljarov. It is based on a resonant states expansion, a rigorous perturbation theory, recently developed in electrodynamics [1] for accurate calculation of eigen wave numbers in open optical system. Here it is applied to non-relativistic quantum mechanical systems in one dimension. The method is used for finding the resonant states in various potentials approximated by combinations of Dirac delta functions. We start our work investigating the full set of resonant states in double and triple quantum well/barrier structures. This includes bound, anti-bound and normal resonant states which are all eigensolutions of Schrödinger's equation with generalised outgoing wave boundary conditions. We analysed the transformation of resonant states and their transitions between different subgroups as well as the role of each subgroup in observables, such as the quantum transmission.

Using the triple quantum well, we verified the resonant

state expansion, showing convergence to the available analytic solution as the number of resonant states in the basis increases. The method is then applied to multiple quantum well and barrier structures, including finite periodic systems. Results are compared with the eigenstates in triple quantum wells and infinite periodic potentials, revealing the nature of the resonant states in the studied systems.

Before going into the regorous formalism of resonant states in quantum mechanincs which is provided further in this introduction, we first look at a well known problem of a forced harmonic oscillator with damping which presents the simplest physcial system showing resonant states.

1.1 Classical harmonic oscillator

In classical mechanics, a harmonic oscillator is a system that, when displaced from its equilibrium position, experiences a restoring force, F, proportional to the displacement, x: $\vec{F} = -k\vec{x}$ where k is a positive constant. If F is the only force acting on the system, the system is called a simple harmonic oscillator, and it undergoes simple harmonic motion: sinusoidal oscillations about the equilibrium point, with a constant amplitude and a constant frequency (which does not depend on the amplitude). The common equation to harmonic oscillators is the equation of motion

$$\ddot{x} + \omega_0^2 x = 0 \tag{1.1}$$

with the well-known solutions

$$x(t) = c_1 \cos \omega_0 t + c_2 \sin \omega_0 t. \tag{1.2}$$

If a frictional force (damping) proportional to the velocity is also present, the harmonic oscillator is described as a damped oscillator

$$\left(\frac{d^2}{dt^2} + 2\gamma \frac{d}{dt} + \omega_0^2 \right) X(t) = e^{i\omega t} \tag{1.3}$$

with a solution

$$X(t) = X_0(\omega) e^{i\omega t} \tag{1.4}$$

where

$$X_0(\omega) = \frac{-1}{(\omega - \omega_1)(\omega - \omega_2)} \tag{1.5}$$

is the Green's function (GF) having 2 poles, at ω_1 and ω_2. These are the eigen frequencies of the system, which are given by

$$\omega_{1,2} = \pm\Omega - i\Gamma \tag{1.6}$$

with the real part as

$$\Omega = \sqrt{\omega_0^2 - \gamma^2} \tag{1.7}$$

and imaginary part as $\Gamma = \gamma$. These poles present resonances in the system response, as demonstrated by Fig. 1.1

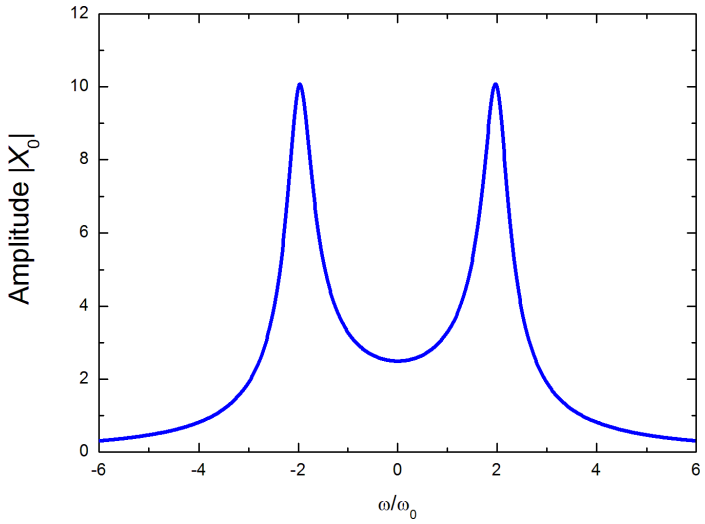

Figure 1.1: This figure shows classical resonance at $\omega \approx \omega_0 = 1$ with width $\sim 2\gamma$ ($\gamma = 0.5$).

By taking the limit as $\gamma \to 0$ (no damping), ω_1 and ω_2 on the real axis resembles the energies of bound states and the expression for Eq. (1.3) is reduced to the previous expression Eq. (1.1). The appearance of these bound states in two dimensional photonic crystal waveguides is investigated in [2], and in quantum mechanics the creteria for their existence in one dimension was also discussed in [3].

1.2 Bound states in a finite square well

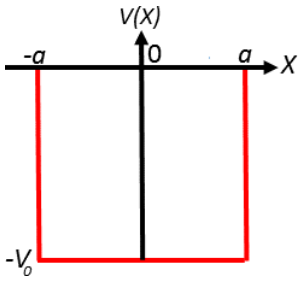

Figure 1.2: Form of a 1D potential along the x-axis.

The finite square well problem nicely introduces bound states in quantum mechanics. We consider the finite square well of width $2a$ defined by a potential $V(x)$ given by

$$V(x) = \begin{cases} -V_0, & \text{if } |x| < a \\ 0, & \text{if } |x| > a \end{cases} \tag{1.8}$$

which contributes to Schrödinger's equation. The wavefunction $\psi(x)$ of a bound states having $-V_0 < E < 0$ are then piecewise continuous functions:

$$\psi(x) = \begin{cases} Ce^{-\beta x}, & \text{if } x > a \\ A\sin\alpha x + B\cos\alpha x, & \text{if } |x| \leq a \\ De^{\beta x}, & \text{if } x < -a \end{cases} \tag{1.9}$$

where

$$\beta = \sqrt{-E} \tag{1.10}$$

and

$$\alpha = \sqrt{V_0 + E} \tag{1.11}$$

where we have used $\hbar = 1$ and $m = 1/2$. The condition that characterizes the finite wells bound states takes the form of a transcendental equation that cannot be solved analytically. Due to the symmetric nature of our wave functions, the bound states come in pairs: even and odd states. This results in two secular transcendental equations that we need to solve in order to find the energies

at which bound states occur: Even states: $A = 0$, $B \neq 0$, $C = D$;

$$\alpha \tan \alpha a = \beta. \tag{1.12}$$

Odd states: $A \neq 0$, $B = 0$, $C = -D$;

$$\alpha \cot \alpha a = -\beta. \tag{1.13}$$

To find the energies of the allowed bound states, root-finding techniques must be employed. In this case a Newton-Raphson procedure in Matlab is used and details of its implementation are given in Sec. 2.2. There is also a continuum of state in quantum well for energies $E > 0$ which is usually treated as scattering states. Resonant states (RSs) allow treating the continuum on equal footing with bound states: Both types of states are discrete eigen solutions of Schrödinger's equation.

1.3 Resonant states (RSs)

The concept of RSs, originates from non-relativistic quantum mechanics. This concept was introduced in the original works of Gamow [4] and Siegert [5], see also review articles [6, 7]. Quantum-mechanical RSs are the eigen solutions of the Schrödinger wave equation with purely outgoing wave boundary conditions [4–6]. RSs have generally complex energy eigenvalues $E_n = \hbar\Omega_n - i\hbar\Gamma_n$, with negative imaginary part having the meaning of the inverse lifetime of the quantum state, exponentially decaying in

time as $e^{-\Gamma_n t}$ which results by substituting the energy E_n to the time-dependent wave function $\psi_n(r,t) = \psi_n(r)e^{-iE_n t/\hbar}$. Already in the early works on RSs, it has been understood that owing to this decay, the wave function grows in space exponentially at large distances, reflecting the fact that the probability density leaks out of the open system [8]. These exponentially increasing tails of RSs outside the system makes the wave function not square integrable, thus preventing from using the standard normalization condition. Therefore, a special normalization and orthogonality conditions for RSs were proposed [5, 6]. The RSs can then be used to calculate the Green's function of the system via its spectral representation [9, 10] using the Mittag-Leffler theorem. The Green's function in turn provides the complete system response and allows to calculate observables such as local density of states, scattering, or transmission.

It has been also realized that the full set of the RSs is complete inside the finite area of space occupied by an open system [9, 10], and therefore the RSs can be used as a basis for expanding solutions of the Schrödinger equations, also with modified potential. Using this approach, the Schrödinger wave equation is reduced to a linear matrix eigenvlue problem, which can be solved by diagonalizing a complex symmetric matrix. This is called the resonant state expansion method (RSE).

1.4 Resonant state expansion

The resonant state expansion (RSE) is a rigorous perturbative method for treating open optical systems, which has been recently developed in electrodynamics [1]. The RSE has been verified and applied to various one-dimensional (1D), 2D and 3D open optical systems [11–17], demonstrating its high efficiency and suitability to treat perturbations of the permittivity of arbitrary strength and shape. The RSE treats the perturbed problem as a combination of an unperturbed problem usually having an analytical solution and a perturbation. It is well known that the presence of a continuum in the spectrum of a system is a significant problem for any perturbation theory. In open quantum systems such a continuum is often the dominating if not the only part of the spectrum. However, going away from the real axis to the complex frequency plane, the continuum can in many cases be effectively replaced by a countable number of discrete resonant states (RSs). In optics, these are vectorial eigen solutions of Maxwell's equations.

The 1D quantum-mechanical analog of the RSE was formulated early in [18] with the only numerical implementation known in the literature [19], which was a calculation of a single bound state in a rectangular quantum well. The conclusion made in [19] was that the convergence of this calculation is not quick enough compared to some other methods also assessed in [19]. Perhaps,

this has become the reason why this approach in quantum mechanics was not developed any further. However, very recently, the RSE has been re-invented in electromagnetics [1], and it has been shown [11] that the RSE actually presents a very efficient computational approach, with a potential to supersede some popular computational methods, such as finite-difference time-domain [20, 21], finite element method [22], Fourier modal method [23, 24], and so on. This indicates clearly that there a need also to study the quantum-mechanical (QM) analogue of the RSE (QM-RSE), which we have started doing in the present work.

The aim of this work is to apply, verify and study the QM-RSE in various 1D quantum systems. We first calculate the RSs of a symmetric double quantum well structure modeled by a delta-function potential. These RSs are then taken as an unperturbed basis for the QM-RSE. Both symmetric and asymmetric triple quantum well or barrier structures, which allow relatively simple analytic solutions, are then used to verify the QM-RSE and to study its convergence. In this case, the potential of the third well or barrier in the middle is treated as a perturbation. The QM-RSE is then applied for an efficient calculation of RSs in multiple quantum well structures and finite periodic quantum lattices of different period and potential strength. The results obtained are compared with infinite quantum lattices described by a Kronig-Penney model [25].

1.5 Resonant states (RSs) and their normalisation in one-dimensional systems

Resonant states (RSs) have been known in quantum mechanics for almost a century, since the pioneering works of Gamow[4] and Siegert [5]. They describe, in a mathematically rigorous way, natural resonances which quantum systems exhibit. People are dealing with resonances in different fields of physics, ranging from classical mechanics and electrodynamics to quantum physics and gravity. Resonant phenomena have attracted significant interest in recent years, in particular, in quantum mechanics due to a rapid progress in the field of semiconductor nanostructures, where different electronic states are formed in various types of quantum potentials. In spite of this growing interest in resonances, many fundamental aspects of RSs in quantum systems are still to be investigated [26].

Perhaps, a more traditional way of dealing with resonances is to study the singularities of the scattering matrix as described in many textbooks (see, e.g. [27]). Finding these singularities is actually equivalent to solving the Schrödinger equation with outgoing wave boundary conditions outside the system. These boundary conditions strictly define the RSs of the system.

Consider the RSs of a one-dimensional (1D) quantum mechanical systems, such as a double or triple quantum well. For

a better understanding of their properties, we will study them in detail in Chap. (2) and (3) and later use in Chap. (4) and (5) for constructing an analytic basis of RSs and varifying the RSE. The basis of RSs of a double well can then be used for treating more complicated potentials with the RSE. In general, RSs of a quantum-mechanical system are eigen solutions of the Schrödinger equation

$$\hat{H}(\mathbf{r})\psi_n(\mathbf{r}) = E_n\psi_n(\mathbf{r})\,, \tag{1.14}$$

satisfying the outgoing wave boundary conditions (BCs). Here $\hat{H}(\mathbf{r})$ is the Hamiltonian of a single particle, $\psi_n(\mathbf{r})$ and E_n are, respectively, its eigen wave function and eigen energy, and $\mathbf{r}$ is a three-dimensional coordinate. Note that one can obtain the time independent Schrödinger equation Eq. (1.14) from the time dependent one, as well as obtain from classical mechanics as shown in App.(A). Having in mind application to e.g. planar semiconductor heterostructures, we reduce our consideration in this work to a non-relativistic one-dimensional Schrödinger's problem. For brevity of notations, we make use of the units $\hbar = 1$ and $m = 1/2$, where m is the particle mass (e.g. the electron effective mass in a semiconductor). It is also convenient to introduce the eigen wave number k_n of the particle associated with a given RS and use it instead of the energy E_n which are linked together via a non-relativistic parabolic dispersion relation

$$E_n = k_n^2\,. \tag{1.15}$$

A 1D time-independent Schrödinger equation then takes the form:

$$\left[-\frac{d^2}{dx^2}+V(x)\right]\psi_n(x)=k_n^2\psi_n(x)\,, \tag{1.16}$$

where $V(x)$ is the potential of the particle, which is chosen in such a way that it vanishes outside the system. In 1D, the outgoing wave BCs for RSs reduce to

$$\psi_n(x)\propto e^{ik_n|x|} \quad \text{for} \quad |x|\to\infty\,, \tag{1.17}$$

which are also known as Siegert BCs [5]. Solving Eq. (1.16) with the BCs Eq. (1.17) inevitably leads to the fact that the energies E_n are generally complex,

$$E_n=(p_n+i\varkappa_n)^2=(p_n^2-\varkappa_n^2)+2ip_n\varkappa_n\,, \tag{1.18}$$

where p_n and $\varkappa_n$ are, respectively, the real and the imaginary part of the eigen wave number: $k_n=p_n+i\varkappa_n$. For bound states $p_n=0$ and $\varkappa_n>0$, so that the energy is real negative $E_n=-\varkappa_n^2<0$, and the general Eq. (1.17) reduces to the standard BC of the wave function vanishing away from the system: $\psi_n(x)\propto e^{-\varkappa_n|x|}\to 0$ at $|x|\to\infty$. For anti-bound states [28], if they exist in the spectrum, $p_n=0$ and $\varkappa_n<0$, corresponding to a purely growing wave outside the system, even though their energies are real. All other RSs have $p_n\neq 0$ and $\varkappa_n<0$ which results in complex eigen energies and wave functions which oscillate and grow exponentially in the exterior: $\psi_n(x)\propto e^{(ip_n-\varkappa_n)|x|}\to\infty$, according to Eq. (1.17).

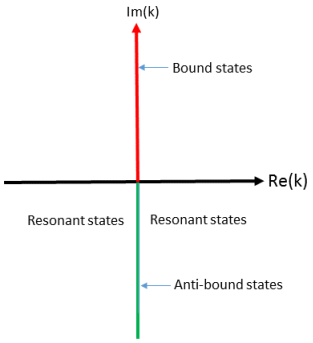

Figure 1.3: Diagram showing the locations of bound, antibound and resonant states wave numbers in a complex k-plane.

As a consequence of this exponential growth the wave functions of the RSs are not orthogonal and not normalizable in the usual way. Indeed RSs require a proper general orthonormality condition which would include the standard one as a special case, valid for bound states. For a one-dimensional system, this general orthonormality of RSs is given [1, 5, 10] by

$$\delta_{nm} = \int_{x_L}^{x_R} \psi_n(x)\psi_m(x)dx - \frac{\psi_n(x_L)\psi_m(x_L) + \psi_n(x_R)\psi_m(x_R)}{i(k_n + k_m)}, \tag{1.19}$$

where δ_{nm} is the Kronecker delta, and x_L and x_R are two arbitrary points outside the system, one to the left of it (x_L) and one to the right (x_R).

The orthogonality ($n \neq m$) is now proven in Appendix (B), while the normalization ($n = m$) can be derived from the Green's function, as done e.g. in [1].

Taking the normalisation ($n = m$) and following from Eq. (1.19) obtain

$$\int_{-a}^{a} \psi_n^2(x)dx - \frac{\psi_n^2(x_L) + \psi_n^2(x_R)}{2ik_n} = 1. \tag{1.20}$$

The integral can be split into 3 different integrals covering the whole range in total:

$$\int_{x_L}^{-a} \psi_n^2(x)dx + \int_{-a}^{a} \psi_n^2(x)dx + \int_{a}^{x_R} \psi_n^2(x)dx - \frac{\psi_n^2(x_L) + \psi_n^2(x_R)}{2ik_n} = 1, \tag{1.21}$$

or

$$\left[\frac{\psi_n^2}{-2ik_n}\right]_{x_L}^{-a} + \int_{-a}^{a} \psi_n^2(x)dx + \left[\frac{\psi_n^2}{2ik_n}\right]_{a}^{x_R} - \frac{\psi_n^2(x_L) + \psi_n^2(x_R)}{2ik_n} = 1. \tag{1.22}$$

$$\frac{\psi_n^2(-a)}{-2ik_n} - \frac{\psi_n^2(x_L)}{-2ik_n} + \frac{\psi_n^2(x_R)}{2ik_n} - \frac{\psi_n^2(a)}{2ik_n} - \frac{\psi_n^2(x_L) + \psi_n^2(x_R)}{2ik_n} + \int_{-a}^{a} \psi_n^2(x)dx = 1 \tag{1.23}$$

Since the wave function is continuous at $x = \pm a$, Eq.(1.23) is reduced to

$$\int_{-a}^{a} |\psi_n^2|(x)dx - \frac{\psi_n^2(-a) + \psi_n^2(a)}{2ik_n} = 1. \tag{1.24}$$

In Eq. (1.19) x_L and x_R can be any (but outside the system). Allowing $x_L \to -\infty$ and $x_R \to +\infty$ and noting that $\psi_n(\pm\infty) = 0$ for bound state Eq.(1.19) becomes the standard orthogonality condition:

$$\delta_{nm} = \int_{-\infty}^{\infty} \psi_n(x)\psi_m(x)dx. \tag{1.25}$$

For exponentially growing wave functions the divergence of the integral at $|x_{R,L}| \to \infty$ is exactly compensated by the second term.

Furthermore, as the normalization does not depend on x_L and x_R, it is usually convenient to take these points exactly at the boundaries of the system.

1.6 Semiconductor heterostructures: Multiple quantum wells and superlattices

Due to the new growth techniques, it has become possible to construct artificial one dimensional (1D) lattice structures by growing different layers of materials on top of each other. A semiconductor heterostructure resembles the atomic lattice: It is a sandwich of two different semiconductors with different band gaps. In general, a number of potential wells separated by potential barriers, is referred to as a multiple quantum wells. If one makes a heterostructure with thin enough layers, quantum interference effects start to dominate in the motion of the electrons. The simplest structure in which these may be observed is a quantum well, which simply consists of a thin layer of a narrower-gap semiconductor between thicker layers of a wider-gap material [29]. The band profile then shows a "rectangular well," as illustrated in Fig. 1.4.

Quantum well heterostructures are key components of many optoelectronic devices, because they can increase the strength of

electro-optical interactions by confining the carriers to small regions [30].

1.6.1 Single and coupled quantum wells

A single quantum well semiconductor structure typically consists of a thin semiconductor layer sandwiched between two layers of a material with a wider bandgap, like aluminium arsenide. The band structure is demonstrated in Fig. 1.4. This structure can be grown by molecular beam epitaxy, a widely used technique in the manufacture of semiconductor devices.

A coupled quantum well structure consists of two single quantum wells separated by a barrier layer. The barrier layer is sufficiently thin enough to allow the tunneling of carriers between the two quantum wells layer. As a result, an electron and a hole can either reside in one of the two quantum wells.

Thin metal films can also support quantum well states, in particular, metallic thin overlayers grown in metal and semiconductor surfaces. The electron (or hole) is confined by the vacuum-metal interface in one side, and in general, by an absolute gap with semiconductor substrates, or by a projected band gap with metal substrates.

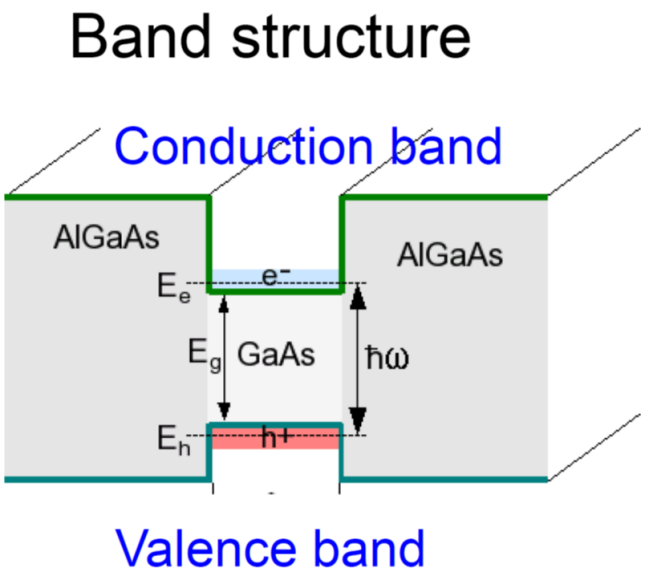

Figure 1.4: Sketch of a realistic semiconductor quantum well showing conduction and valence band edges

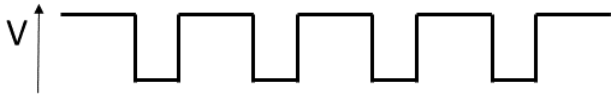

Figure 1.5: Sketch of a superlattice showing conduction and valence band edges

1.6.2 Superlattices

Superlattices are one-dimensional periodic structures that were grown early in 1925 by Johansson and Linde [31]. Typically, the thickness of one layer is several nanometers. It can also refer to a lower-dimensional structure such as an array of quantum dots or quantum wires. The properties of one-dimensional periodic potential and negative differential conductivity in semiconductors were first investigated theoretically in 1970's by L. Esaki and R. Tsu [32]. Later on, superlattices were artificially grown [33–35] by different material growth techniques. By the advancement of semiconductor superlattice structures, unusual optical and electrical properties have been observed and a detailed study of their

band structure has become possible. In principle, superlattices consist of two (or more) materials interleaved in thin layers by depositing them in a repeated pattern. The two different semiconductor materials are deposited alternatively on each other to form a periodic structure in the growth direction.

1.7 Periodic potentials

In this case, we consider a superlattice as an example, therefore we need to study periodic structures in a bit more details. The Schrödinger equation for an electron in one-dimension is

$$H\psi(x) = \left[-\frac{\hbar^2}{2m}\frac{d^2}{dx^2} + V(x)\right]\psi(x) = E\psi(x) \tag{1.26}$$

with a periodic potential

$$V(x+d) = V(x) \tag{1.27}$$

where d is a lattice period. The fundamental theorem regarding the motion of electrons in a periodic potential is that of Bloch (1928) [36] which, in its one-dimensional form, is usually called the Bloch-Floquet theorem.

1.7.1 Bloch's theorem

The concept of the Bloch theorem was first developed in 1928, by Felix Bloch [36], to describe the conduction of electrons in crystalline solids. Independent mathematical proofs was provided by [37, 38]. As a result, a variety of nomenclatures are common: applied to ordinary differential equations, it is called Floquet theory.

Mathematically Bloch's theorem states that for any periodic potential $u(x)$, there is a special fundamental system of solutions with the translational symmetry

$$\psi_{nk}(x) = e^{iqx} u_{kj}(x) \tag{1.28}$$

where

$$u_{kj}(x + nd) = u_{kj}(x) \tag{1.29}$$

The indexes k, j are the electron wave vector and electron bands respectively. Eq.(1.28) and Eq.(1.29) imply that

$$\psi_{kj}(x + nd) = e^{iqd} \psi_{kj}(x). \tag{1.30}$$

Dropping the indexes Bloch's theorem showed that the solutions to the Schrödinger's equation are the product of a plane wave and a periodic function with the periodicity of the lattice:

$$\psi(x + nd) = e^{iqd} \psi(x). \tag{1.31}$$

such that for every period d in the lattice the eigenstates of H can be chosen so that each ψ is associated with a wave vector q. Details of this proof is presented in Appendix (C).

1.7.2 Kronig-Penney model

The Kronig-Penney model was first formulated in 1930 by R. de L. Kronig and W. G. Penney [25]. The Kronig-Penney model was discussed in a number of solid-state physics text books [39]. A schematic of this model describing a one-dimensional periodic potential is shown in Fig. 1.6. This model shows a periodic super-lattice with a δ-functions.

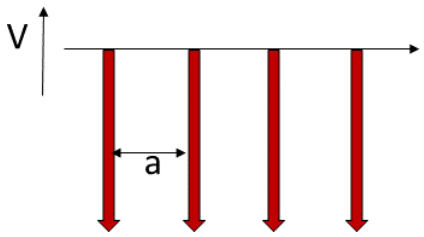

Figure 1.6: Sketche of a Kronig-Penney model with δ function potentials

It does not describe band overlaps which take place in realistic (finite) potentials [40]. Even though the model is highly artificial, yet it illustrates many of the characteristic features of the behaviour of electrons in a periodic lattice (i.e. will open gaps in the energy dispersion relation). The wave functions associated with this model can be calculated by solving the one-dimensional

time independent Schrödinger equation Eq.(1.26). Since the electron moves in a periodic potential

$$V(x) = -\gamma \sum_{n=-\infty}^{\infty} \delta(x - nd), \tag{1.32}$$

where γ is called the barrier/well strength. Its wavefunction must satisfy Bloch's theorem for any choice of superlattice

$$\psi(x + d) = e^{iqd}\psi(x) \tag{1.33}$$

where d is the period of the superlattice potential while k is the eigen-wavenumber associated with the direction of electronic motion. Applying the relevant boundary conditions to our wave functions obtained

$$\cos(qd) = \cos(kd) - \frac{\gamma}{2k}\sin(kd). \tag{1.34}$$

Full derivation of Eq.(1.34) is given in App.(D).There are only two variables in Eq.(1.34) namely k and q. The LHS of Eq.(1.34) is bounded since it can only assume values between $+1$ and -1 for real k. If we plot the left-hand side of this equation against kd, it will be possible to determine those value of k (and hence energy) which are permissible; that is, permit $\cos(kd) - \frac{\gamma}{2k}\sin(kd)$ to take values between $+1$ and -1. This is shown in Fig. 1.7 for barrier and well.

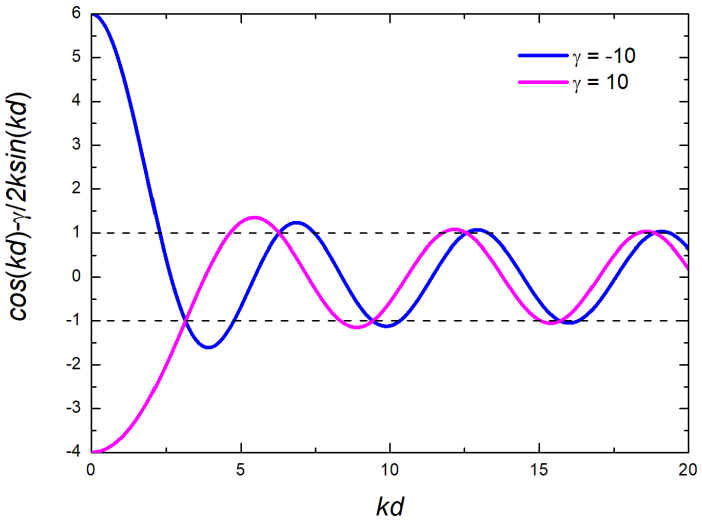

Figure 1.7: Plot of the function $\cos(kd) - \frac{\gamma}{2k}\sin(kd)$ for barrier and well. For barrier we use the parameter $\gamma = -10$ while for the well we use $\gamma = 10$

1.8 Overview

In chapter two, we present the concept of RSs in a finite square quantum well. We derive first the analytic secular transcendental equations for even and odd states by applying the outgoing wave boundary conditions. The complex roots of these equations are found using Newton-Raphson method implemented in Matlab. We consider all types of RSs present in such a system. We also calculate the wave functions of RSs.

In chapter three, we investigate the full spectrum of eigensolutions of the one-dimensional Schrödinger's equation for double and triple quantum wells/barriers structures. We model a double and triple quantum wells structures with Dirac delta-function potentials working out and analysing analytic solutions. The transformation of RSs and their transitions between different subgroups as well as the role of each subgroup in observables, such as the

quantum transmission, is analysed. We also revisit in this chapter the well known problem of bound states in delta-like potentials.

Using triple quantum wells in chapter three we were able in chapter four to verify and study the quantum mechanical RSE (QM-RSE) in 1D quantum systems. This verification is made using available simple exact solutions for triple QWs. The comparison demonstrates high accuracy and quick convergence of the QM-RSE.

We complete the research overview of the thesis with the final chapter where we apply the QM-RSE to multiple quantum well structures and finite periodic and random quantum lattices. The application of QM-RSE to 1D quantum lattices has its application to a semiconductor heterostructures: Multiple quantum wells and superlattices. The QM-RSE allowed us to study RSs of multiple QW systems with a large number of QWs. The RSs of multiple QW structures are analysed and compared with the band structure in the Kronig-Penney model.

Chapter 2

Resonant states in a finite rectangular quantum well

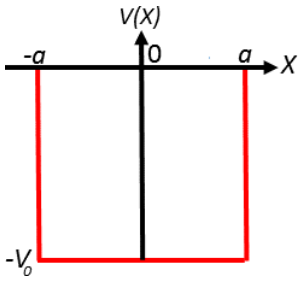

Figure 2.1: Form of a 1D potential along the x-axis.

In this chapter, we consider a well-known problem in quantum mechanics [27], the one-dimensional finite rectangular well, to study the spectrum of RSs. Quite long ago Nussenzveig [41] studied the behaviour of RSs in a rectangular potential well (barrier) as a function of the well depth (barrier height). In his work he observed the flow of RSs in a complex plane by varying the depth of the potential. For over a decades little has been done to improve on those results. In this chapter, we accurately calculated such RSs numerically using Newton-Raphson method implemented in

Matlab. We demonstrate how the bound states appear or disappear in the spectrum transforming into anti-bound states as the strength of the potential V_0 changes [28, 42–44]. Then we extend our consideration to study properties of RSs wave functions and discuss the physical meaning of the normal RSs, also paying attention to the their evolution and transformation into/from bound and anti-bound states.

2.1 Derivation of the secular equation

In quantum mechanics, RSs are eigen solutions of the Schrödinger equation Eq.(1.14) with outgoing wave boundary conditions (BCs).

A 1D time-independent Schrödinger equation then takes the form:

$$\left[-\frac{d^2}{dx^2} + V(x)\right] \psi_n(x) = k_n^2 \psi_n(x)\,, \tag{2.1}$$

where $V(x)$ is the potential of the particle, which is chosen in such a way that it vanishes outside the system.

$V(x)$ is a general potential with compact support. Here we reduce it to rectangular :

$$V(x) = \begin{cases} -V_0, & \text{if } |x| < a \\ 0, & \text{if } |x| > a \end{cases} \tag{2.2}$$

This potential is illustrated in Fig. 2.1. Solutions in this potential has been covered in depth by many texbooks such as [27]. However, RSs in general are usually not considered in textbooks. Therefore, in this chapter it is interesting to study RSs of this potential and to see in particular how the RSs move in the complex k-plane as we change the depth of the well. We find a general eigen solutions of Eq.(2.1) with BCs Eq. (1.17). Thus the wave function has the form

$$\psi(x) = \begin{cases} Ae^{ikx}, & \text{if } x > a \\ B(e^{iqx} + pe^{-iqx}), & \text{if } |x| \leq a \\ Ae^{-ikx}, & \text{if } x < -a \end{cases} \tag{2.3}$$

where $p = \pm 1$ is the parity and we have omitted the RS index n for brevity of notation. A and B are normalisation coefficients to be shown later and k and q are the wave numbers which are related via

$$q = \sqrt{k^2 + V_0} \tag{2.4}$$

and the energy of the states are given by

$$E = k^2 \,. \tag{2.5}$$

For simplicity we use in $m = \frac{1}{2}$ and $\hbar = 1$. To find the eigenvalues, k, we require that $\psi(x)$ and $\psi'(x)$ are continuous at $x = \pm a$.

$$\psi(a + 0_+) = \psi(a - 0_+), \tag{2.6}$$

$$\psi'(a+0_+) = \psi'(a-0_+), \tag{2.7}$$

$$Ae^{ika} = B(e^{iqa} + pe^{-iqa}), \tag{2.8}$$

$$ikAe^{ika} = iqB(e^{iqa} - pe^{-iqa}) \tag{2.9}$$

where 0_+ is a positive infinitesimal. Expressing Eqs.(2.8) and (2.9) obtained

$$\frac{q}{k} = \frac{e^{iqa} + pe^{-iqa}}{e^{iqa} - pe^{-iqa}}. \tag{2.10}$$

From this we get

$$pe^{2iqa} = \frac{q-k}{q+k}, \tag{2.11}$$

which after some algebra leads to

$$k = iq_n \tan(qa) \tag{2.12}$$

for even and

$$k = -iq_n \cot(qa) \tag{2.13}$$

for odd states.

After finding solutions of the transcendental equations, we then substitute the values of k and q back into Eq.(2.11) in order to obtain the wave functions. We found that: if

$$\frac{q-k}{q+k} = +e^{2iqa} \tag{2.14}$$

the solutions are even and the wavefunctions are symmetric. If

however,

$$\frac{q-k}{q+k} = -e^{2iqa} \tag{2.15}$$

the solutions are odd and the wavefunctions are antisymmetric.

The secular transcendental equations Eq.(2.12) and Eq.(2.13) are solved below together with Eq.(2.4) in order to find the eigen wave numbers in the complex k-plane. Equations Eq.(2.12) and Eq.(2.13) cannot be solved analytically. So, in this work, we employ the Newton-Raphson method implemented in MATLAB, which is very efficient in finding roots of a complex function. Solving Eq.(2.12) and Eq.(2.13), we find all types of states, which include bounds, antibound and normal RSs. For both even and odd solutions the wave functions have to be normalized but care has to be taken during the calculations. For bound states this is an easy task, see Eq.(1.25) but for the resonant states which has exponentially increasing tails, an additional term must be considrered to normalize them correctly Eq.(1.19). An outer limit is required for their normalization and is given by a. We use $x_L = -a$ and $x_R = a$ in Eq.(1.19). It is found that the value of x_L, x_R can be any and thus for convenience we are free to choose the boundaries of the well as the limits of this normalization (see Sec.(1.5)). The orthonormality condition is given as [1, 5, 10]:

$$\delta_{nm} = \int_{-a}^{a} dx \psi_n(x)\psi_m(x) - \frac{\psi_n(a)\psi_m(a) + \psi_n(-a)\psi_m(-a)}{i(k_n + k_m)} \tag{2.16}$$

where we have restored RS indices in order to distinguish different RSs which contribute to Eq. (2.16). Using the normalization condition Eq.(2.16) the constants are found as [14] (for derivation, see App.(E)):

$$A_n = \frac{(-1)^n q_n e^{-ik_n a}}{\sqrt{V(a + \frac{i}{k_n})}} \tag{2.17}$$

and

$$B_n = \frac{(-i)^n}{2\sqrt{a + \frac{i}{k_n}}} \tag{2.18}$$

2.2 Numerical procedure of finding the eigen wave numbers

There are many numerical procedures for solving Eq.(2.12) and Eq.(2.13). While the equations cannot be solved analytically, they can be solved numerically up to any desired accuracy. Below are the few steps we used in order to find the solutions:

1) We use the relation between q and k in Eq.(2.4). This makes the final equations to solve written in terms of k only.

2) We define a function $f(k)$ such that the equation we solve becomes $f(k) = 0$.

3) We set the physical parameter values, such as V_0 and a.

4) We create a mesh of guess values for k in the complex k-plane *i.e.* real $k = -100 : 1 : 100$ and imag $k = (-3 : 1 : 0)i$ and perform the followin few steps for each point:

5) In the Newton-Raphson method we find k which fulfil condition

(2) above by changing k iteratively with $k - \frac{f(k)}{f'(k)}$.

6) We repeat until $f(k)$ is smaller than certain tolerance, in this case 10^{-9}.

7) We then perform the Newton-Raphson for all the points in the mesh.

8) We remove all the solutions that didn't converge and also all the solutions that are similar, meaning that the absolute values of all the real and imaginary part has to be larger than the tolerance.

9) Lastly, we plot the solutions for k in the complex k-plane (see for e.g. Fig. 2.2 and Fig. 2.3) for different parameters, and then calculate also the wave functions.

The MATLAB code implemented using Newton-Rapson method for the calculation of the resonant states wave numbers is now given in Appendix (F).

2.3 Bound states

Bound states have localised wave function with exponentially decaying tails at outside the system. For bound states the energy is real. For potential vanishing at $|x| \to \infty$, the bound state energies are negative [45]. Applying the asymptotic boundary conditions, the bound states wavefunctions have the asymptotic behaviour as

$$\psi_n(x) = \pm e^{-\varkappa_n |x|}, \; |x| \to \infty \tag{2.19}$$

with $\varkappa_n > 0$, where we have used in Eq.(2.3)

$$k_n = i\varkappa_n \tag{2.20}$$

Therefore the bound state energy E is

$$E_n = k_n^2 = -\varkappa_n^2, \tag{2.21}$$

taking negative values.

The eigen wave numbers of bound states are located on a positive imaginary k-plane [43], (see Fig. 2.2 and Fig. 2.3) for a rectangular quantum well with $V_0 = 3$ and 16 respectively and their wave functions are shown in Fig. 2.4.

2.4 Eigen wave numbers of the RSs

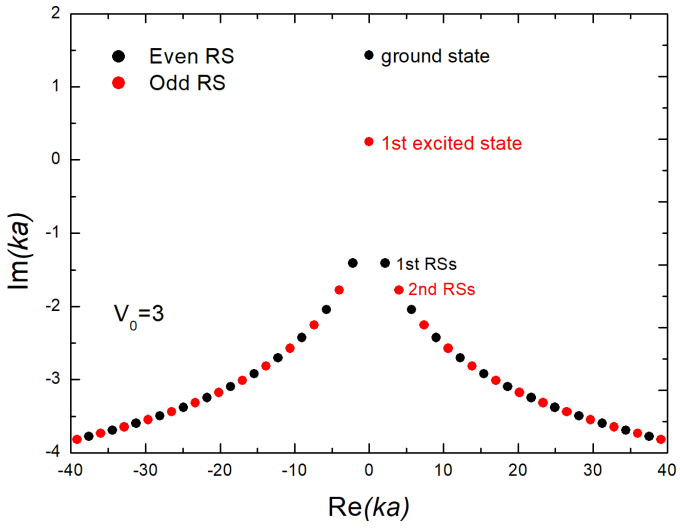

Figure 2.2: RS eigen wave numbers of the Schrödinger equation with a rectangular well potential of depth $V_0 = 3$ with outgoing waves boundary conditions plotted in the complex k-plane

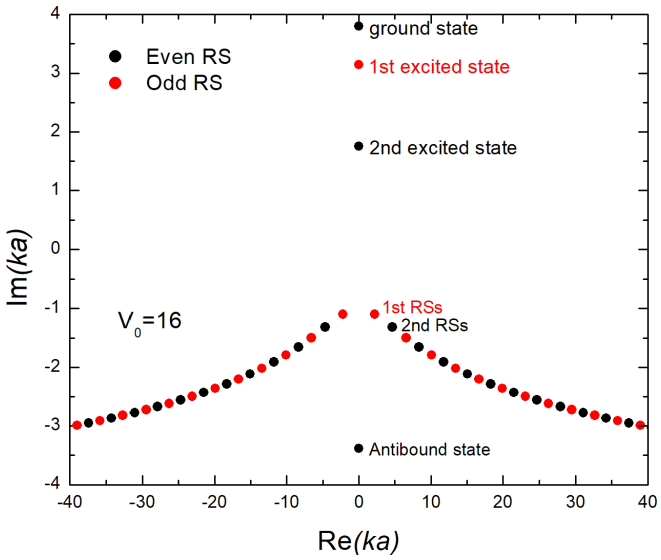

Figure 2.3: As Fig. 2.2 but for $V_0 = 16$

Fig. 2.2 and Fig. 2.3 show the plots of the complex roots in Eq.(2.12) and Eq.(2.13) which contain all types of RSs. As we can see, there are different types of modes, we call the resonant states as a general class of eigenstates, which includes all kind of states: bound, antibound and normal resonant states. For a shallow well like the one considered in Fig. 2.2, there are only two bound states and the RSs look similar to those in [26]. Increasing the depth of the well V_0, the normal RSs wave numbers move upwards parallel to the imaginary axis, and also the number of bound and antibound states is increased. When the pair of conjugate RSs hits the imaginary axis it splits up into a bound-antibound states pair [28, 41] which gets more bound when increasing the depth further (see for e.g., Fig. 2.3). The number of bound and antibound states depends on the choice of parameter V_0. The normal resonant states all have non zero real and imaginary parts of k_n. Each normal resonant state with $\mathrm{Re(k_n)} > 0$ has a partner in the left half plane with $\mathrm{Re(k_n)} < 0$. The positions

of a normal resonant state and corresponding anti-resonant state are symmetric with respect to imaginary axis. Their locations are mirror images with respect to the imaginary axis $k_{-n} = -k_n^*$ and $\psi_{-n}(x) = \psi_n^*(x)$. Depending on the system parameters, there are also discrete states on the imaginary axis. These states are called bound and antibound states. The bound states of the system considered in Fig. 2.3 are the ground state, 1st excited state and 2nd excited state. The bound states are located on the positive imaginary axis $\mathrm{Im(k_n)} > 0$ while the antibound states are located in the negative imaginary axis $\mathrm{Im(k_n)} < 0$. Since the energy of bound states is negative, the ground state corresponds to the highest RSs on the positive imaginary axis.

2.5 Wave functions of the RSs

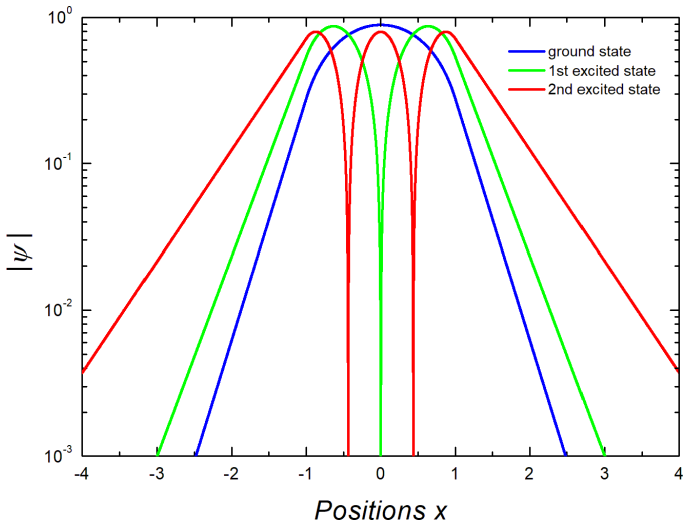

Figure 2.4: The absolute value of the wave function for the ground state, 1^{st} excited and 2^{nd} excited states with the rectangular well potential of depth $V_0 = 16$

Fig. 2.4 shows the plots of the absolute values of the wave

function for the ground state, 1^{st} excited and 2^{nd} excited state. These states are obtained by applying the boundary conditions to our wave function. The wave functions form two discrete sets, one remains unchanged under a mirror transformation (i.e. if we change x to -x), and the other changes sign. It is observe that, the wavefunctions exhibit even and odd symmetries about $x = 0$ as expected. Functions with this kind of behaviour are said to have a definite parity [46]. If $\psi_n(x) = \psi_n(-x)$ the parity is said to be even, and if $\psi_n(-x) = -\psi_n(x)$ the parity is said to be odd (for proof, see Appendix (I)). As we can see from Fig. 2.4, the wave function has exponentially decreasing tails outside of the well (see straight lines in log scale). Little is being discussed on these bound states since they have been covered in depths in many journals and textbooks.

2.5.1 Normal RSs

The resonant state can be defined as an eigenstate of the stationary Schrödinger equation with boundary conditions of outgoing or incoming waves only.

$$\psi_n(x) = \pm e^{ik_n|x|}, x = \pm \to \infty \tag{2.22}$$

which is also called Siegert condition [5]. For evaluation of resonant states, we seek a solution of Eq.(2.1) with complex energy Eq.(1.18) with $p_n > 0$ and $\varkappa_n > 0$ such that the wavefunctions

behaves asymptotically as:

$$\psi_n(x) = \begin{cases} e^{ip_n x + \varkappa_n x}, & \text{if } x \to +\infty \\ \pm e^{-ip_n - \varkappa_n x}, & \text{if } x \to -\infty \end{cases} \tag{2.23}$$

This nature of the wavefunction shows the positive real part of energy state since $p_n^2 > \varkappa_n^2$. We can see from Fig. 2.5, Fig. 2.6, and Fig. 2.7 that $|\psi|$ diverges exponentially as $e^{\varkappa_n |x|}$.

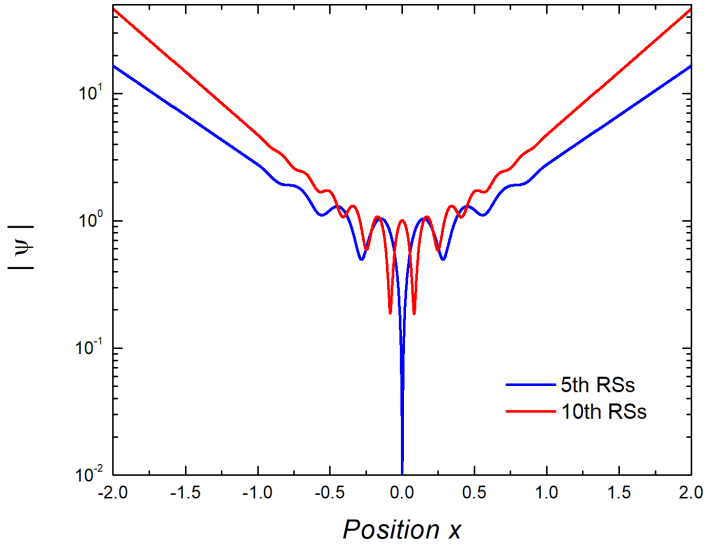

Figure 2.5: Plots of the absolute value of the 5^{th} and 10^{th} RSs wave function for $V_0 = 16$

In Fig. 2.5 are plots of the absolute value of the 5^{th} and 10^{th} RSs wave function. We can see that the wave function have even and odd symmetry about $x = 0$. With each subsequent state the symmetry switches and the wave function vanishes only for odd states. This is also observed in Fig. 2.6 and Fig. 2.7.

2.5.2 Antibound states

An antibound state shares physical features with the bound states and resonant states but it is called as a separate type of states. Wave functions for antibound states are not square integrable. Like for normal RS they diverge exponentially at large $|x|$ (see Fig. 2.6). The solution inside the well is similar to that of the bound state having energy $E < 0$. We can see the wave function is symmetric around the origin, which indicates that there must be solutions of defined parity also for antibound states.

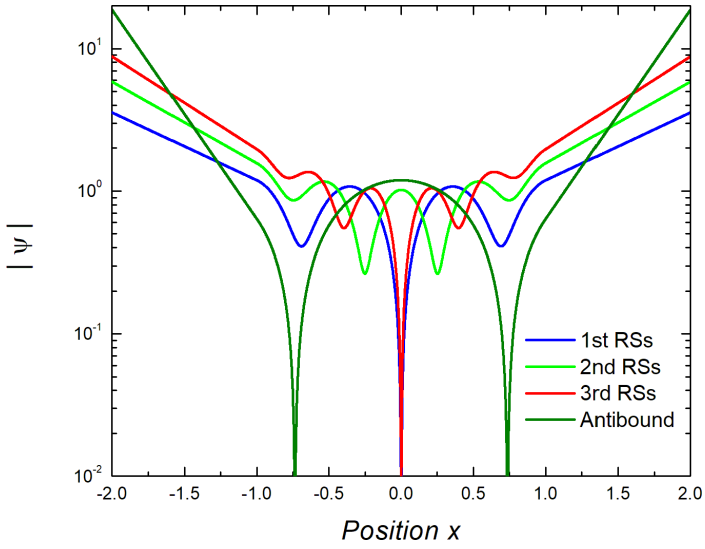

Figure 2.6: Plots of the absolute values of the antibound state, 1^{st}, 2^{nd} and 3^{rd} resonant states wave functions for $V_0 = 16$

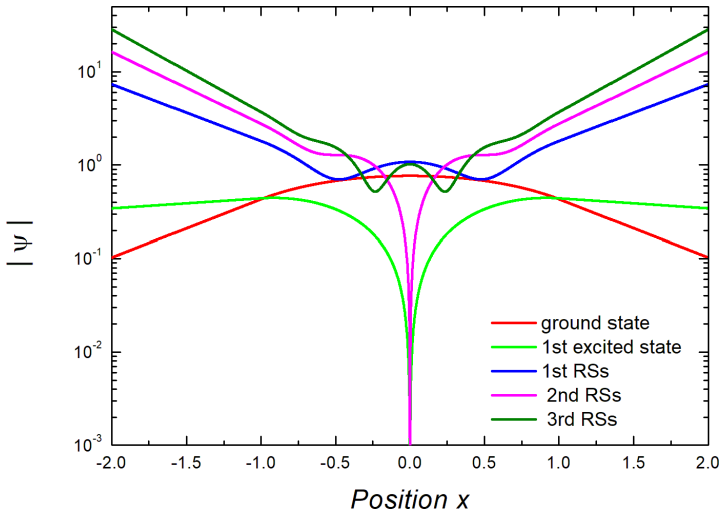

Figure 2.7: Plots of the absolute values of the ground state, first excited state, 1^{st}, 2^{nd} and 3^{rd} resonant states wave functions for $V_0 = 3$

Fig. 2.6 shows the plots of the absolute values of the antibound state, 1^{st}, 2^{nd} and 3^{rd} normal RSs wave functions while Fig. 2.7 shows the ground, first excited states, 1^{st}, 2^{nd} and 3^{rd} resonant states wave functions for comparison. The antibound states show a similar features to the bound states wave functions having a defined parity within the well. Unlike the bound states (see for e.g. Fig. 2.4), we can see that in a normal RSs and antibound states the wave functions grows exponentially at large distance. Strong oscillation is observed in Fig. 2.6 for a well depth of $V_0 = 16$ as compared to Fig. 2.7 which has a shallow well ($V_0 = 3$). It is found that for normal RSs the number of oscillations in wave functions depends on the size of well depth.

The larger the size of well depth the more stronger oscillation is observed within the full spectral range (see Fig. 2.6). Since the bound states and normal RSs wave functions alternate between even and odd states with ground state wave function as even,

therefore, the wave functions of the 1^{st} and 5^{th} RSs in Fig. 2.6 and Fig. 2.5 respectively are considered to be odd states. Unlike in Fig. 2.6, the wave function for the 1^{st} RSs in Fig. 2.7 is even because of the symmetry brakage due to higher number of bound states in Fig. 2.7. It is found that the wave functions for odd states vanishes at $x = 0$ (see for e.g. 5^{th} RSs in Fig. 2.5, 1^{st}, 3^{rd} RSs in Fig. 2.6 and 1^{st} excited and 2^{nd} RSs for Fig. 2.7).

2.5.3 Symmetry of the wave functions

In this part we discuss the symmetric/asymmetric nature of the 1^{st} and 2^{nd} RSs wave functions for $V_0 = 3$ and $V_0 = 16$. We can see that Figs (2.8) - (2.11) shows the real and imaginary parts of the wave function of the 1^{st} and 2^{nd} resonant states. For Figs (2.8) and (2.9) we used the parameter $V_0 = 3$ while for Figs (2.10) and (2.11) we used $V_0 = 16$ for comparison.

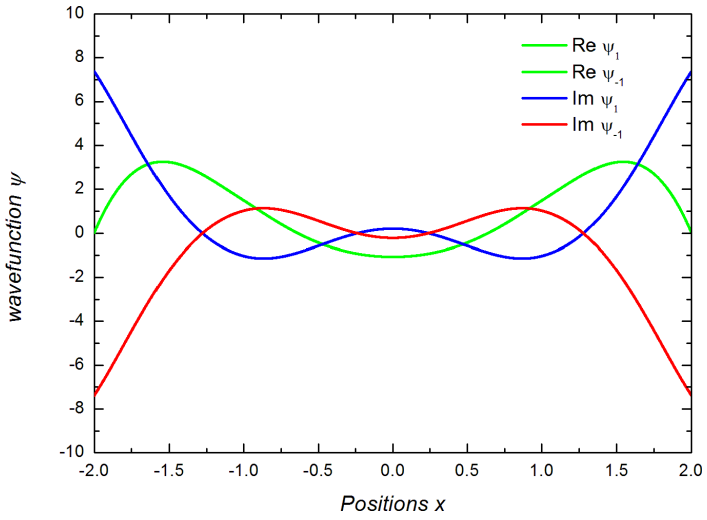

Figure 2.8: The plot shows the wave functions of the real and imaginary part of the 1^{st} resonant state for $V_0 = 3$

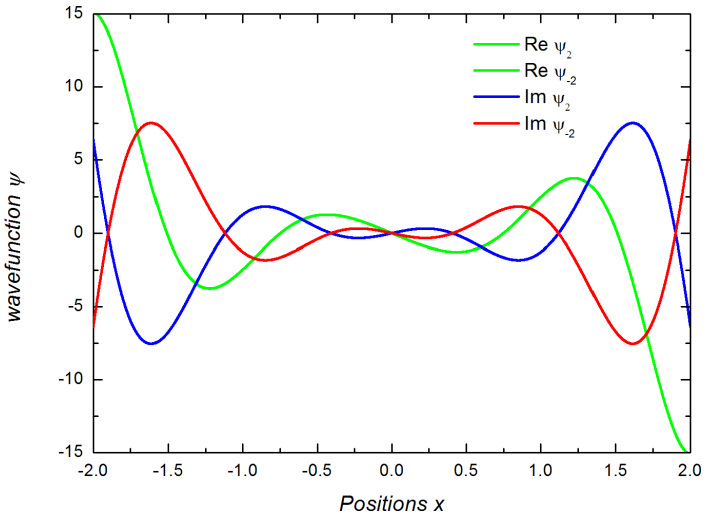

Figure 2.9: The plot shows the wave functions of the real and imaginary part of the 2^{nd} resonant state for $V_0 = 3$

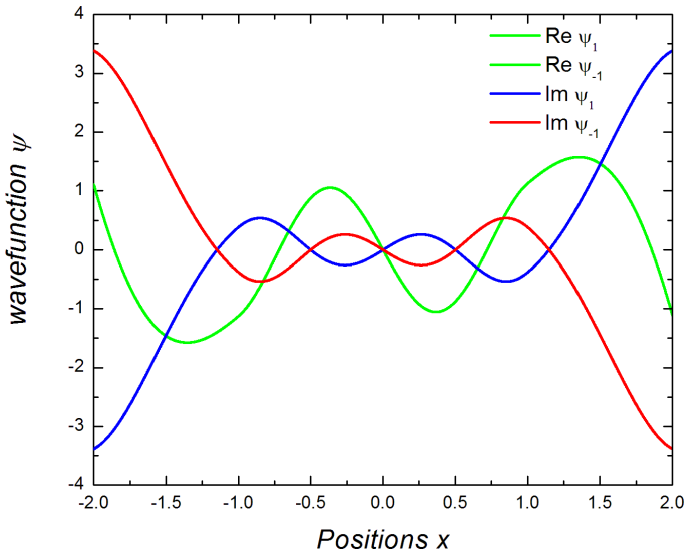

Figure 2.10: The plot shows the wave functions of the real and imaginary part of the 1^{st} resonant state for $V_0 = 16$

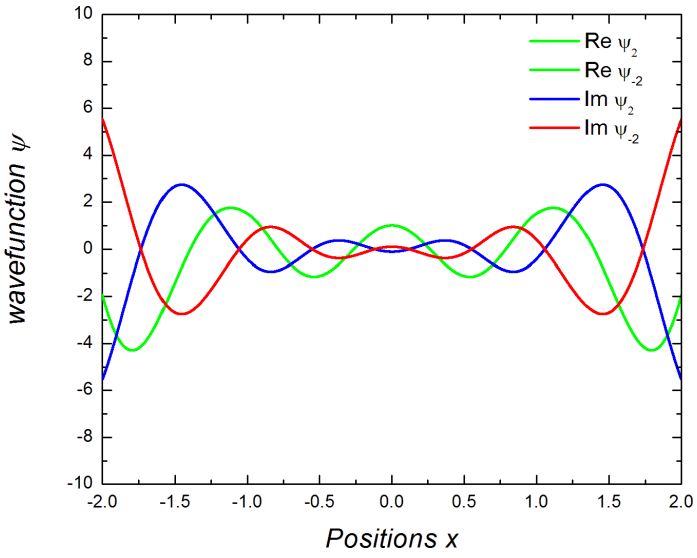

Figure 2.11: The plot shows the wave functions of the real and imaginary part of the 2^{nd} resonant state for $V_0 = 16$

It is shown that in Fig. 2.8 the wave function of the 1^{st} resonant state has an even function while it is odd in Fig. 2.10. We can also see that the wave function of the 2^{nd} resonant state in Fig. 2.9 has an odd function while it is even in Fig. 2.11. This switch between even and odd symmetry happen due to the change in system size. The 1^{st} resonant state is the next member in a sequence of RSs starting from the ground state and going to the highest excited state.

We found that the real part of the wave function is not changing throughout, while the imaginary part changes. This demonstrates that the wave function of the RSs are symmetric across the imaginary axis and contain symmetric pair of states which are complex conjugates of each other. This gives the relation $\psi_n(x) = \psi_n^*(x)$ with index $n = \pm 1, 2$ as shown in Figs (2.8) - (2.11).

2.6 Summary

In this chapter, the concept of RSs was introduced and discussed in a 1D finite square well potential. RSs were studied by seeking solutions to the time independent Schrödinger equation with outgoing boundary conditions. After application of boundary conditions to the problem, a system of equations was generated and written in terms of secular transcendental equations for even and odd states. Solutions of these equations were analytically obtained using Newton-Raphson method in Matlab. The full spectrum obtained include bound states associated with pure imaginary and positive wave numbers, the antibound states associated with pure imaginary and negative wave numbers and the normal RSs with a complex wave numbers which lie in the lower half of the complex k-plane. The properties of RSs were considered and discussed in details. The wave function of state of all types were plotted and compare with each other, demonstrating probability leakage of antibound and normal RSs. The symmetric nature of the RSs wave function was also discussed. We demonstrate that each resonant state wave function contains a symmetric pair of states which are complex conjugate of each other.

Chapter 3

Resonant states in double and triple quantum wells and barriers

In this chapter, we investigate the full spectrum of eigensolutions of the 1D Schrödinger equation for double and triple quantum well/barrier systems. The full spectrum of RSs includes bound, anti-bound and normal RSs, all together determining the spectral properties of a quantum system, such as local density of states and transmission [14].

We concentrate on double and triple quantum well structures where the delta potential approximation is a lot more appropriate, as it picks up the main resonant properties and features of these systems, at the same time omitting unimportant spectral details related to finite widths of realistic potentials, which in turn lead to additional quantum reflections. A single quantum

well modeled by a delta potential shows no resonant states either (apart from a single bound state), see for e.g. App.(D). This is because such a system has a zero width, in clear contrast with finite systems size.

3.1 RSs in a double well/barrier structures

We model a symmetric double quantum well structure with a superposition of two Dirac delta functions,

$$V(x) = -\gamma\delta(x-a) - \gamma\delta(x+a)\,, \tag{3.1}$$

where $2a$ is the distance between the wells and γ is the strength of the potential which has the meaning of the depth of each quantum well multiplied by its width. Fig. 3.1 sketches this potential along with a realistic coupled quantum well structure it models. An obvious advantage of the model is its simplicity and explicit analytical solvability. The solution for this potential, in terms of bound states, has been covered in depth in many texbooks, see e.g. [47]. We revisit this problem again, in order to study the full spectrum of RSs and their properties, which has not been done in the literature. This is also of practical importance, as the full set of RSs can be further used as a basis in the RSE.

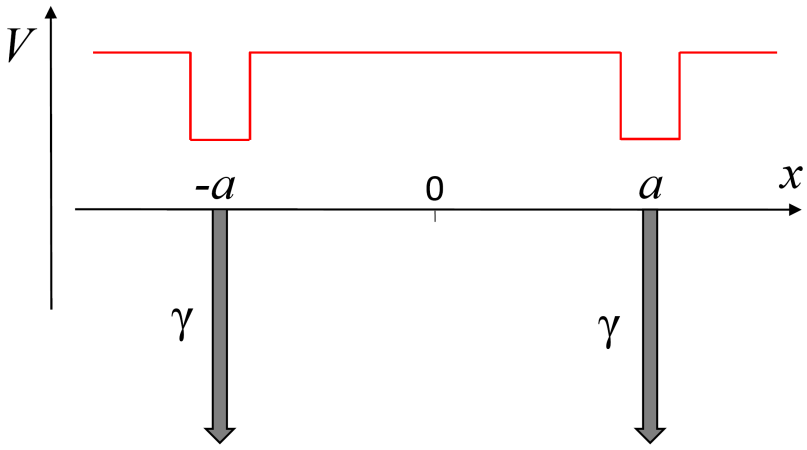

Figure 3.1: A sketch of the potential of a symmetric double well structure (red line) approximated by two delta-functions (grey arrows).

3.1.1 Exact solution

A general solution of Eq. (1.16) with the potential Eq. (3.1) has the form (for brevity of notations, we drop in this and the following section the index n labeling RSs):

$$\psi(x) = \begin{cases} Ae^{ikx} + Be^{-ikx} & x > a, \\ C_1 e^{ikx} + C_2 e^{-ikx} & |x| \leqslant a, \\ De^{ikx} + Fe^{-ikx} & x < -a, \end{cases} \tag{3.2}$$

with constant coefficients standing at the exponentials. Applying the outgoing wave BCs leads to $B = D = 0$. Furthermore, using the mirror symmetry of the potential, $V(-x) = V(x)$, splits all the solutions into two groups: even and odd states, having the property

$$\psi(-x) = \pm\psi(x)\,. \tag{3.3}$$

From this we obtain $F = \pm A$ and $C_1 = \pm C_2 = C$. Then the wave function takes the form

$$\psi(x) = \begin{cases} Ae^{ikx} & x > a, \\ C\left(e^{ikx} \pm e^{-ikx}\right) & |x| \leqslant a, \\ \pm Ae^{-ikx} & x < -a. \end{cases} \tag{3.4}$$

The wave function $\psi(x)$ must be continuous at any point but its derivative $\psi'(x)$ is discontinuous at $x = \pm a$. The break in the derivative can be evaluated by integrating Eq. (1.16) across the delta-function potential wells. This yields to four boundary conditions determining the relation between the coefficients A and C, as well as the eigenvalues k. However, as the symmetry of the potential has been already taken into account leading to Eq. (3.4), only one pair of BCs (e.g. at $x = a$) provides a unique information:

$$\psi'(a + 0_+) - \psi'(a - 0_+) = -\gamma\psi(a)\,, \tag{3.5}$$

$$\psi(a + 0_+) - \psi(a - 0_+) = 0\,, \tag{3.6}$$

where 0_+ is a positive infinitesimal. The other pair of BCs (at $x = -a$) is then fulfilled automatically. Substituting the wave function Eq. (3.4) into the BCs Eqs. (3.5) and (3.6), obtain

$$ikAe^{ika} - ikC(e^{ika} \mp e^{-ika}) = -\gamma Ae^{ika}\,, \tag{3.7}$$

$$Ae^{ika} - C(e^{ika} \pm e^{-ika}) = 0\,, \tag{3.8}$$

Expressing the ratio A/C from Eqs. (3.5) and (3.6) and combining the results obtain

$$\frac{A}{C} = \frac{ik(e^{ika} \mp e^{-ika})}{(ik+\gamma)e^{ika}} = \frac{e^{ika} \pm e^{-ika}}{e^{ika}}\,, \tag{3.9}$$

After rearrangement this leads to a transcendental secular equation,

$$1 + \frac{2ik}{\gamma} = \mp e^{2ika}\,, \tag{3.10}$$

determining all the RS eigenvalues k_n. Note that the upper (lower) sign corresponds to even (odd) RSs.

3.1.2 Bound and anti-bound states

To find bound and anti-bound states of the system, we make a substitution $k = i\varkappa$ in Eq. (3.10) and solve the latter for real values of $\varkappa$. Then the eigen energy $E = -\varkappa^2$ takes real negative numbers. For bound states, $\varkappa$ should be positive, as required by evanescent wave function outside the system. For anti-bound states instead the wave function has a pure exponential growth to the exterior which is provided by $\varkappa < 0$.

While the secular equation Eq. (3.10) apparently depends on two parameters, γ and a, this parametric space reduces to a single parameter

$$\alpha = \gamma a \tag{3.11}$$

which can be treated as the effective system size or the effective strengths of the potential. Concentrating on the dependence of

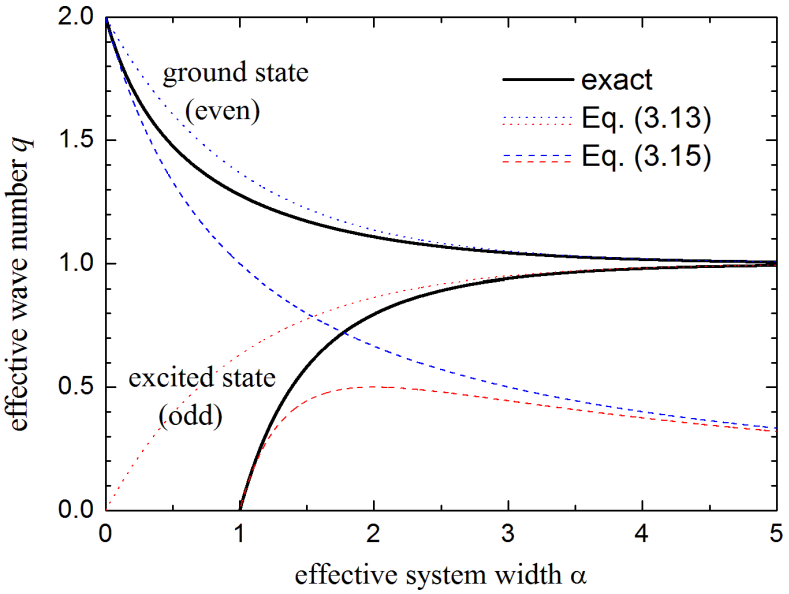

Figure 3.2: Exact (black solid lines) and approximate (blue and red dashed and dotted lines) effective wave numbers $q = -2ik/\gamma$ of the two bound states in a double quantum well system modeled by a double delta function potential, as functions of the effective system width $\alpha = \gamma a$.

the eigen states on the system size, it is convenient to introduce a dimensionless wave number $q = 2\varkappa/\gamma$. Then Eq. (3.10) takes the form

$$q_{\pm} = 1 \pm e^{-q_{\pm}\alpha}\,, \tag{3.12}$$

where we introduce an index $+$ $(-)$ labeling even (odd) parity states. The full solution of Eq. (3.12) found numerically with the help of the Newton-Raphson method implemented in MATLAB is shown in Fig. 3.2 for positive values of α and q. It demonstrates the dependence of the imaginary wave vector for two bound (even and odd) states in the system as function of its effective width α.

At large distances between the wells ($\alpha \gg 1$) the two states

are quasi-degenerate,

$$q_{\pm} \approx 1 \pm e^{-\alpha}\,, \tag{3.13}$$

illustrating the fact that each isolated delta-like quantum well accommodates only one bound state at $q = 1$. As clear from Fig. 3.2, Eq. (3.13) is a good approximation of the full solution Eq. (3.12) for $\alpha \gtrsim 3$. As α increases, the splitting between the levels becomes exponentially small, reflecting the vanishing tunnel coupling between the wells.

In the opposite limit of small width a or small wave number $\varkappa$ (i.e. small binding energy), we obtain a simple analytic approximation, based on the Taylor expansion of the exponential in Eq. (3.12),

$$e^{-q\alpha} \approx 1 - q\alpha + q^2\alpha^2/2\,, \tag{3.14}$$

valid for $|q\alpha| = |\varkappa a| \ll 1$. For the even parity state, it is sufficient to use the expansion Eq. (3.14) up to 1st order, while the same level of approximation for the odd parity state requires the 2nd order to be taken into account. Then approximate solutions of Eq. (3.12) take the form:

$$q_{+} \approx \frac{2}{\alpha+1}\ \text{(even)}, \quad q_{-} \approx 2\frac{\alpha-1}{\alpha^2}\ \text{(odd)}. \tag{3.15}$$

They are shown in Fig. 3.2 by dashed lines matching the exact solution (solid lines) at small α (for the even state) or at small q (for the odd state).

The analytic approximation Eq. (3.15) also allows us to find

a condition for bound states to exist in the system [3], which requires that $q > 0$. Indeed, when a bound state disappears from the spectrum, its binding energy vanishes, meaning that $q \to 0$. This makes the approximation Eq. (3.15) valid, so that it precisely determines the critical values of the system parameters when the bound state disappears. While the ground state exists for any $\alpha > 0$ (q_+ is always positive), the excited (odd) bound state exists for only

$$\alpha > 1 \tag{3.16}$$

and disappears at $\alpha = 1$ (when q_- is vanishing), as the width of the system becomes insufficient to accommodate it, given the tunnel coupling between the wells. However, a quantum state itself cannot disappear from the system completely and is transformed into an anti-bound state which can be observed for $\alpha < 1$.

To see it more clearly and also to investigate the dependence on the potential strength (e.g. keeping the width $2a$ fixed), we introduce another dimensionless imaginary wave number $s = 2\varkappa a$, so that Eq. (3.10) becomes

$$\alpha = \frac{s}{1 \pm e^{-s}} \tag{3.17}$$

and can be easily plotted due to the explicit functional dependence on s, see Fig. 3.3. Since $a > 0$, the region of positive s corresponds to bound states. We see two bound states for $\alpha > 1$ and only one for $0 < \alpha < 1$. The odd state transforms at $\alpha = 1$ from the bound

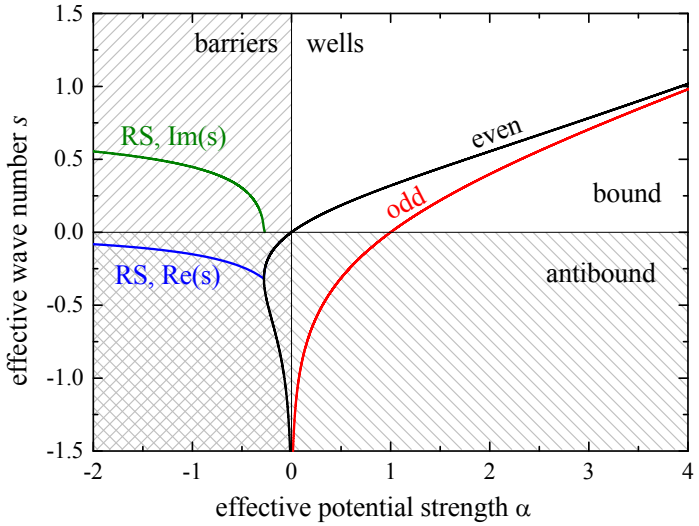

Figure 3.3: Effective wave number $s = -2ika$ as function of the effective potential strength $\alpha = \gamma a$ plotted for even and odd eigen states using the explicit functional dependence Eq. (3.17). The plot demonstrates transitions from bound to anti-bound states and then to normal RSs. Regions for potential wells ($\alpha > 0$) and barriers ($\alpha < 0$) are indicated, as well as for bound ($s > 0$) and anti-bound ($s < 0$) states. Blue and green lines show the real and imaginary parts of the wave numbers s for the pair of the lowest energy normal RSs formed from a pair of degenerate anti-bound states at $\alpha \approx -0.27$.

into an anti-bound state, as negative s corresponds to growing exponentials outside the systems, see Eq. (3.4) for $k = is/2a$ and $s < 0$. Another anti-bound state forms from the even bound state at $\alpha = 0$ when the wells switch into barriers. At the same time, as α changes its sign from positive to negative, the odd anti-bound state goes away to infinity as $s \to -\infty$ and then comes back at small negative values of α as an even anti-bound state, coexisting with the other even anti-bound state up to $\alpha \approx -0.27$. At that point the two anti-bound states merge, now transforming into a pair of normal RSs, which then evolve as α decreases further. Both RSs have the same imaginary part and the opposite real part of

k, shown in Fig. 3.3 by blue and greens lines, respectively.

3.1.3 Resonant states

We now consider all possible solutions of Eq. (3.10) in the complex k-plane, generating bound, anti-bound and normal RSs, as shown in Fig. 3.4 for the case of a double well and a double barrier structure. For the wells ($\gamma a = 3$), one can see two bound states and an infinite countable number of normal RSs with nonzero real and imaginary parts of k. These normal RSs all have complex wave functions which cannot be made real by redefining the normalization constant, unlike bound or anti-bound states. These RSs appear in pairs: Each RS with the eigen wave number k and the eigen function ψ has a counterpart with the eigen wave number $-k^*$ and the eigen function ψ^*, so that the spectra of RSs shown in Fig. 3.4 possess a mirror symmetry about the imaginary axis, which is a general property of an open system, not related to its spatial symmetry. For the barriers ($\gamma a = -3$), there are only normal RSs seen in the spectrum, as this potential strength is too big for anti-bound states to exist, see Fig. 3.3. In both spectra, normal RSs of even and odd parity appear in alternating order and are almost equally spaced for large k dominated by the real part. The reason for that is that these states have the same nature as Fabry-Pérot modes in an optical system, with a half integer multiple of their De-Broglie wavelength $\lambda = 2\pi/k$ approximately matching the system size $2a$ Indeed, the spacing between the wave numbers

plotted in Fig. 3.4 is $\delta k \approx \pi/2a$. These RSs are formed owing to the constructive interference of waves created by multiple reflection from the potential inhomogeneities at $x = \pm a$. The absolute value of the imaginary part of k grows monotonically with the real part of k (and consequently with the resonance energy), showing an increasing probability of a particle to leave the system as its energy increases.

Interestingly, at large k the even RS wave numbers of the double well structure approach asymptotically the odd RS wave numbers of the double barrier structure, and vice versa, provided that the absolute values of $|\gamma a|$ are the same for the barriers and wells. This can be understood, looking again at Eq. (3.10) and noticing that if the first term was neglected, Eq. (3.10) would become invariant with respect to a simultaneous flip of the sign of γ (switching between barriers and wells) and the sign standing at the exponential (switching between even and odd solutions), thus making the above two cases equivalent. Indeed, this equivalence is asymptotically achieved at large k, when the first term in Eq. (3.10) is getting small compared to the other two and can be neglected.

Applying the normalization condition Eq. (1.19) to the wave function Eq. (3.4) and excluding exponentials with the help of the secular equation Eq. (3.10), we find the normalization constants in

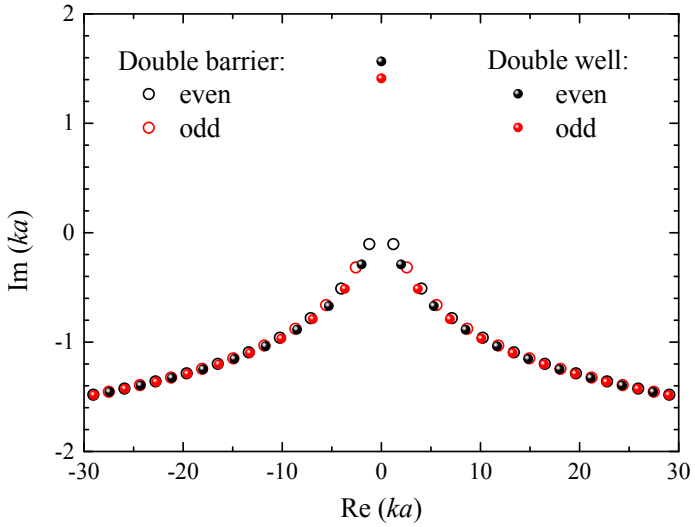

Figure 3.4: Complex eigen wave numbers k_n of RSs in a double delta-potential structure, with two wells ($\gamma a = 3$, shiny balls) and two barrier ($\gamma a = -3$, open circles). Even and odd parity states are shown, respectively, in black and red.

Eq. (3.4), for derivation, see Appendix (H)

$$A = C\left(1 + \frac{\gamma}{2ik}\right)^{-1} \text{ and } C = \frac{1}{2\sqrt{\pm[a - (\gamma + 2ik)^{-1}]}}\,. \qquad (3.18)$$

The normalized wave functions of a double well or a double barrier system are now ready to use in the RSE in Chap. 4 which can be applied for various perturbations.

3.2 RSs in a triple well/barrier structures

We now add a third well (barrier) positioned at $x = b$, somewhere between the two equal wells (barriers): $-a < b < a$.

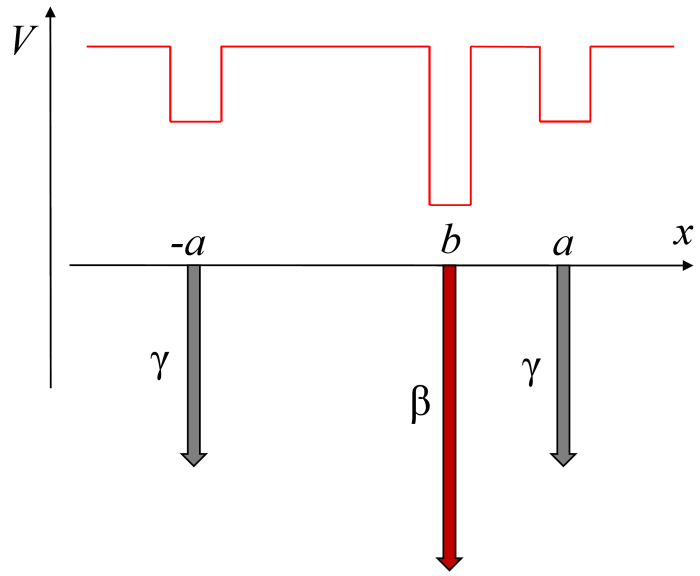

Figure 3.5: As Fig. 3.1 but for a triple delta-function potential.

It is modeled in the same way, so that the potential is given by

$$V(x) = -\gamma\delta(x-a) - \gamma\delta(x+a) - \beta\delta(x-b)\,, \tag{3.19}$$

where the strength β is in general different from that of two other wells, with $\beta > 0$ ($\beta < 0$) corresponding to an additional well (barrier). A sketch of this potential and its relation to a more realistic semiconductor heterostructure is provided in Fig. 3.5.

We use the same approach as in Sec. 3.1 to solve Eq. (1.16) with the potential Eq. (3.19), taking the wave function of a RS in the following form:

$$\psi(x) = \begin{cases} Ae^{ikx} & x > a, \\ C_1 e^{ikx} + C_2 e^{-ikx} & b \leqslant x \leqslant a, \\ D_1 e^{ikx} + D_2 e^{-ikx} & -a \leqslant x < b, \\ Be^{-ikx} & x < -a. \end{cases} \tag{3.20}$$

3.2.1 Exact solution for a symmetric structure

We first consider the case of a symmetric potential, having $b = 0$ and arbitrary β. Then using Eq. (3.3), we find $B = \pm A$ for the solution outside the system and

$$C_1 e^{ikx} + C_2 e^{-ikx} = D_1 e^{ikx} + D_2 e^{-ikx} \tag{3.21}$$

for the region inside. Equating coefficients at the same exponentials in Eq. (3.21), obtain $D_2 = \pm C_1 = \pm C$ and $C_2 = \pm D_1 = \pm D$, where we have introduced constants C and D for brevity of notations. Then the wave function takes a simplified form:

$$\psi(x) = \begin{cases} Ae^{ikx} & x > a, \\ Ce^{ikx} \pm De^{-ikx} & 0 \leqslant x \leqslant a, \\ De^{ikx} \pm Ce^{-ikx} & -a \leqslant x < 0, \\ \pm Ae^{-ikx} & x < -a. \end{cases} \tag{3.22}$$

The existence of the third delta-function in the potential Eq. (3.19) has lead to a new break point in the wave function, which is at $x = 0$, and to two more BCs:

$$\psi'(\varepsilon) - \psi'(-\varepsilon) = -\beta\psi(0)\,, \tag{3.23}$$

$$\psi(+\varepsilon) - \psi(-\varepsilon) = 0\,, \tag{3.24}$$

in addition to the pair of BCs given by Eqs. (3.5) and (3.6). Using Eq. (3.24) for an odd parity state [the lower sign in Eq. (3.22)] results in a condition $C = D$ meaning that $\psi(0) = 0$, as should be for any anti-symmetric state. This makes however the odd state insensitive to the potential well or barrier if the latter is placed exactly in the center, thus keeping $\psi'(x)$ continuous at $x = 0$. The odd parity solution of the Schrödinger equation with the potential Eq. (3.19) and $b = 0$ is thus the same as for the double delta potential Eq. (3.1) and is described in detail in Sec. 3.1. We therefore concentrate below on even parity states.

For even parity states Eq. (3.24) is automatically fulfilled due to Eq. (3.3), but Eq. (3.23) brings in a unique information about the middle well/barrier: $2ik(C - D) = -\beta(C + D)$, or

$$\sigma = \frac{D}{C} = -\frac{1 + 2ik/\beta}{1 - 2ik/\beta}\,. \tag{3.25}$$

At the same time, Eqs. (3.5) and (3.6) now give

$$ikAe^{ika} - ik(Ce^{ika} - De^{-ika}) = -\gamma Ae^{ika}\,, \tag{3.26}$$

$$Ae^{ika} - (Ce^{ika} + De^{-ika}) = 0\,, \tag{3.27}$$

which result, after they are combined with Eq. (3.25), in two different expressions for the ratio A/C,

$$\frac{A}{C} = \frac{ik(e^{ika} - \sigma e^{-ika})}{(ik + \gamma)e^{ika}} = \frac{e^{ika} + \sigma e^{-ika}}{e^{ika}}\,, \tag{3.28}$$

determining a secular transcendental equation for even parity states:

$$1 + \frac{2ik}{\gamma} = \frac{1 - 2ik/\beta}{1 + 2ik/\beta} e^{2ika} \,. \tag{3.29}$$

In the limit $\beta \to 0$, Eq. (3.29) transforms into the double-well secular equation (3.10) for even parity.

3.2.2 Bound and anti-bound states

Repeating the procedure used in Sec. 3.1.2, we first introduce a purely imaginary wave number $k = i\varkappa$, expressed in terms of a real valued $\varkappa$ and then use an effective dimensionless wave number $q = 2\varkappa/\gamma$, in order to study the dependence of the bound state on the system size. In addition to the effective width/strength α defined by Eq. (3.11), we introduce a relative strength of the middle well/barrier:

$$\varepsilon = \frac{\beta}{\gamma} \,. \tag{3.30}$$

Equation (3.29) then takes the form

$$q = 1 + \frac{q + \varepsilon}{q - \varepsilon} e^{-q\alpha} \tag{3.31}$$

[compare with Eq. (3.12) for +]. The exact numerical solution of Eq. (3.31) for $\varepsilon = 0.5$ is shown in Fig. 3.6 by black solid lines displaying two even parity bound states, as well as the odd parity state which is the same as in Fig. 3.2. While the ground state

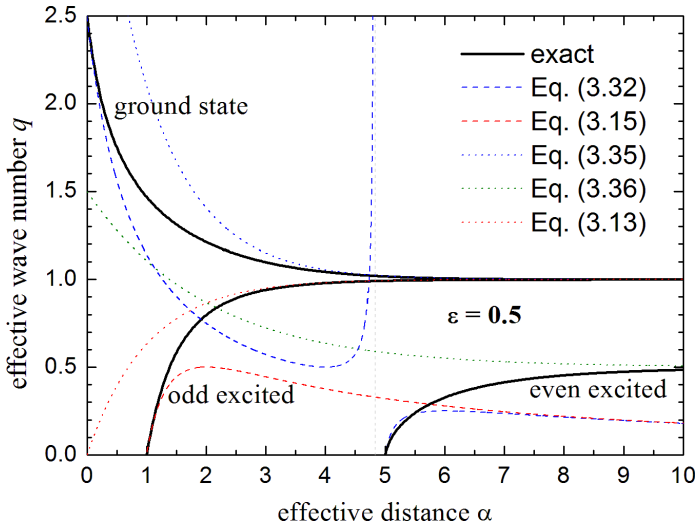

Figure 3.6: As Fig. 3.2 but for a triple-delta potential with $b = 0$ and $\varepsilon = 1/2$.

having the highest value of q exists for any size of the system (i.e. for all $\alpha > 0$), the 2nd excited (even) state disappears in this case at $\alpha = 5$.

To understand this behavior, we again use the Taylor expansion Eq. (3.14) up to 2nd order, obtaining from Eq. (3.31) an approximation for even states:

$$q \approx \frac{2 - \varepsilon(\alpha - 1)}{1 + \alpha(1 - \alpha\varepsilon/2)} \,. \tag{3.32}$$

Obviously, for $\varepsilon = 0$, Eq. (3.32) is equivalent to the approximation Eq. (3.15) for the even parity values q_+. The approximation Eq. (3.32) is shown for $\varepsilon = 0.5$ in Fig. 3.6 by dashed blue lines, demonstrating a good agreement with the full solution for $\alpha \to 0$ (ground state) and for $q \to 0$ (2nd excited states). The latter limit allows us to obtain the following inequality for ε and α, showing

under which conditions an even bound state exists:

$$\alpha > 1 + \frac{2}{\varepsilon}\,. \tag{3.33}$$

When both $\gamma > 0$ and $\beta > 0$, this inequality refers to the 2nd excited state in a triple well. In particular, for the example in Fig. 3.6, the even excited state disappears at $\alpha = 1 + 2/\varepsilon = 5$.

If, however, there is a barrier in the middle of two wells, i.e. $\gamma > 0$ but $\beta < 0$, there is a maximum of two bound states in the spectrum, one even (the ground state) and one odd (the excited state), and the same Eq. (3.33) now becomes a condition for the ground state to exist. Indeed, if the barrier is high enough, namely if $\beta < -2\gamma$, the ground state also disappears from the spectrum at the system size smaller than that determined by Eq. (3.33). This case presents an interesting situation when a one-dimensional symmetric potential well structure cannot accommodate any bound states. An illustration for $\varepsilon = -4$ is provided in Fig. 3.7 showing that the ground state disappears at $\alpha = 1/2$, in agreement with Fig. 3.9 below.

To analyze the behavior at a large system size, we take the limit $\alpha \to \infty$, which makes the exponential term in Eq. (3.31) small. This results in a quadratic equation for q:

$$q^2 - q(1 + \varepsilon + e^{-q\alpha}) + \varepsilon(1 - e^{-q\alpha}) = 0 \tag{3.34}$$

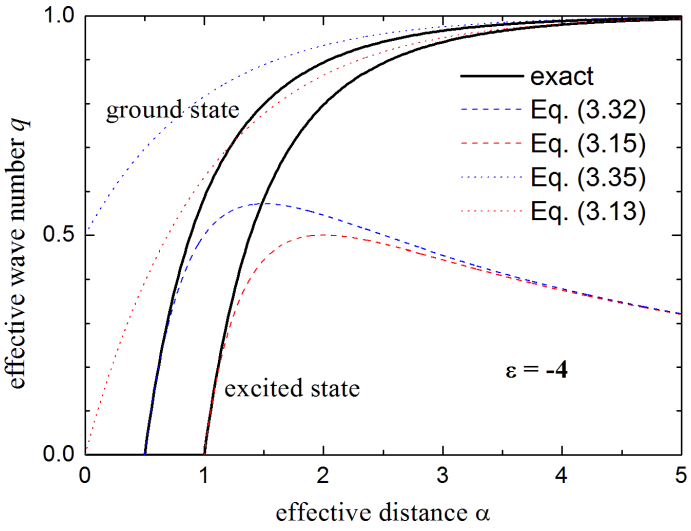

Figure 3.7: As Fig. 3.6 but for $\varepsilon = -4$.

giving solutions

$$q_0 \approx 1 + \frac{1+\varepsilon}{1-\varepsilon} e^{-\alpha} \tag{3.35}$$

for the ground and

$$q_2 \approx \varepsilon + \frac{\varepsilon}{1-\varepsilon} e^{-\varepsilon\alpha} \tag{3.36}$$

for the 2nd excited state. These approximate values are also plotted in Figs. 3.6 and 3.7 showing a good agreement with the full solution.

To study the dependence on the quantum well strength γ (i.e. α for a fixed a), we introduce, as in Sec. 3.1.2, the effective wave number $s = 2\varkappa a$. Then Eq. (3.29) becomes

$$\frac{s}{\alpha} = 1 + \frac{s/\alpha + \varepsilon}{s/\alpha - \varepsilon} e^{-s} \tag{3.37}$$

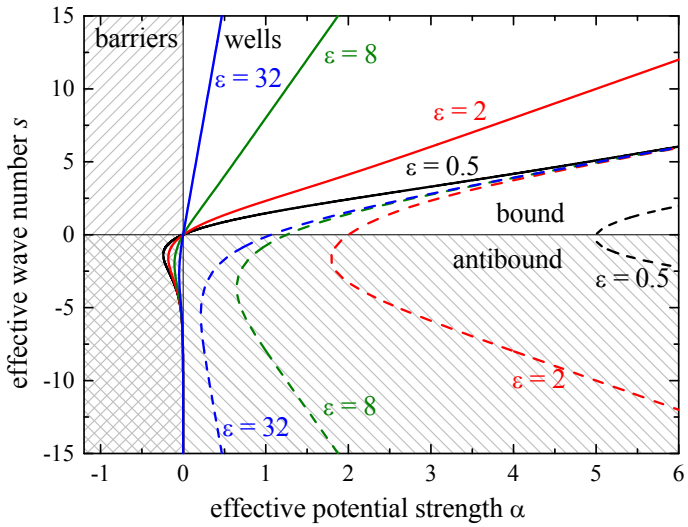

Figure 3.8: As Fig. 3.3 but for a triple delta potential with $b = 0$ and different ε as labeled. All the curves are obtained by plotting the inverse of the function Eq. (3.38). Note that only even parity solutions are displayed, with an excited state branch shown by a dashed curve for each ε.

which has an explicit solution for $\alpha(s)$:

$$\alpha = \frac{2s}{1+\varepsilon+e^{-s} \pm \sqrt{(1-\varepsilon)^2+2(1+3\varepsilon)e^{-s}+e^{-2s}}}\,, \qquad (3.38)$$

[compare with Eq. (3.17)]. Again, the advantage of representing the solution in the form of Eq. (3.38) is that it can be displayed without solving the secular equation. The plots of it are presented in Fig. 3.8, showing the evolution of bound and anti-bound states with the effective potential strength α. We see that as α decreases the bound states transform into anti-bound states and then to normal RSs (not shown in Fig. 3.8), as in the case of a double barrier, see Fig. 3.3.

Finally, by fixing α (i.e. the product of the potential strength γ and the width a) the dependence $q(\varepsilon)$ or $s(\varepsilon)$ on the relative

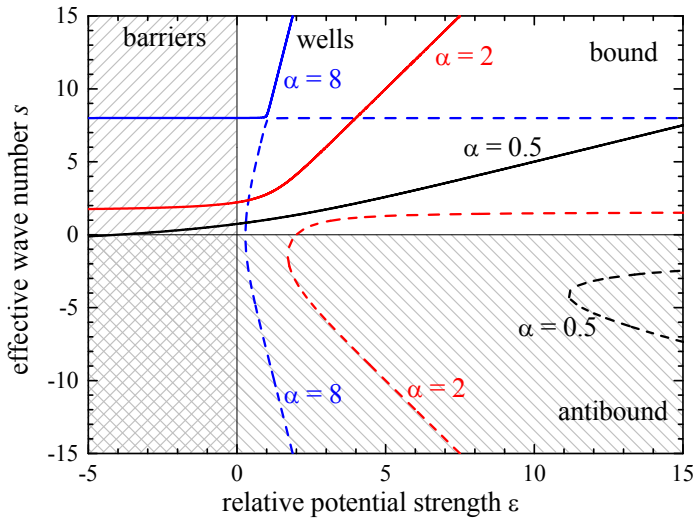

Figure 3.9: As Fig. 3.8 but for the relative potential strength dependence given by Eq. (3.39), for different values of α as labeled.

potential strength ε, given by Eq. (3.30), can be extracted. Expressing ε from Eq. (3.31) obtain

$$\varepsilon = q\,\frac{1-q+e^{-q\alpha}}{1-q-e^{-q\alpha}} = \frac{s}{\alpha}\,\frac{1-s/\alpha+e^{-s}}{1-s/\alpha-e^{-s}}\,. \tag{3.39}$$

Taking the inverse of this function, we find the dependence $s(\varepsilon)$ [or $q(\varepsilon)$] which is displayed in Fig. 3.9, showing the evolution of states with the potential ratio ε continuously changing between positive and negative values, thus covering also an important case of mixed potentials (with a barrier in the middle). Interestingly the two even states displayed show a sort of avoided crossing which is getting sharper with increased potential strength/width α, i.e. the separation between the two states decreases with α owing to a smaller tunnel coupling between the wells.

3.2.3 Solutions for an asymmetric case

Let us now consider a more general case of an arbitrary position of the middle well/barrier at $x = b$, with $-a < b < a$. To find the secular equation for RSs and relations between 6 amplitudes in the wave function Eq. (3.20), one needs to satisfy 3 pairs of BCs, describing the continuity of the wave function and discontinuity of its first derivative at $x = -a$, b and a. We skip all the details of derivation which can be made in a way similar to those outlined in Secs.3.1.2 and 3.2.2. We present a resulting secular equation for k, which can be written compactly as

$$\xi^2(1-\eta) - 2\xi\cos(2kb) + 1 + \eta = 0\,, \tag{3.40}$$

after introducing

$$\xi = \frac{e^{2ika}}{1 + 2ik/\gamma} \quad \text{and} \quad \eta = \frac{2ik}{\beta}\,. \tag{3.41}$$

For derivation, see App.(J).

We again first study the dependence of the full solution of Eq. (3.40) for bound states on the potential strength γ, for fixed a, b and β. Introducing $\alpha = \gamma a$ and $s = -2ika$, as before, and solving the quadratic equation (3.40) for ξ, obtain two branches of the solution:

$$\alpha_\pm(s) = \frac{s}{1 - e^{-s}/\xi_\pm(s)}\,, \tag{3.42}$$

where

$$\xi_{\pm}(s) = \frac{c \pm \sqrt{c^2 + \eta^2 - 1}}{1 - \eta}\,, \tag{3.43}$$

$$c(s) = \cosh(sb/a) \quad \text{and} \quad \eta(s) = -\frac{s}{\beta a}\,. \tag{3.44}$$

It is instructive to see that for $b = 0$, the two branches become

$$\xi_{-} = 1 \quad \text{and} \quad \xi_{+} = \frac{1 + \eta}{1 - \eta} \tag{3.45}$$

corresponding to the odd and even parity states and coinciding which the solution for a symmetric triple structure given by Eq. (3.10) with the lower sign used and by Eq. (3.29), respectively. Taking further the limit $\eta \to \infty$ (corresponding to $\beta \to 0$), obtain solutions for a double well structure: $\xi_{\mp} = \pm 1$ which, after substitution into Eq. (3.43), give exactly Eq. (3.17).

Finally, expressing η from Eq. (3.40), we find an explicit dependence of the wave numbers k on the middle well/barrier strength β:

$$\beta a = s\,\frac{1 - 2\xi c + \xi^2}{1 - \xi^2}\,, \tag{3.46}$$

where $\xi = e^{-s}/(1 - s/\alpha)$, in accordance with Eq. (3.41). The function $k(\beta)$ can be obtained by simply inverting the function $\beta(k)$ given by Eq. (3.46). Taking $c = 1$ Eq. (3.46) reduces to

$$\beta a = s\,\frac{1 + \xi}{1 - \xi} \tag{3.47}$$

for a symmetric structure ($b = 0$), which is exactly the same as Eq. (3.39).

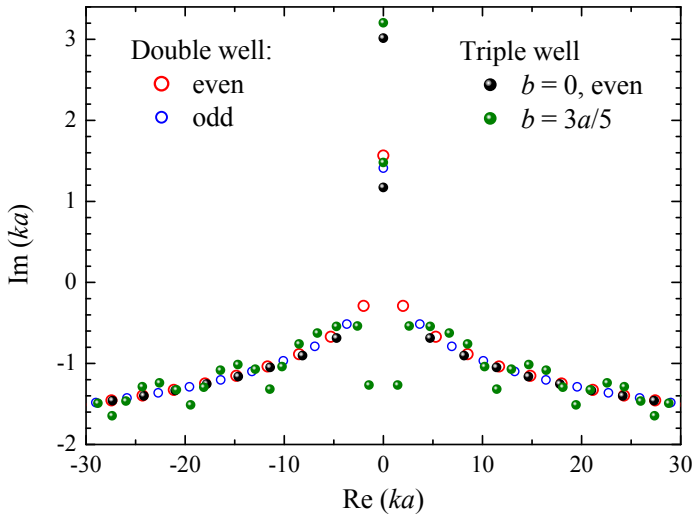

Figure 3.10: As Fig. 3.4, for double ($\gamma = 3/a$), triple symmetric ($b = 0$, $\gamma = 3/a$, $\beta = 6/a$) and triple asymmetric ($b = 3a/5$, $\gamma = 3/a$, $\beta = 6/a$) quantum well structures.

3.2.4 Resonant states

RSs for both symmetric and asymmetric triple well structures are shown in Fig. 3.10. The spectrum of RSs for the symmetric structure is quite similar to that of the double well which is also shown for comparison (the same as demonstrated in Fig. 3.4). Note that odd RSs remain the same for both systems. For the triple well, we now see two bound states, in accordance with our analysis in Sec. 3.2.2. Indeed, for $\alpha = 3$ and $\varepsilon = 2$ the inequality Eq. (3.33) is fulfilled allowing the second excited state to exist.

The spectrum of RSs for an asymmetric triple well structure with $b = 3a/5$, $\gamma = 3/a$ and $\beta = 6/a$ is quite different. First of all, the middle well is 3 times deeper than for the symmetric structure. Being shifted from the center of the structure, the middle

quantum well mixes even and odd RSs. As a result, stronger deviations from the double well spectrum of RSs is seen. Choosing the ratio $2a/(a-b)$ equal to an integer, as in the present case, the third well in the middle splits the structure into two resonators having commensurable widths (in our case $a_L = 8a/5$ and $a_R = 2a/5$, respectively, splitting the width in 4:1 proportion). Therefore resonances accommodated in the right (narrower) subsystem can be enhanced by the left (wider) subsystem. As a result, one can see a quasi-periodic modulation in the spectrum with the period of about $2\pi/a_R$, which is five times larger than the separation between the RS wave numbers, which is approximately π/a.

3.3 Role of the resonant states in the transmission

In this section, we study the role of RSs in observables, such as the local density of states or the scattering matrix. Below we consider, as an example, the transmission of a particle through a quantum system consisting of two Dirac delta wells. A particle traveling in free space is described by a wave function in the form of plane wave with a wave number k. We first calculate analytically its transmission amplitude $t_a(k)$ as a function of the *real* wave number k of the particle. This transmission can be found by choosing appropriate BCs outside the system, namely by allowing the system to be excited with an incoming wave. To do so, we keep in Eq. (3.2) the term with an incoming wave which now has a

non-vanishing amplitude $D \neq 0$, while requiring that $B = 0$. The BCs at $x = \pm a$, given by Eqs. (3.5) and (3.6), are the same as for the RSs. Applying them and solving a set of algebraic equations, we find the transmission amplitude

$$t_a(k) = \frac{A}{D} = \frac{4k^2}{4k(k - i\gamma) - \gamma^2(1 - e^{4ika})}\,, \tag{3.48}$$

$$\tilde{t}_a(k) = t_a(k)e^{ika}. \tag{3.49}$$

For detail derivation of Eq. (3.48), see App.(K). Now taking the analytic continuation of this function into the complex k plane, it is easy to see that $\tilde{t}_a(k)$ has simple poles at $k = k_n$, where k_n are the wave numbers of all possible RSs (including bound, anti-bound and normal RSs), which satisfy the secular Eq. (3.10). Also, the function Eq. (3.48) is vanishing on an infinitely large circle in the complex k plane, and therefore, one can apply to it the Mittag-Leffler (ML) theorem [1, 10, 14], writing the transmission function in the form of an infinite series over all poles:

$$t(k) = e^{-ika} \sum_n \frac{\tilde{R}_n}{k - k_n}\,, \tag{3.50}$$

Here $\tilde{R}_n$ are the residues of the analytic function $\tilde{t}_a(k)$ at its poles, which are given by

$$\tilde{R}_n = \frac{k_n^2 e^{ik_n a}}{2k_n - i\gamma + ia\gamma^2 e^{4ik_n a}}\,. \tag{3.51}$$

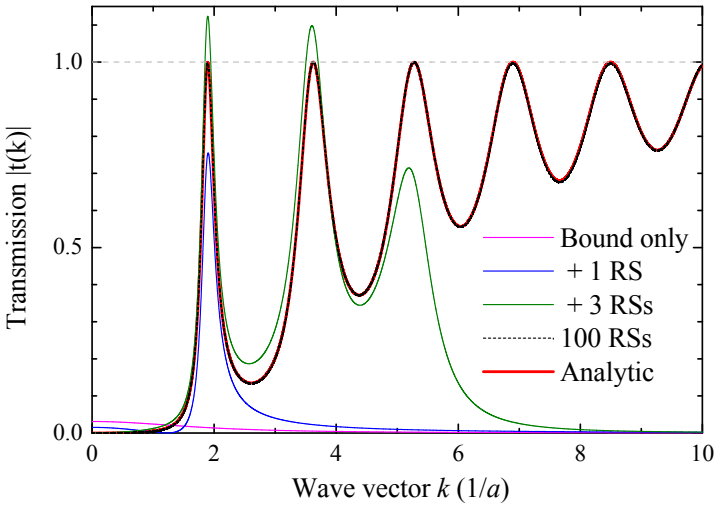

Figure 3.11: The amplitude of the analytic transmission $|t_a(k)|$ (thick red curve) trough a double Dirac delta well structure with $\gamma = 3/a$ and its spectral representation $t(k)$ calculated for different number of RSs taken into account in the Mittag-Leffler expansion: bound states only (magenta), bound states and 1 pair of RSs (dark blue), bound states and 3 pairs of RSs (dark green), and 100 RSs in total including all bound and anti-bound states (black dashed curve).

Using the ML expansion Eq. (3.50) we study in Fig. 3.11 the role of different RSs in the transmission.

For an *arbitrary* one-dimensional potential with compact support, i.e. vanishing (or constant) outside the system area $|x| \leqslant a$, the transmission amplitude is given by

$$t(k) = 2ike^{-2ika}G_k(a,-a)\,, \tag{3.52}$$

see e.g. [11]. Here, $G_k(x,x')$ is the Green's function of the Schrödinger equation (1.16) for a given fixed wave number k. For the coordinates x and x' within the system, the Green's function is also vanishing on an infinitely large circle in the complex k plane, and

therefore, one can apply to it the Mittag-Leffler (ML) theorem of the form [1, 10, 14]

$$G_k(x, x') = \sum_n \frac{\psi_n(x)\psi_n(x')}{2k_n(k - k_n)}\,, \tag{3.53}$$

where $\psi_n(x)$ are the RS wave functions normalized according to Eq. (1.19).

For illustration, we apply the general result given by Eqs. (3.52) and (3.53) to the particular case of the double delta-function potential Eq. (3.1). Using the explicit form of the wave functions Eq. (3.4), their normalization Eq. (4.11), and the secular equation (3.10), one can write the transmission, with the help of Eqs. (3.52) and (3.53), in the form of an infinite series over its poles:

$$t(k) = ke^{-2ika} \sum_n \frac{R_n}{k - k_n}\,, \tag{3.54}$$

where

$$R_n = \pm \frac{ik_n a^2}{\gamma[(\gamma + 2ik_n)a - 1]}\,. \tag{3.55}$$

The results of Eq. (3.50) and Eq. (3.54) can be compared with the analytic transmission $\tilde{t}_a(k)$, given by Eq. (3.49), which is done in Fig. 3.11 and Fig. 3.12. Using the ML expansion Eqs. (3.50) and (3.54), we also study in Fig. 3.11 and Fig. 3.12 the role of different RSs in the transmission. We first note that in these representations, bound states play a small but non-negligible role, producing some background contribution. The maxima of the transmission reaching the value of 1 for this symmetric quantum structure

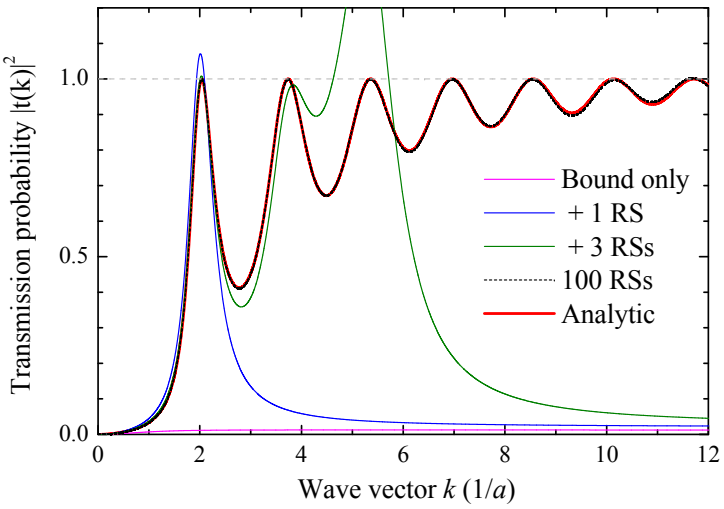

Figure 3.12: The probability of transmission trough a double Dirac delta well structure with $\gamma = 3/a$, evaluated using the analytic transmission $\tilde{t}_a(k)$ (thick red curve) and its spectral representation $t(k)$ calculated for different number of RSs taken into account in the Mittag-Leffler expansion: bound states only (magenta), bound states and 1 pair of RSs (dark blue), bound states and 3 pairs of RSs (dark green), and 100 RSs in total, including the bound states (black dashed curve).

can be described by only taking into account in the summations Eq. (3.50) and Eq. (3.54) the corresponding normal RSs. Adding the very first pair of normal RSs already describes quite well the first peak in the transmission. The agreement is further improved by adding more RSs. With three pairs of RSs, the first peak of the transmission is fully reproduced, but the other two are described only qualitatively. To correct this and to describe other peaks, more RSs in Eq. (3.50) and Eq. (3.54) are needed. Taking all of them into account, the correct transmission is fully reproduced.

3.4 Summary

In this chapter, we have studied the full set of resonant states of a one-dimensional Schrödinger problem with double and

triple quantum wells or barriers approximated by Dirac delta functions. This includes bound, anti-bound and normal resonant states which are all eigensolutions of Schrödinger's equation with generalised outgoing wave boundary conditions. We have analysed the transformation of resonant states and their transitions between different subgroups as well as the role of each subgroup in observables, such as the quantum transmission. As part of this study we have revisited the well known problem of bound states in the quantum well potentials modeled by Dirac delta functions. We have finally shown and demonstrated that the normal resonant states determine the main spectral features in quantum transmission, and taking the full set of resonant states, allows one to precisely determine the transmission via its Mittag-Leffler expansion.

Chapter 4

Resonant state expansion in quantum mechanics

In this chapter, we outline the formalism of the QM-RSE which have been developed earlier in [1, 18]. We have chosen as an unperturbed basis for the QM-RSE, solution to a simple 1D Schrödinger equation with a potential described by a double quantum well composed of two delta functions. The QM-RSE is applied to triple quantum wells and verify using the exact solution showing the convergence as the number of basis states increases. The interference effect in triple quantum wells was also studiesd.

4.1 Formalism of the QM-RSE

The QM-RSE treats a perturbation $\Delta V(x)$ of the quantum potential in the time-independent Schrödinger equation,

$$\left[-\frac{\hbar^2}{2m}\frac{d^2}{dx^2} + V(x) + \Delta V(x)\right]\psi_\nu(x) = E_\nu\psi_\nu(x)\,, \qquad (4.1)$$

by using as a basis the RSs for the unperturbed potential $V(x)$ and transforming Eq. (4.1) into a matrix eigenvalue problem. Here, for simplicity, we concentrate on the 1D Schrödinger equation for a particle with mass m. $\psi_\nu(x)$ is the wave function of a perturbed RS of the particle and E_ν is its energy. It is useful to introduce also the RS wave numbers $\varkappa_\nu$ defined as $E_\nu = \hbar^2\varkappa_\nu^2/(2m)$. The corresponding wave functions and the wave numbers of the RSs in the unperturbed potential $V(x)$ are denoted by $\varphi_n(x)$ and k_n, respectively, where index n labels the unperturbed RSs. The QM-RSE is applicable to potentials with compact support and perturbations included in the area occupied by the unperturbed system [1, 13].

Using the Green's function of the Schrödinger equation for the unperturbed quantum potential $V(x)$ and treating the term with perturbation $\Delta V(x)\psi_\nu(x)$ in Eq. (4.1) as an inhomogeneity, one can find a formal solution of Eq. (4.1). Then, applying the Mittag-Leffler expansion to the Green's function, and expanding the perturbed RSs into the unperturbed ones,

$$\psi_\nu(x) = \sum_n C_{n\nu}\sqrt{\frac{\varkappa_\nu}{k_n}}\varphi_n(x)\,, \tag{4.2}$$

the Schrödinger equation (4.1) is converted into a linear complex eigenvalue problem [1, 18]

$$\sum_m H_{nm}C_{m\nu} = \varkappa_\nu C_{n\nu}\,, \tag{4.3}$$

where

$$H_{nm} = k_n \delta_{nm} + \frac{\Delta V_{nm}}{2\sqrt{k_n}\sqrt{k_m}}\,, \tag{4.4}$$

$$\Delta V_{nm} = \int_{-a}^{a} \varphi_n(x) \Delta V(x) \varphi_m(x) dx\,, \tag{4.5}$$

and δ_{nm} is the Kronecher delta. Here we assumed, without loss of generality, that the perturbation is located within the region $|x| \leqslant a$.

The perturbed wave numbers $\varkappa_\nu$ and the expansion coefficients $C_{n\nu}$ can be found by diagonalizing the complex symmetric matrix H_{nm}, consisting of the diagonal matrix of the unperturbed eigen wave numbers k_n and a perturbation matrix ΔV_{nm}. The $\sqrt{k_n}$ factors are introduced in Eqs. (4.2) and (4.4), in order to symmetrize the eigenvalue problem.

The perturbation matrix Eq. (4.5) is determined by the unperturbed wave functions $\varphi_n(x)$ which have to be properly nomalized. As shown in [1, 13, 18], the proper normalization in 1D, leading to the eigenvalue problem Eq. (4.3), has the following form:

$$1 = \int_{-a}^{a} \varphi_n^2(x) dx - \frac{\varphi_n^2(a) + \varphi_n^2(-a)}{2ik_n}\,, \tag{4.6}$$

where we have used the fact that the inhomogeneity of the unperturbed potential is located within the region $|x| \leqslant a$, so that $x = \pm a$ are the boundaries of the unperturbed open quantum system. More detailed discussions of the normalization of the RSs in quantum-mechanical systems can be found in [10, 48–50].

The complete basis of RSs usually contains an infinite countable number of functions. Therefore, the matrix equation (4.3) of the QM-RSE has infinite size and for practical use requires a truncation. This truncation presents the only limitation of the QM-RSE, which is an asymptotically exact method. Moreover, the RSE is capable of treating arbitrarily strong perturbations [1], provided that a sufficient number of RSs is kept in the basis, in order to guarantee the required accuracy of calculation.

4.2 Unperturbed resonant states: Double quantum well

To apply the QM-RSE for particular quantum systems, we need to choose a suited basis of RSs. These are the solutions of the Schrödinger equation with an unperturbed potential $V(x)$ which in principle can be chosen arbitrary, though both $V(x)$ and $\Delta V(x)$ have to be functions with compact support, and the perturbation $\Delta V(x)$ must be non-vanishing only within the area of inhomogeneity of $V(x)$, as already noted. Usually, the optimal choice of the unperturbed potential is such that the Schrödinger equation with $V(x)$ has an analytic solution and at the same time is close to the full potential to be treated, in this way minimizing the effect of the perturbation.

In this work, however, we have chosen as unperturbed, or the basis system the most simple 1D quantum potential containing RSs: a double symmetric quantum well described by two Dirac

delta functions. We fix this choice for all perturbed examples considered below, varying only the parameters of the basis system, where necessary. We also use the convenient units of $\hbar = 1$ and $m = 1/2$ throughout this work.

The unperturbed quantum potential is thus given by

$$V(x) = -\gamma\delta(x-a) - \gamma\delta(x+a)\,, \tag{4.7}$$

which models a symmetric double quantum well (barrier) structure for $\gamma > 0$ ($\gamma < 0$). Here, $\delta(x)$ is the Dirac delta function, $2a$ is the distance between the wells, and γ is the strength of the potential which has the meaning of the depth of each quantum well multiplied by its width, having in mind a comparison of this model with the corresponding rectangular quantum wells. An obvious advantage of the model is its simplicity and explicit analytical solvability. The solution of the unperturbed Schrödinger equation in Chap. 3 is given by

$$\varphi_n(x) = \begin{cases} A_n e^{ik_n x}, & x > a, \\ C_n(e^{ik_n x} \pm e^{-ik_n x}) & |x| \leqslant a, \\ \pm A_n e^{-ik_n x}, & x < -a, \end{cases} \tag{4.8}$$

where the basis RS wave numbers k_n satisfy the secular equation

$$1 + \frac{2ik_n}{\gamma} = \mp e^{2ik_n a}\,, \tag{4.9}$$

with the upper (lower) sign corresponding to even (odd) parity states. Note that Eq. (4.9) generates a complete set of the basis RSs which include bound, anti-bound and normal RSs, as classified and discussed in detail in Chap. 3. They all need to be taken into account in the QM-RSE.

The normalization of RSs was also calculated in Chap. 3, using the definition Eq. (4.6). The result is given by

$$A_n = C_n \left(1 + \frac{\gamma}{2ik_n}\right)^{-1}, \tag{4.10}$$

$$C_n = \frac{1}{2\sqrt{\pm[a - (\gamma + 2ik_n)^{-1}]}}\,. \tag{4.11}$$

4.3 Verification of the QM-RSE: Triple quantum wells

To verify the QM-RSE and to study its convergence, we take another exactly solvable system, having a relatively simple analytic solution: a triple quantum well described by three delta functions. For simplicity, we keep the strength of the left and right wells/barriers (separated by the distance $2a$) the same, while the position and the strength of the middle well/barrier can be any. In this way, our triple well/bar rier system is described by the potential $V(x) + \Delta V(x)$, where $V(x)$ is given by Eq. (4.7) and

$$\Delta V(x) = -\beta\delta(x - b)\,, \tag{4.12}$$

where the position b and the strength β of the middle well/barrier are arbitrary parameters, with $|b| < a$ and $\beta > 0$ corresponding to a well and $\beta < 0$ to a barrier.

4.3.1 Analytic solution

A general analytic solution of the Schrödinger equation with the triple delta potential $V(x) + \Delta V(x)$, where $V(x)$ and $\Delta V(x)$ are given by Eqs. (4.7) and (4.12), respectively, is also provided in Chap. 3. The secular equation for the RS wave numbers $\varkappa$ of this perturbed quantum system is given by

$$\xi^2(1-\eta) - 2\xi\cos(2\varkappa b) + 1 + \eta = 0\,, \tag{4.13}$$

where

$$\xi = \frac{e^{2i\varkappa a}}{1 + 2i\varkappa/\gamma}\,, \qquad \eta = \frac{2i\varkappa}{\beta}\,. \tag{4.14}$$

Both secular equations (4.9) and (4.13), for double and triple quantum wells, are solved numerically to find the exact RSs wave numbers of the unperturbed and perturbed problem, respectively. This is done using the Newton-Raphson method implement in MATLAB. Exact wave numbers of the RSs in double and triple quantum wells are presented in the complex k-plane in Figs. 4.1–4.4 and compared with QM-RSE (see a discussion of this comparison in Sec. 4.3.3 and Sec. 4.3.4 below).

Since a single delta-function potential well always has only one bound state for any strength of the potential ($\gamma > 0$), it is clear

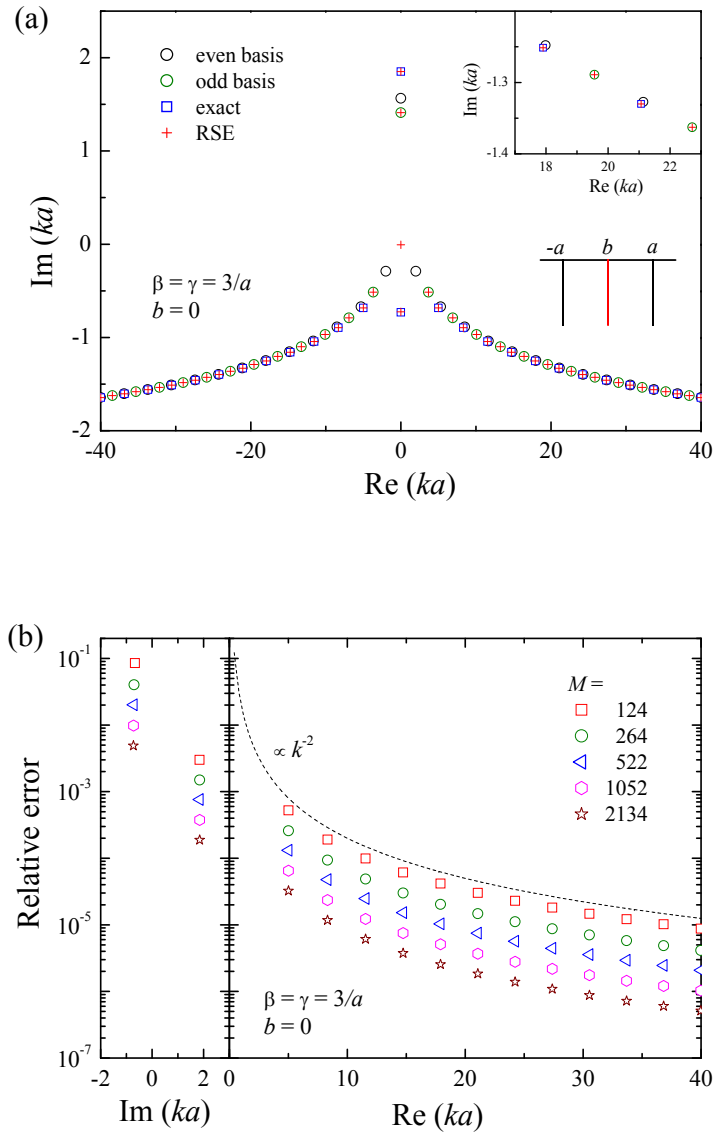

Figure 4.1: (a) Eigen wave numbers of the resonant states for a double symmetric quantum well with $\gamma = 3/a$ (open circles) and a triple symmetric quantum well with $b = 0$ and $\gamma = \beta = 3/a$, calculated using the QM-RSE (red crosses) and the analytic secular equation (4.13) (blue squares). The wave numbers of even (black circles) and odd (green circles) unperturbed RSs for a double quantum well structure are calculated via Eq. (4.9). The insets show a zoom-in of a particular area and a sketch of the perturbed potential (black lines) and the perturbation used (red line). (b) Relative error of the QM-RSE values of the RS wave numbers as function of the real or imaginary part of the wave number, for different basis sizes M as given. The dashed line shows a power law dependence as labeled.

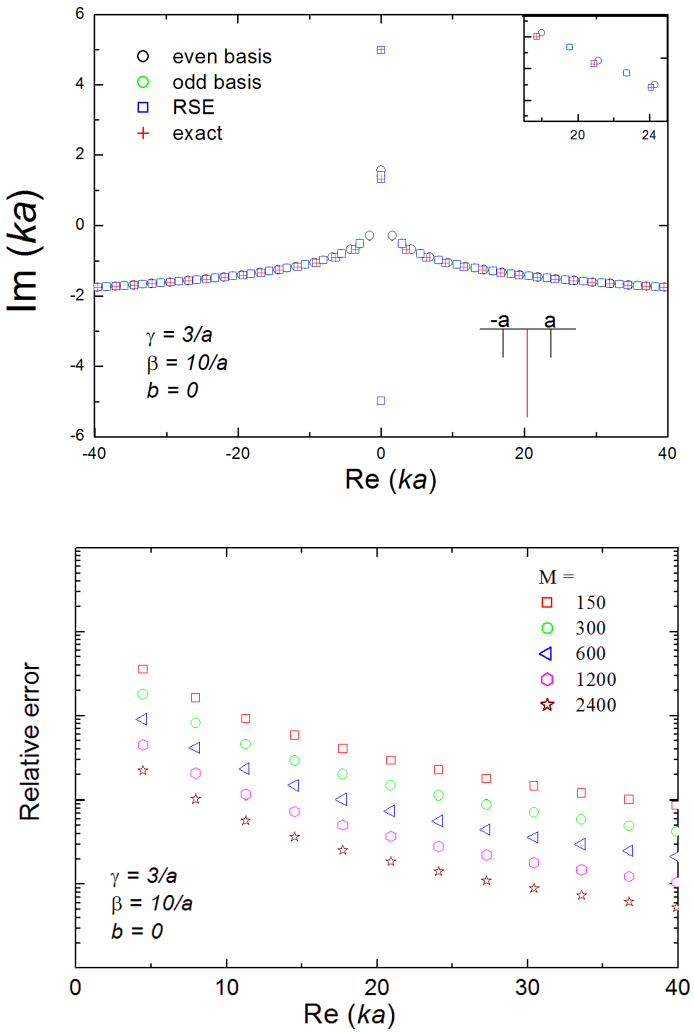

Figure 4.2: As Fig. 4.1 but $\beta = 10/a$

that a double-delta potential can accommodate the maximum of two bound states as shown in Chap. 3. For the parameters used for the double well ($\gamma = 3/a$ and $\gamma = 10/a$), these two bound states are present in the spectrum and are seen in 4.1 (a) and 4.2 (a) respectively, on the imaginary k-axis (black and green circles). All other eigenmodes of the double well system are the normal RSs which always exist in pairs, thus providing the mirror symmetry of the full spectrum of RSs, which is a general property of any open system. As it is clear from Eqs. (4.9) and (4.13), there is an infinite countable number of RSs in the spectrum, which is another general property of an open system. Furthermore, Fig. 4.1 (a) and

4.2 (a) shows that the normal RSs are almost equally spaced when the real part of k_n is much larger than the imaginary part. This quasi-periodicity of the RS wave numbers can be understood as a result of constructive interference of quantum waves propagating back and forth within the system and experiencing multiple reflections from the wells/barriers at the boundaries $x = \pm a$. From this resonant condition for the constructive interference one can estimate the distance between the neighboring RSs in the complex k-plane to be $\sim \pi/(2a)$, which is observed in Fig. 4.1 (a).

The spectrum of RSs for a symmetric triple well structure, also shown in Fig. 4.1 (a) (blue squares), is quite similar to that of the double well. We see from the inset that in spite of a rather strong potential of the middle well perturbing the double well system, the wave numbers of the even parity RSs are only slightly modified, while those of the odd parity states remain unchanged since $\Delta V(0) = 0$. The only significant change observed in the spectrum is that there are two antibound states which appeared on the negative imaginary half axis. These antibound states are formed from the closest to the origin pair of normal RSs of the double well spectrum, as it was discussed in detail in Chap. 3.

At the same time, the asymmetric triple well spectra are quite different, see Figs. 4.3 (a) and 4.4. They also show the same quasi-periodicity with the period of about $\pi/(2a)$, determined by the fixed width of the system $2a$, not changed by the perturbations used in the QM-RSE. However, one can see additionally another

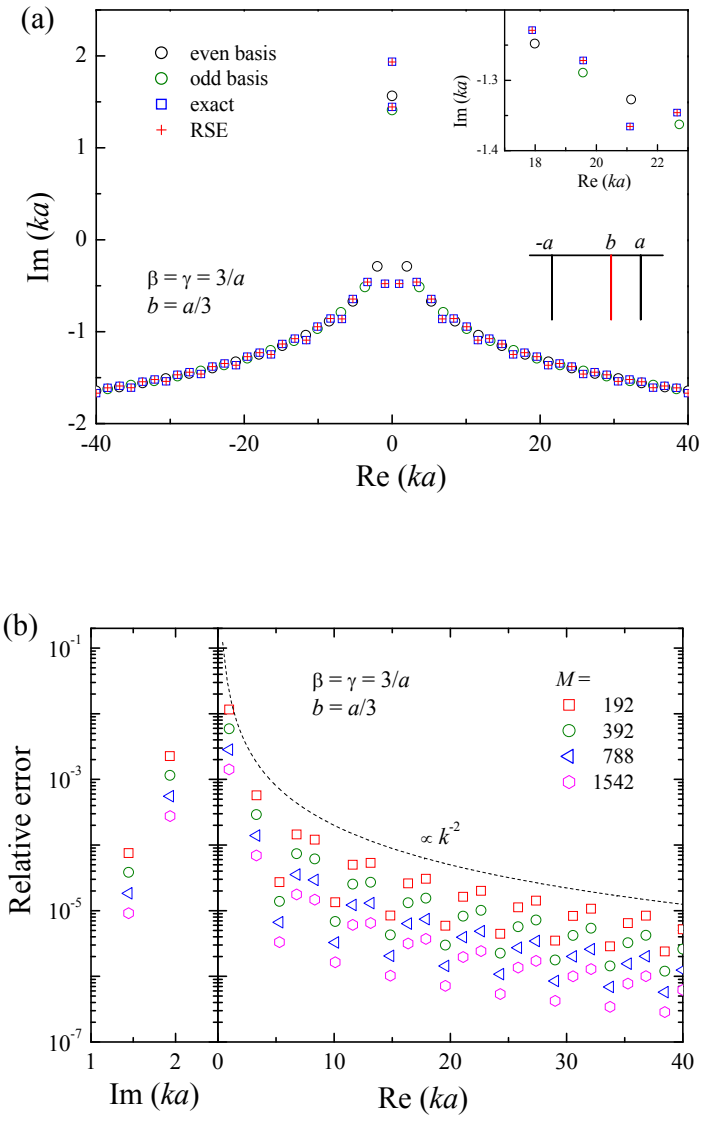

Figure 4.3: As Fig. 4.1 but $b = a/3$.

quasi-periodic behavior of the RS wave numbers, with a larger period, which depends on the position b of the middle quantum well as it is clear from Fig. 4.4.

To study this effect, we have chosen the position of the middle well in such a way that it splits the system into two subsystems with the smaller one being L times narrower than the full system. The results are shown in Figs. 4.3 (a) and 4.4 (a-c) for $L = 3$, 4, 5, and 10, respectively. The RS spectra for these systems show

a quasi-periodicity with L neighboring RSs forming a period, as it is clear from these figures. Physically, this can be understood by looking again at the resonant condition for the constructive interference of waves experiencing multiple reflections. Due to the commensurability of the sizes of the full system and the smaller subsystem, the effect of constructive interference forming the RSs can be enhanced for some of them owing to additional reflections from the middle well.

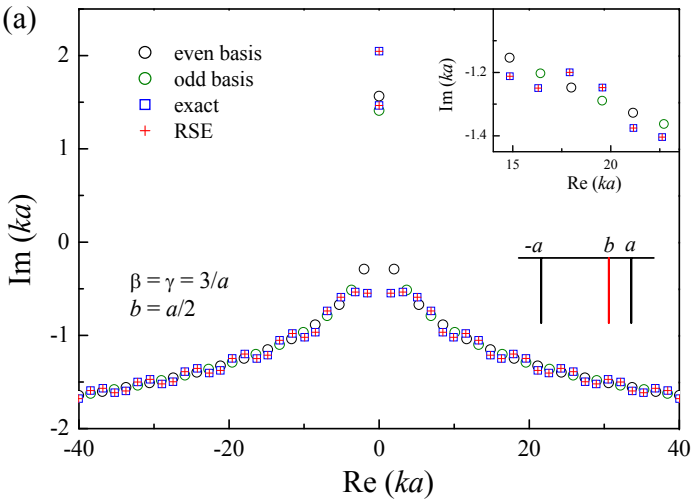

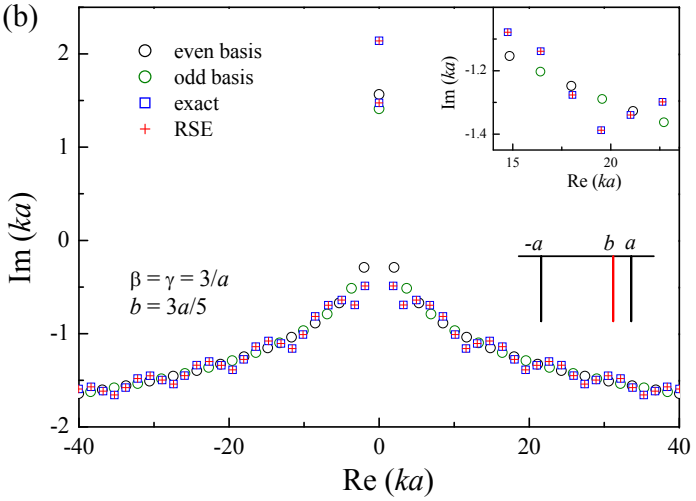

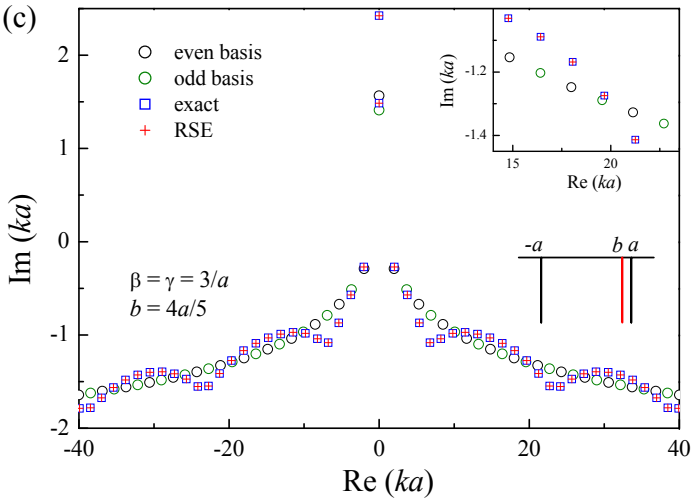

Figure 4.4: As Fig. 4.3 (a) but for $b = a/2$ (a), $b = 3a/5$ (b), and $b = 4a/5$ (c).

4.3.2 Matrix elements of the perturbation

To use the QM-RSE, one needs to calculate the matrix elements of the perturbation Eq. (4.5). For the basis RSs wave functions given by Eq. (4.8) and the perturbation Eq. (4.12), we find

$$\Delta V_{nm} = -\beta \varphi_n(b) \varphi_m(b)\,, \tag{4.15}$$

where

$$\varphi_n(b) = 2C_n \times \begin{cases} \cos k_n b & \text{for even RSs}\,, \\ \\ i \sin k_n b & \text{for odd RSs}\,, \end{cases} \tag{4.16}$$

and the normalization constants C_n are given by Eq. (4.11).

In general, if both the unperturbed and perturbed potentials are symmetric, the RS wave functions for both potentials are either even or odd. In other words, the perturbation matrix ΔV_{nm} does not lead to any mixing of RSs of different parity. However, for the delta-like perturbation Eq. (4.15), if it is symmetric, i.e. if $b = 0$, not only even and odd states do not mix, but, moreover, odd basis RSs do not perturb. This is clear from the fact that the matrix elements are non-vanishing only between even parity states. In this case the matrix elements are given by

$$\Delta V_{nm} = -4\beta C_n C_m\,. \tag{4.17}$$

The vanishing effect of the perturbation on the odd RSs is also

confirmed by the exact solution for the symmetric triple well presented in Fig. 4.1 (a) which shows that the wave numbers of the odd RSs of both double and triple quantum wells coincide.

4.3.3 QM-RSE for a triple symmetric quantum well

We treat with the QM-RSE the symmetric triple quantum well first. The QM-RSE results are generated by solving numerically the linear matrix eigenvalue problem Eq. (4.3) with ΔV_{nm} defined by Eq. (4.17). The infinite matrix H_{nm} in Eq. (4.3) is truncated in such a way that all RSs within a circle of radius R centered at $k = 0$ in the complex k-plane are kept in the basis. This introduces the total number of the basis RSs M. We use this definition of the basis for all the examples treated in this work.

We compare in Fig. 4.1 (a) the QM-RSE result for the RS wave numbers (red crosses) for a symmetric triple quantum well with the exact solution of Eqs. (4.13) and (4.14) (blue squares). The unperturbed wave numbers for both even and odd parity RSs are shown by black and green circles respectively. We see that applying the perturbation does not change the wave numbers of the odd RSs of the basis system, as discussed above. At the same time, all even RSs are modified due to the perturbation, including the ground state of the system (shown by the topmost square/cross on the imaginary k-axis).

It is clear from the comparison in Fig. 4.1 (a) that the QM-RSE is reproducing the exact values. The only RSs having no exact solution to compare with is an antibound states with the wave number close to zero. To quantify this agreement we show in Fig. 4.1 (b) the relative error $|(\varkappa_\nu^{\mathrm{RSE}} - \varkappa_\nu^{\mathrm{ex}})/\varkappa_\nu^{\mathrm{ex}}|$, where $\varkappa_\nu^{\mathrm{RSE}}$ and $\varkappa_\nu^{\mathrm{ex}}$ are the QM-RSE and the exact wave numbers of a given perturbed RS ν. The relative error is shown for different basis sizes M demonstrating the convergence of the QM-RSE to the exact solution as the basis size increases. Note that the shown values of M include also odd basis states which remain unperturbed in this example. Figure 4.1 (b) allows us also to quantify the convergence: The relative error is approximately inversely proportional to the basis size M. Interestingly, for any fixed M the relative error scales for different normal RSs as as $1/k^2$, see the dashed line in Fig. 4.1 (b).

4.3.4 QM-RSE for a triple asymmetric quantum well

Applying the QM-RSE to an asymmetric triple quantum well structure shows a very similar quality of the calculation, even though the perturbation now mixes even and odd RSs of the basis system, effectively doubling the actual linear size of the matrix eigenvalue problem. Indeed Figs. 4.3 (a) and 4.4 (a-c) demonstrate a visual agreement between the QM-RSE and the exact solution, confirming the spectral changes caused by the additional quantum

interference effects in these structure, as discussed in Sec. 4.3.1. Note that Newton-Raphson solutions of the secular equations are much sensitive to the initial guess values use for finding the roots. As a consequence, some RSs can be missing in the analytic spectrum (which is however not the case of the present calculation). At the same time, the RSE finds *all solutions* in a selected spectral range at the same time producing *no spurious solutions*. Indeed, the RSE is based on a complete (though, truncated) set of RSs of the unperturbed system, and as a result of the calculation, it returns also a complete set of perturbed RSs. Therefore, there can be no RSE solutions which are missing or spurious.

Figure 4.3 (b) demonstrates the convergence of the QM-RSE to the exact solution for the asymmetric triple well, which is very similar to the symmetric case. The comparison with the exact solutions in Figs. 4.1-4.4 and the study of the relative errors for the RS wave numbers thus provides a verification of the QM-RSE in 1D. We can now take the advantages of the QM-RSE, applying it to more complex potentials, such a multiple quantum wells and finite quantum lattices, where the exact solutions are more difficult to find by other means.

4.4 Summary

In this chapter, we have studied the resonant state expansion in various simple one-dimensional quantum mechanical systems. The method is used here for finding the resonant states in

various potentials approximated by combinations of Dirac delta functions. The resonant state expansion is verified for a triple quantum well system, showing convergence to the available analytic solution as the number of resonant states in the basis increases. We have demonstrated that the relative error scales as the inverse of the basis size. For a fixed basis size, it scales as $1/k^2$ for normal RSs. We have studied, using the RSE, the interference effect where the system is divided into two resonators of commensurable widths.

Chapter 5

QM-RSE applied to finite quantum lattices

In this chapter, we apply the QM-RSE to finite periodic quantum potentials. We keep using the model of delta functions and define a finite periodic potential in such a way that it consists of N equally spaced delta-like quantum wells of strength γ. The separation between the quantum wells, or the period of the potential is

$$d = \frac{2a}{N-1}\,, \tag{5.1}$$

where $2a$, is the width of the system. The full potential of the system, $V(x) + \Delta V(x)$, thus consists of the unperturbed potential $V(x)$ of a double well, which is given by Eq. (4.7) and a perturbation

$$\Delta V(x) = -\gamma \sum_{k=2}^{N-1} \delta(x - b_k)\,, \tag{5.2}$$

in which

$$b_k = -a + d(k-1) \tag{5.3}$$

are the positions of the quantum wells. According to Eq. (4.5), the perturbation matrix of the QM-RSE is then given by

$$\Delta V_{nm} = -\gamma \sum_{k=2}^{N-1} \varphi_n(b_k)\varphi_m(b_k) \tag{5.4}$$

with $\varphi_n(b)$ provided in Eq. (4.16).

5.1 QM-RSE calculation of the resonant states wave numbers and convergence

We use the QM-RSE to calculate the RS wave numbers for increasing number of wells N. The $N = 2$ case is the unperturbed system, and the $N = 3$ case is already treated in Sec. 4.3.3 above, see Fig. 4.1. So, increase N further, we now first look at the $N = 4$ case. The wave numbers of both unperturbed and perturbed RSs for this case are shown in Fig. 5.1 (a). The spectrum looks very similar to the ones considered before in what concerns the normal RSs, showing again a bigger period which we discuss below in more depth. However, a significant difference compared to the spectra in Figs. 4.3 and 4.4 is the presence of two anti-bound states on the negative imaginary half-axis. This is due to two facts. First of all, the considered systems has a larger depth of the quantum wells:

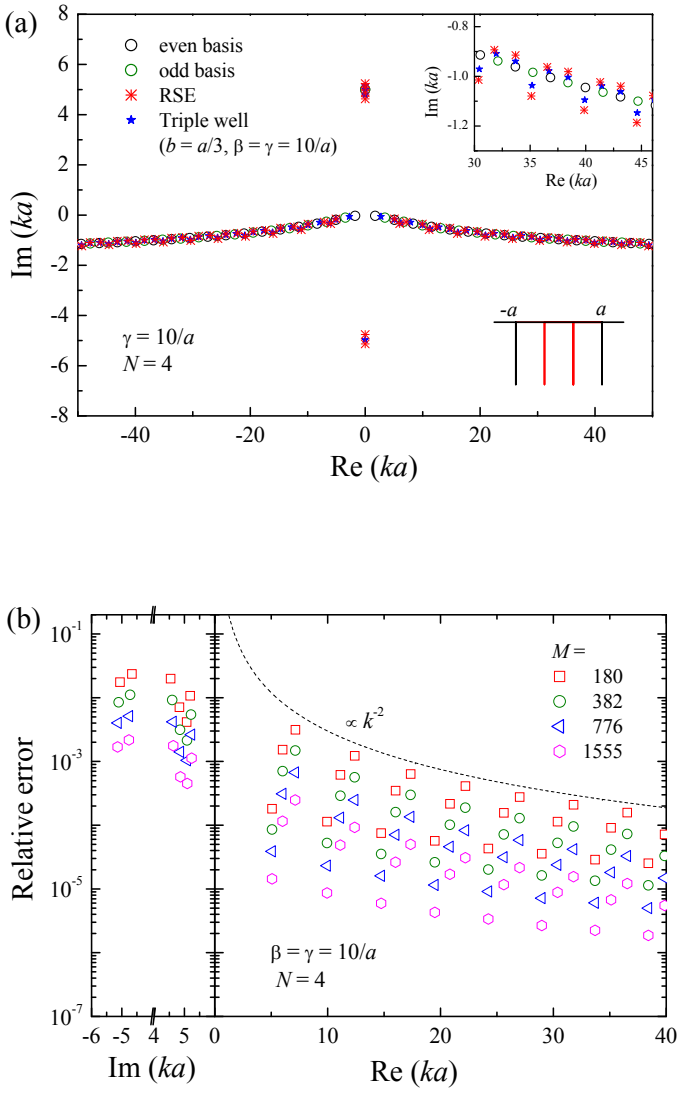

Figure 5.1: As Fig. 4.1 but for a finite periodic potential with $N = 4$ quantum wells of depth $\gamma = 10/a$. The perturbation used in the QM-RSE is given by Eq. (5.2). The resonant states of a triple well structure with $\beta = \gamma = 10/a$ and $b = a/2$ are shown additionally (blue stars). The relative error in (b) is calculated using the QM-RSE values for $M = 4480$ replacing the exact solution.

$\gamma = 10/a$. Secondly, the number of quantum wells is increased to 4. These two factors result in a stronger overall quantum potential which is able to accommodate a larger number of bound states: One can see that there are 4 bound states in this system, which are produced by a hybridization of the bound states of four individual quantum wells. Increasing the depth of the potentials reduces the tunnel coupling between these bound states, which allows us to consider this coupling as a rather small perturbation not affecting much the individual states. At the same time, the presence of two more bound states inevitably leads to two anti-bound states showing up in the spectrum. One can understand the presence of these four states in the spectrum as a result of transformation of two pairs of normal RSs into bound and anti-bound states as the strength of the quantum wells increases, see Chap. 3 for a more detailed discussion of this phenomenon.

The convergence of the QM-RSE is quantified in Fig. 5.1 (b) where we again show the relative error of the calculation of the RS wave numbers for four different basis sizes: $M \approx M_0$, $2M_0$, $4M_0$, and $8M_0$. However, this time we do not find the exact solution, which would be a complicated, though not impossible task. Instead of the exact solution we take the values calculated with a much larger value of M. We see that the relative error is in principle very similar to that presented in Figs. 4.1 (b) and 4.4 (b), where the exact solution was used. Again, the $1/k^2$ dependence of the relative error for a fixed M is observed, and the error scales inversely

proportional to M. We therefore conclude that the convergence of the QM-RSE does change when one makes the perturbation more complex.

5.2 Comparison with triple well spectra

Increasing N further, the computational complexity of finding RSs using some alternative methods, such as transfer or scattering matrix approaches, increases dramatically. This is not only due to an increasing number of interfaces (or inhomogeneities) present in the system, determining the size of the linear algebra problem, but mainly because some of the eigenmodes are becoming prohibitively difficult to find. These are usually modes having the most interesting properties, such as superradiant states [51] or bound states in the continuum [52]. At the same time, the complexity of the QM-RSE remains almost the same. Of course, the overall strength of the perturbation increases proportionally to N which requires taking into account more RSs in the basis in order to keep the accuracy of calculation the same.

Looking at Fig. 5.2 where the RSs for $N = 5$, 6 and 11 are shown, we see that the number of bound and antibound states further increases (up to 6 and 4, respectively). However $N = 6$ and $N = 11$ have the same number of bound/antibound states. This can be understood in the following way. The quantum tunneling between the wells increases with N, since the well separation d

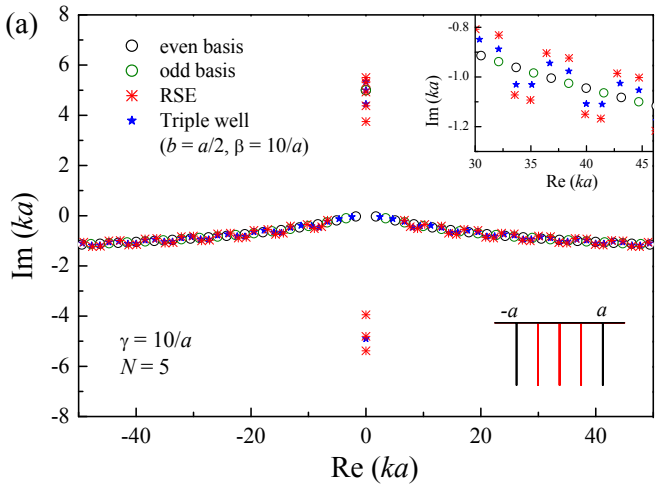

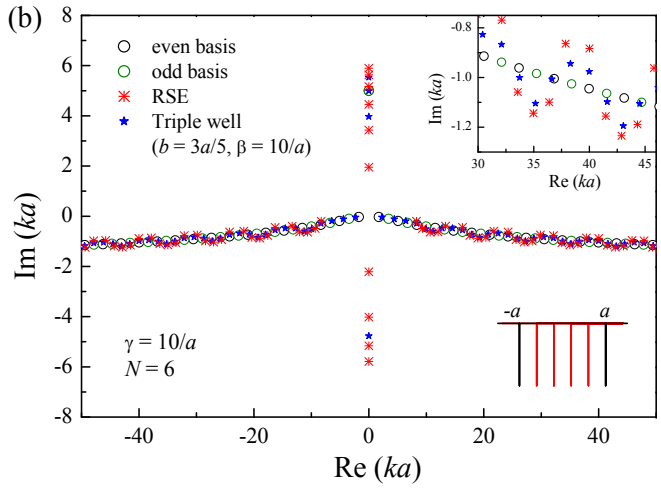

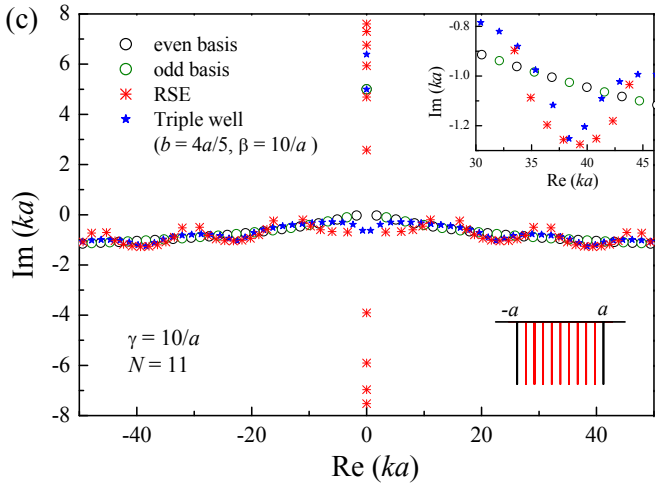

Figure 5.2: As Fig. 5.1 (a) but for $N = 5$, 6, and 11. Additionally, the resonant states for a triple well structure with $\beta = \gamma = 10/a$ and $b = a/3$, $3a/5$, and $4a/5$ are shown, in (a), (b), and (c), respectively.

decreases. With increasing tunneling one goes further away from the picture of nearly independent quantum wells, from which the tunneling is only a small perturbation, in which case the total number of bound states is equal to the number of wells. With a larger tunneling instead, the whole potential has to be treated more like one common wide quantum well which can accommodate a limited number of bound states. As for the antibound states, their number is usually two less the number of bound states [43].

We also see in Fig. 5.2 a quasi-periodic behavior of the RS wave number, similar to the phenomenon observed for triple quantum wells and discussed in Sec. 4.3.1. Increasing N, the number of states in the period increases – it is actually equal to $N-1$, as can be seen from the graphs. To confirm that this is a manifestation of the same effect of an additional resonant enhancement, owing to the splitting of the whole system into two or more resonator, we compare in Fig. 5.2 the RSs of finite periodic systems with those of the corresponding triple well system. We have chosen the smallest separation between the wells in the triple well system equal to d, the period of the quantum lattice, which is given by Eq. (5.1).

This comparison reveals close similarities between the finite periodic and the corresponding triple well systems, with the same quasi-periodicity in the spectra observed for both. One can see from the insets in Figs. 5.1(a) and 5.2(a)-(c) that the spectra of the two systems are in a good qualitative agreement. In other words, the RS spectrum of a finite periodic system does

not change much if one removes from the potential all the inner quantum wells except the rightmost one. The physical reason for the quasi-periodic oscillations is essentially the same as mentioned above and discussed in more detail in Sec. 4.3.1. The finite periodic potential with N quantum wells splits the full system into $N-1$ resonators of width d similar to one such resonator present in the corresponding triple well. The presence of multiple resonators of a commensurable width in finite periodic structures only enhances the effect already observed in the triple wells: Indeed, the amplitudes of the quasi-periodic oscillations in the RS spectra are stronger in the case of the quantum lattices.

5.3 Comparison with the Kronig-Penney model

Taking the limit $N \to \infty$ while keeping the period (the distance between the neighboring wells) fixed, we end up with the famous Kronig-Penney potential [25]

$$V(x) = -\gamma \sum_{n=-\infty}^{\infty} \delta(x - nd) \tag{5.5}$$

describing an infinite periodic system, or an infinite quantum lattice. The Kronig-Penney model is known to have an exact analytic solution showing allowed bands and band gaps in the energy spectrum or the wave number spectrum of a particle.

The exact solution of the Kronig-Penney model is given

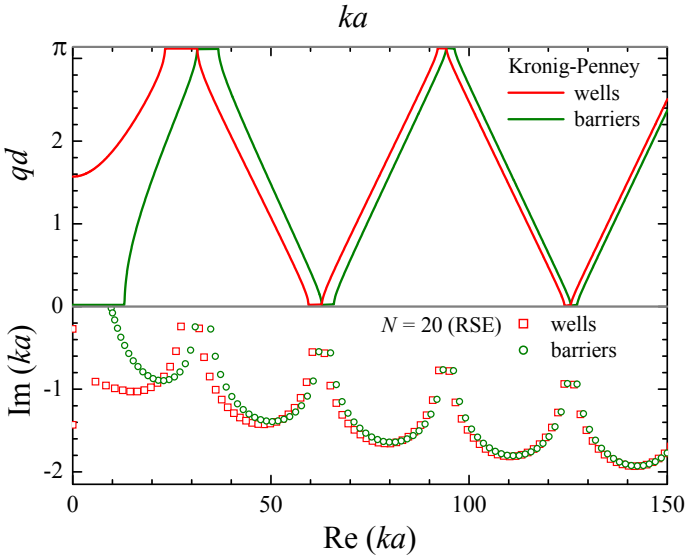

Figure 5.3: (top) Solution of the Kronig-Penney model Eq. (5.6). (bottom) Resonant state wave numbers of a finite periodic quantum lattice with $N = 20$ calculated using the QM-RSE, for $\gamma = 10/a$ (wells) and $\gamma = -10/a$ (barriers).

by [25]

$$\cos(qd) = \cos(kd) - \frac{\gamma}{2k}\sin(kd)\,. \tag{5.6}$$

where q the wave number of the quasi-particle in the periodic potential which is a conserved quantity. According to Bloch's theorem, the wave function of the particle has the form $\psi(x+d) = e^{iqd}\psi(x)$ containing this wave number.

We compare in Fig. 5.3 the spectra of RSs for a potential of $N = 20$ wells (barriers) with the spectra of allowed and forbidden bands of a particle in the periodic potential Eq. (5.5) corresponding to $N = \infty$. For the former, we again use the complex k-plane, see the bottom part of Fig. 5.3. For the latter, we use the (q, k) plane with real values of q and k, see the top part of Fig. 5.3. For the comparison, we use the same parameters of both structures: $\gamma =$

$10/a$ and $d = 2a/19$. One can see a clear qualitative agreement between the allowed band and the groups (periods) of RSs in the quasi-periodic RS spectra. The Kronig-Penney model thus helps us to clarifies on the actual physical meaning of these periodic groups of RSs: In the limit $N \to \infty$ they just form the allowed band in a periodic potential. Figure 5.3 shows results for wells and barriers, demonstrating a good agreement and correlation between finite and infinite periodic structures.

5.4 Effect of varying strength of periodic quantum lattice

We finally study the dependence of the RS wave numbers on the potential strength of a finite periodic structure of $N = 20$ quantum barriers. We see from Fig. 5.4 that each group of RSs of the quasi-periodic spectrum (discussed in Sec. 5.3) is quite robust to changes of the potential strength. However, the separation between the groups which would correspond to a band gap in the spectrum of an ideal periodic system strongly depends on γ. This is consistent with the result of Kronig-Penney model also showing the dependence of the band gap width on the potential strength. We do not provide here any quantitative comparison, though.

Another important effect is a decrease of the imaginary part of the RS wave numbers as potential strength γ increases. In other words, increasing γ improves the quality factor (Q-factor) $Q = |\mathrm{Re}k_n/(2\,\mathrm{Im}k_n)|$ of all the resonances. This is expected, as

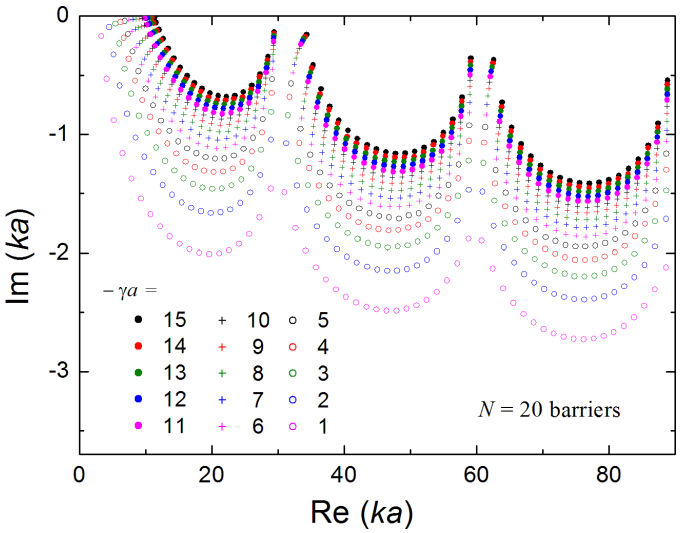

Figure 5.4: Resonant state wave numbers of a finite periodic lattice of $N = 20$ quantum barriers, calculated using the QM-RSE for different barrier strength γ as given.

higher values of γ provide a better reflection from the potential inhomogeneities, in this way helping the given probability density to stay longer within the system. For some resonant states, the Q-factor becoming really large, see, for example the very RS having $Q \approx 400$. The physical reason of formation of such states might be similar to that of bound states in the continuum [52]. The true bound states, however, have an infinite Q-factor.

5.5 Random quantum lattice

Here we apply the RSE to finite random potentials and calculated their wavenumbers for 10 different realisations, unlike in Chap. 4 where we fixed our parameters. Here the parameters used are $N = 20, a = 1, \gamma = -10, \alpha = 0.2, 0.5,$ and 0.8. Since β

from Eq.(5.2) is not fixed, in this case, it is given in the form

$$\beta = b_{min} + (b_{max} - b_{min})r \tag{5.7}$$

where $b_{max} = \gamma(2-\alpha)$, $b_{min} = \alpha\gamma$ and r is a random number taken between 0 and 1. In all the realisations we use average values of β instead given as

$$\bar{\beta} = \sum_{k=2}^{N-1} \frac{\beta_k}{N-2} \tag{5.8}$$

where N is the number of lattices within the quantum well. It is however noted that from Eq.(5.7) if $r = 0$ then $\beta = b_{min}$ and we expect a very strong disorder while, if $r = 1$ then $\beta = b_{max}$ which leads to no disorder in the system.

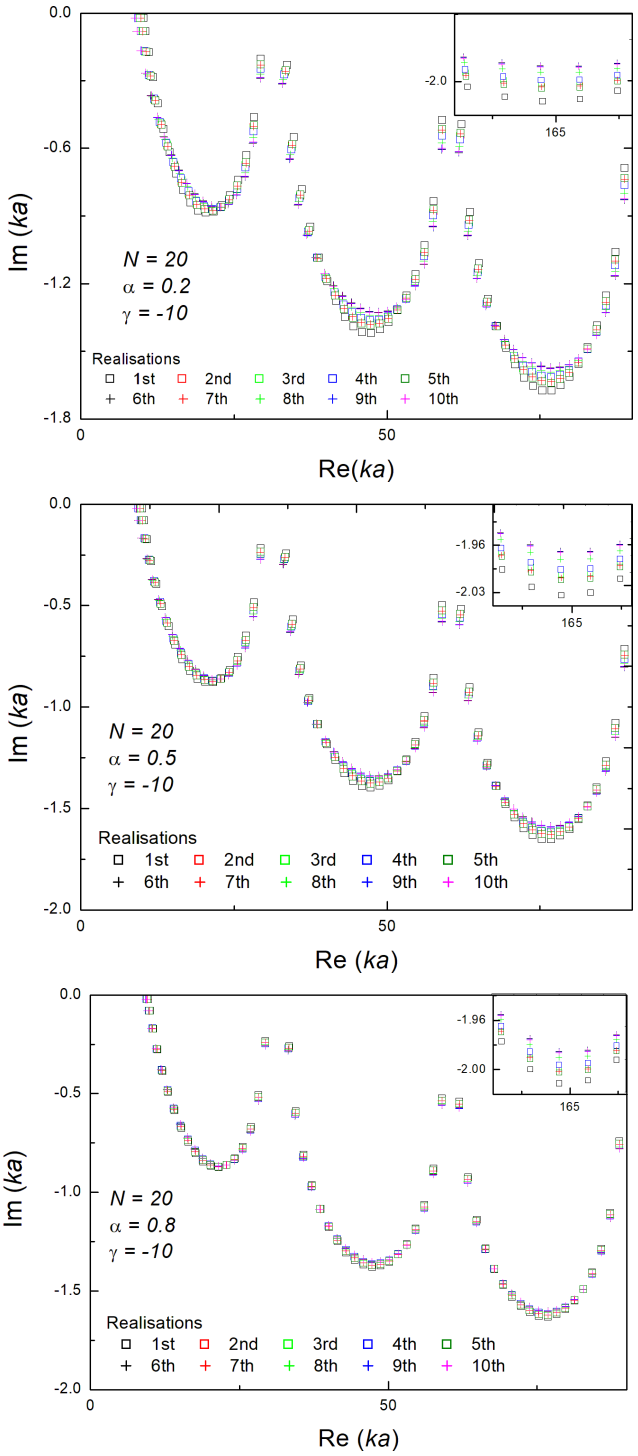

Figure 5.5: As Fig. 4.1 but for a finite random potential with $N = 20$ quantum barriers of depth $\gamma = -10/a$ for 10 different realisations. The number of realisations was calculated using $\alpha = 0.2$, 0.5, and 0.8 as shown, in (a), (b), and (c), respectively.

It is observed that there is a stronger disorder for smaller α and a weaker disorder for larger α getting closer to 1. This can be seen from Fig. 5.5 (a-c) where $\alpha = 0.2$, 0.5 and 0.8 are

presented. Similar quasi-periodicity of the spectra are observed also with disorder.

5.6 Summary

In this chapter, we further apply a resonant state expansion to a more complicated quantum systems. The systems include multiple quantum well and barrier structures, and finite random and periodic systems. Results of these are compared with the eigenstates in triple quantum wells studied in Chap. 4, and with the Kroniq-Penney model revealing the nature of the resonant states in the studied systems.

We found in perticular, that the spectrum of the normal RSs looks very similar to the one considered in Chap. 4. However, a significant difference observed, is the increase in the number of bound states and presence of antibound states on the negative imaginary half axis. We have demonstrated that the transformation of these bound/antibound states results with an increasing number of quantum wells and also with a larger depth of the quantum well in the considered systems.

We again demonstrated in this chapter, the convergence of the QM-RSE, where we presented the results of the relative error calculations of the RSs wave numbers for different basis sizes.

The effect of varying the strength of a finite periodic structure was discussed. We found that the region of each sub-groups which would correspond to band gaps in the spectral range of this

finite periodic system is strongly depends on potential strength γ.

We finally, applied the QM-RSE to the finite random potentials and studied the disorder of the system considered. We demonstrated that the disorder in this system depends on the choice of strength α. We found that the stronger disorder is observed for a smaller choice of α.

Chapter 6

Conclusion and outlook

We have applied the resonant state expansion (RSE), a novel powerful theoretical method recently developed in electrodynamics, to non-relativistic quantum-mechanical systems in one dimension, modeling all potentials with Dirac delta functions. We have verified the method, which we call here quantum-mechanical resonant state expansion (QM-RSE), testing it on systems with triple quantum wells while using the resonant states of a double quantum well as a basis. We have studied the full set of resonant states of a one dimensional Schrödinger problem with double and triple quantum wells or barriers approximated by Dirac delta functions. This full set includes bound, anti-bound and normal resonant states. We have revisited the problem of finding bound states in delta-well potentials and have worked out simple analytic expressions for important limiting cases and compared them with the full numerical solution. The latter is in turn presented here as universal

dependencies containing the minimal number of parameters. Furthermore, we have studied the transition between different types of resonant states, demonstrating in particular how bound states disappear from the spectrum continuously transforming into anti-bound states, which are in turn transform further into normal resonant states. We have shown that these normal resonant states determine the main spectral features in observables, such as the quantum transmission, and that taking the full set of resonant states, including the bound and anti-bound states, allows one to precisely determine the transmission via its Mittag-Leffler expansion. Complicated potentials like finite Kronig-Penney lattices are easy to add resonances using the RSE, as the RSE provides the full Green's function in terms of the RSs, and the Green's function gives access to all the observables, including the transmission. We have also, analysed the RSs of double and triple quantum wells in terms of the constructive interference of quantum waves supported by these structures.

We have studied the convergence of the QM-RSE to the exact solutions. In particular, we have demonstrated that the QM-RSE is asymptotically exact, with the number of basis resonant states being the only technical parameter of the method, and that the relative error scales inversely proportional to the basis size. We have further demonstrated that the QM-RSE enables

an accurate and efficient study of complicated quantum structures, such as multiple quantum wells and finite periodic potentials, which are harder to address by alternative methods. Some complicated quantum systems can exhibit interesting physical phenomena, such as formation of quasi-periodic bands of resonances or bound states in the continuum, and thus have to be investigated with an accurate and efficient tool. The QM-RSE can offer such a tool, as we have demonstrated in this work. Furthermore, it is straightforward to expand the QM-RSE beyond one dimension, as it has been demonstrated in numerous publications on the RSE applied to open optical systems [12–15].

A feature research may include applying the QM-RSE to higher dimensions noting that with the successful application of the RSE in electrodynamics and wave optics allows us to expect that using the QM-RSE in higher dimensions is straight forward and does not require any modification of the formalism. Moreover, it is technically a lot easier than in electrodynamics, as the Schrödinger equation is a scalar wave equation. The only open question at the moment is how quick would be the convergence of the QM-RSE in 2D and 3D. We do not know the answer on this question yet but expect it not to be very different from that in electromagnetic problems.

Another area of future application of the QM-RSE is in the physics of semiconductor nanostructures, where calculating the eigenstates of electrons, holes, and excitons in quantum wires and

dots of non-trivial shape and material composition is a challenging computational task for existing commercial solvers.

Appendix A

The Schrödinger equation

In 1925, Erwin Schrödinger and Werner Heisenberg independently developed the new quantum theory. Schrödinger's method involves partial differential equations, whereas Heisenberg's method employs matrices; however, a year later the two methods were shown to be mathematically equivalent. Most textbooks begin with Schrödinger's equation, since it seems to have a better physical interpretation via the classical wave equation. Indeed, the Schrödinger equation can be viewed as a form of the wave equation applied to matter waves.

A.1 The time-independent Schrödinger equation

The general solution to the Schrödinger equation starts from the classical description of the total energy, E, which is equal

to the sum of the kinetic energy, T, and the potential energy, V

$$E = T + V = \frac{p^2}{2m} + V(x) \tag{A.1}$$

going from classical to quantum mechanics, p becomes an operator $\hat{p} = -i\hbar\frac{d}{dx}$. A wavefunction, ψ, is defined to convert the energy equation into a wave equation Eq.(A.2) [53]. This is achieved by multiplying each term in the energy equation by the defined wavefunction, ψ

$$E\psi(x) = \frac{\hat{p}^2}{2m}\psi(x) + V(x)\psi(x) \tag{A.2}$$

To incorporate the de Broglie wavelength of the particle, we introduce the operator $-\frac{\hbar^2 d^2}{dx^2}$, which provides the square of the momentum, $\hat{p}^2$. When applied to a plane wave we obtain Eq.(A.3) [53, 54]

$$-\hbar^2\frac{d^2\psi}{dx^2} = \hbar^2 k^2\psi = p^2\psi, \tag{A.3}$$

where

$$\psi = e^{i(kx-\omega t)} \tag{A.4}$$

and k is the wavenumber ($k = \frac{2\pi}{\lambda}$). Replacing the momentum squared, $\hat{p}^2$, in Eq.(A.2) by this operator yields the one-dimensional time-independent Schrödinger Eq.(A.5).

$$-\frac{\hbar^2}{2m}\frac{d^2\psi(x)}{dx^2} + V(x)\psi(x) = E\psi(x) \tag{A.5}$$

This single-particle one-dimensional equation can easily be extended to the case of three dimensions, where it becomes

$$-\frac{\hbar^2}{2m}\nabla^2\psi(\mathbf{r}) + V(\mathbf{r})\psi(\mathbf{r}) = E\psi(\mathbf{r}) \tag{A.6}$$

A.2 The time-dependent Schrödinger equation

The wave function of a particle of fixed energy E could be written as a linear combination of wave functions of the form

$$\Psi(x,t) = Ae^{i(kx-\omega t)} \tag{A.7}$$

representing a wave travelling in the positive x direction, and a corresponding wave travelling in the opposite direction [55]. The wave function in Eq.(A.7) is regarded as a wave function for a free particle of momentum $p = \hbar k$ and energy $E = \hbar\omega$. With this in mind, we can then note that

$$\frac{\partial^2\Psi}{\partial x^2} = -k^2\Psi \tag{A.8}$$

which can be written, using $E = \frac{p^2}{2m} = \frac{\hbar^2k^2}{2m}$:

$$-\frac{\hbar^2}{2m}\frac{\partial^2\Psi}{\partial x^2} = \frac{p^2}{2m}\Psi. \tag{A.9}$$

Similarly

$$\frac{\partial \Psi}{\partial t} = -i\omega\Psi \tag{A.10}$$

which can be written, using $E = \hbar\omega$:

$$i\hbar\frac{\partial \Psi}{\partial t} = \hbar\omega\psi = E\Psi. \tag{A.11}$$

We now generalize this to the situation in which there is both a kinetic energy and a potential energy present, then $E = \frac{p^2}{2m} + V(x)$ so that

$$E\Psi = \frac{p^2}{2m}\Psi + V(x)\Psi \tag{A.12}$$

where Ψ is now the wave function of a particle moving in the presence of a potential $V(x)$. But if we assume that the results Eq.(A.9) and Eq.(A.11) still apply in this case then we have

$$-\frac{\hbar^2}{2m}\frac{\partial^2\Psi}{\partial x^2} + V(x)\Psi = i\hbar\frac{\partial \psi}{\partial t} \tag{A.13}$$

which is the famous time-dependent Schrödinger equation.

Appendix B

Derivation of the Orthogonality condition

In this section we derive the orthogonality condition leading to a special normalisation condition as given by Eq.(1.19). In general, a one-dimensional wave equation for a closed system occupying the interval $a \leq x \leq b$ (for example, a particle in a box with infinite walls at $x = a$ and $x = b$) can be formulated as follows: Take

$$H\psi_n(x) = E_n\psi_n(x), \tag{B.1}$$

multiply Eq.(B.1) by ψ_m and integrate. Then obtain:

$$\int_a^b \psi_m(x)H\psi_n(x)dx = E_n \int_a^b \psi_m(x)\psi_n(x)dx. \tag{B.2}$$

Similarly, from

$$H\psi_m(x) = E_m\psi_m(x), \tag{B.3}$$

we have

$$\int_a^b \psi_n(x) H \psi_m(x) dx = E_m \int_a^b \psi_n(x) \psi_m(x) dx. \tag{B.4}$$

Subtract Eq.(B.4) form Eq.(B.2) and use the fact that the Hamiltonian H is Hermitian for any closed system. Then we obtain:

$$\int_a^b \left(\psi_n(x) H \psi_m(x) - \psi_m(x) H \psi_n(x)\right) dx = (E_n - E_m) \int_a^b \psi_n(x) \psi_m(x) dx = 0. \tag{B.5}$$

Obviously, for $E_n \neq E_m$ the last integral vanishes.

Now consider an open system like a rectangular quantum well Fig.(2.1). The Schrödinger equation in this case is the same (but written here in term of the eigen wave numbers):

$$H \psi_n(x) = k_n^2 \psi_n(x). \tag{B.6}$$

Multiplying Eq.(B.6) by ψ_m and integrating over a finite interval, from x_L to x_R which are both outside the system, obtain:

$$\int_{x_L}^{x_R} \psi_m(x) H \psi_n(x) dx = k_n^2 \int_{x_L}^{x_R} \psi_m(x) \psi_n(x) dx. \tag{B.7}$$

Similarly,

$$H \psi_m(x) = k_m^2 \psi_m(x), \tag{B.8}$$

then

$$\int_{x_L}^{x_R} \psi_n(x) H \psi_m(x) dx = k_m^2 \int_{x_L}^{x_R} \psi_n(x) \psi_m(x) dx, \tag{B.9}$$

with

$$H = -\frac{d^2}{dx^2} + V. \tag{B.10}$$

Subtract Eq.(B.9) from Eq.(B.7) to obtain

$$\int_{x_L}^{x_R} \left(\psi_n(x) H \psi_m(x) - \psi_m(x) H \psi_n(x)\right) dx = (k_n^2 - k_m^2) \int_{x_L}^{x_R} \psi_n(x)\psi_m(x) dx. \tag{B.11}$$

Using Eq.(B.10), Eq.(B.11) becomes

$$\int_{x_L}^{x_R} \left(\psi_n \left(-\frac{d^2}{dx^2} + V\right) \psi_m - \psi_m \left(-\frac{d^2}{dx^2} + V\right) \psi_n\right) dx = (k_n^2 - k_m^2) \int_{x_L}^{x_R} \psi_n(x)\psi_m(x) dx. \tag{B.12}$$

This can be simplified to

$$-\int_{x_L}^{x_R} \left(\psi_n \psi_m'' - \psi_m \psi_n''\right) dx = (k_n^2 - k_m^2) \int_{x_L}^{x_R} \psi_n(x)\psi_m(x) dx. \tag{B.13}$$

Integrating Eq.(B.13) by parts and noting that outside the system $\psi_n(x) = A_n e^{ik_n x}$ for $x > a$, so that $\psi_n' = ik_n \psi_n(x)$, we finally obtain for $n \neq m$ a proper orthogonality condition Eq.(1.19)

$$\delta_{nm} = \int_{x_L}^{x_R} \psi_n(x)\psi_m(x) dx - \frac{\psi_n(x_L)\psi_m(x_L) + \psi_n(x_R)\psi_m(x_R)}{i(k_n + k_m)}, \tag{B.14}$$

For $n = m$, a rigorous approach requires to involve Green's function which is done e.g. in [1, 5, 10].

Appendix C

Derivation of the Bloch theorem

In this section we derive the Bloch theorem described by a one-dimensional periodic potential.

Consider an N identical periodic lattice, each separated by a lattice constant a

$$\psi(x+a) = e^{ika}\psi(x), \tag{C.1}$$

with a periodic boundary condition

$$\psi(x+Na) = \psi(x), \tag{C.2}$$

The symmetry of this potential implies that we can find a solution to the wave equation

$$\psi(x+a) = B\psi(x). \tag{C.3}$$

If we apply this translational symmetry N times we will return to the initial lattice point:

$$\psi(x + Na) = B^N \psi(x) = \psi(x). \tag{C.4}$$

This requires $B^N = 1$ and has the general solution of the form

$$B^N = e^{2\pi n i}\, n = 0, \pm 1, \pm 2, ... \tag{C.5}$$

or

$$B = e^{2\pi n i/N} = e^{ika} \tag{C.6}$$

where k is the Bloch wavevector given as

$$k = \frac{2\pi n}{Na}. \tag{C.7}$$

Using Eq. (C.6) we can re-write Eq. (C.3) as

$$\psi(x + a) = B\psi(x) = e^{ika}\psi(x) \tag{C.8}$$

which implies Blochs theorem.

Appendix D

Derivation of the energy dispersion in the Kronig-Penney model

In this section we derive the energy dispersion in the Kronig-Penney model Eq.(5.6). We start from the one-dimensional time independent Schrödinger equation Eq.(1.26) using again $m = 1/2$ and $\hbar = 1$. Since a particle moves in a periodic potential

$$V(x) = -\gamma \sum_{n=-\infty}^{\infty} \delta(x - nd), \tag{D.1}$$

its wavefunction must satisfy Bloch's theorem for any choice of superlattice

$$\psi(x + d) = e^{iqd}\psi(x). \tag{D.2}$$

where d is the period of the superlattice potential while q is the eigen-wavenumber associated with the direction of particle motion.

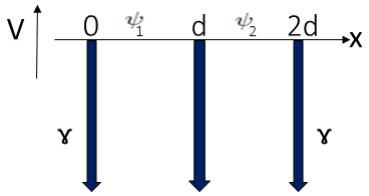

Figure D.1: A sketch of a potential profile of a Kronig-Penney model approximated by Dirac-δ functions.

In region (1) the wave function is given by:

$$\psi_1(x) = Ae^{ikx} + Be^{-ikx} \tag{D.3}$$

The wave function in region (2) can be written interms of Bloch theorem Eq.(1.31)

$$\psi_2(x) = \psi_1(x-d)e^{iqd} = \left[Ae^{ik(x-d)} + Be^{-ik(x-d)}\right] e^{iqd} \tag{D.4}$$

where $k = \sqrt{E}$ and $q = \sqrt{k^2 + \gamma}$. Applying the continuity condition to the wavefunction, *i.e.*

$$\psi_1(d) = \psi_2(d) \tag{D.5}$$

which gives

$$(A+B)e^{iqd} = Ae^{ikd} + Be^{-ikd} \tag{D.6}$$

Therefore

$$A(e^{iqd} - e^{ikd}) = B(e^{-ikd} - e^{iqd}) \tag{D.7}$$

The continuity of the first derivative is not satisfied since $V(x)$

consist of δ-functions. Integrating the Schrödinger equation

$$\int_{d-\delta}^{d+\delta} \frac{d}{dx}\left(\frac{d\psi}{dx}\right) dx = \psi'(d+\delta) - \psi'(d-\delta) \tag{D.8}$$

This is express as

$$\int_{d-\delta}^{d+\delta} \frac{d}{dx}\left(\frac{d\psi}{dx}\right) dx = -\frac{2m}{\hbar}\int_{d-\delta}^{d+\delta} \left[\gamma\delta(x-d) - E\right]\psi_2(x)dx = -\gamma\psi_2(d). \tag{D.9}$$

Applying the discontinuity relation to the wave function in Eq.(D.4) obtain

$$\left[ike^{iqd} - ike^{ikd} + \gamma e^{iqd}\right] A = \left[ike^{iqd} - ike^{-ikd} - \gamma e^{iqd}\right] B. \tag{D.10}$$

Solving Eq.(D.7) and Eq.(D.10) leads to the following final expression

$$\cos(qd) = \cos(kd) - \frac{\gamma}{2k}\sin(kd) \tag{D.11}$$

The importance of this equation is that it provides a restriction on the allowed values of k_n in the periodic potential. The LHS of Eq.(D.11) is bounded in the region of $(-1, 1)$ which leads to that restrictions. (See for e.g. Fig. D.2 for different wells/barrier strengths).

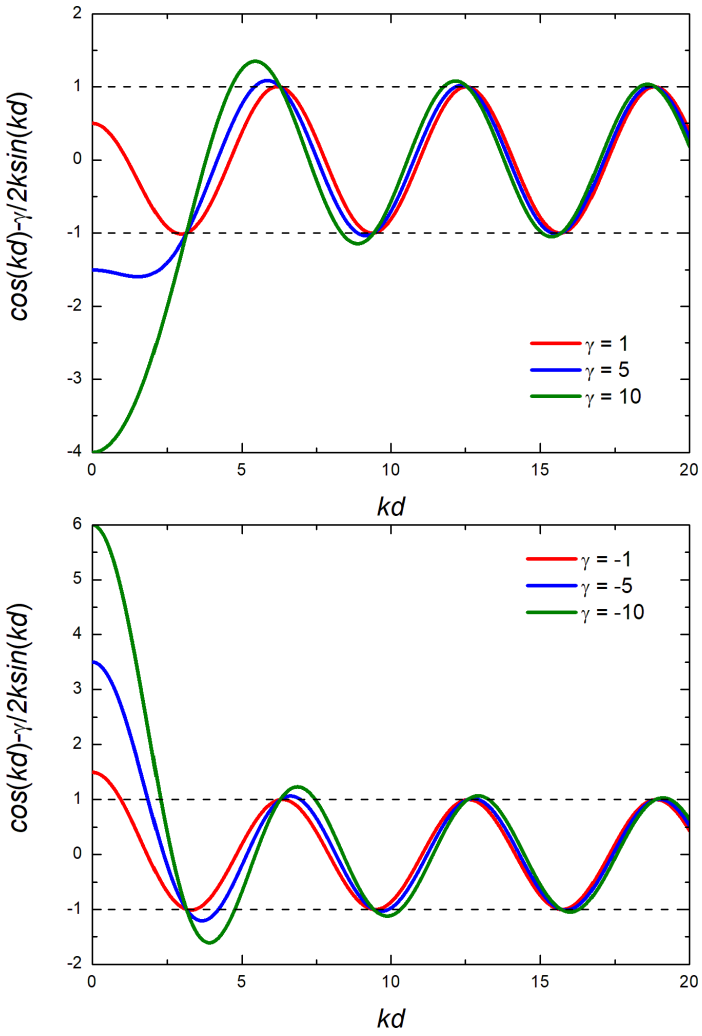

Figure D.2: Plot of the function $\cos(kd) - \frac{\gamma}{2k}\sin(kd)$ for wells (barriers) $\gamma > 0$ ($\gamma < 0$).

Appendix E

Calculation of the normalisation coefficients for RSs in a rectangular well

In this section we calculate the normalisation coefficients for a rectangular well in Chap. 2 as given by Eq.(2.17) and Eq.(2.18).

We use the proper normalisation condition as given by the orthonomality condition

$$\int_{-a}^{a} \psi^2(x)dx - \frac{\psi^2(-a) + \psi^2(a)}{2ik} = 1. \tag{E.1}$$

The wave function as given by Eq.(2.3) is

$$\psi(x) = \begin{cases} Ae^{ikx}, & \text{if } x > a \\ B(e^{iqx} + pe^{-iqx}), & \text{if } |x| \leq a \\ Ae^{-ikx}, & \text{if } x < -a \end{cases} \tag{E.2}$$

where $E = k^2$, $q = \sqrt{k^2 + V_0}$ and $p = \pm 1$ is the parity.

Applying the boundary conditions to the wave functions get

$$Ae^{ika} = B(e^{iqa} + pe^{-iqa}), \tag{E.3}$$

and

$$ikAe^{ika} = iqB(e^{iqa} - pe^{-iqa}). \tag{E.4}$$

we multiply Eq.(E.3) by ik and get

$$ikAe^{ika} = ikB(e^{iqa} + pe^{-iqa}), \tag{E.5}$$

Expressing Eqs.(E.4) and (E.5) obtain

$$\frac{q}{k} = \frac{e^{iqa} + pe^{-iqa}}{e^{iqa} - pe^{-iqa}} \tag{E.6}$$

from this we get Eq. (2.11)

$$pe^{2iqa} = \frac{q-k}{q+k}. \tag{E.7}$$

Using Eq.(E.7) we can write the wave function within the finite

range $|x| \leq a$ as

$$\psi^2 = B^2(e^{2iqx} + e^{-2iqx} + 2p) \tag{E.8}$$

Using $\psi^2(a)$=$\psi^2(-a)$ from Eq. (E.1) obtain

$$\int_{-a}^{a} \psi^2(x)dx - \frac{\psi^2(a)}{ik} = 1. \tag{E.9}$$

Using Eq.(E.8) we can write $\frac{\psi^2(a)}{ik}$ in Eq.(E.9) as

$$\frac{\psi^2(a)}{ik} = \frac{B^2}{ik}(e^{2iqa} + e^{-2iqa} + 2p). \tag{E.10}$$

Eq.(E.10) can be written interms of Eq.(E.7) as

$$\frac{\psi^2(a)}{ik} = \frac{4q^2B^2p}{ik(q^2 - k^2)} = \frac{4q^2B^2p}{ikV_0}. \tag{E.11}$$

were

$$V_0 = q^2 - k^2. \tag{E.12}$$

Similarly, from Eq.(E.9) and usin Eq.(E.8) we can write

$$\int_{-a}^{a} \psi^2(x)dx = B^2\left(\frac{e^{2iqa} - e^{-2iqa}}{iq} + 4pa\right) \tag{E.13}$$

Simplifying Eq.(E.13) using Eq.(E.7) get

$$\int_{-a}^{a} \psi^2(x)dx = B^2p\left(4a + \frac{4kq}{iq(q^2 - k^2)}\right) \tag{E.14}$$

This can be written in terms of Eq.(E.12) as

$$\int_{-a}^{a} \psi^2(x)dx = B^2 p\left(4a + \frac{4k}{iV_0}\right). \tag{E.15}$$

We now substitute Eq.(E.11) and Eq.(E.15) into Eq.(E.9)

$$B^2 p\left(4a + \frac{4k}{iV_0}\right) - \frac{4q^2 B^2 p}{ikV_0} = 1. \tag{E.16}$$

Rearranging this we get

$$4B^2 p\left[a + \frac{k}{iV_0} - \frac{q^2}{ikV_0}\right] = 1 \tag{E.17}$$

using Eq. (E.12) we can write from Eq. (E.17).

$$\frac{k^2 - q^2}{iV_0 k} = -\frac{1}{ik} = \frac{i}{k} \tag{E.18}$$

Putting Eq. (E.18) in Eq. (E.17) we get the normalisation coefficient B as

$$B = \frac{(-i)^n}{2\sqrt{p\left(a + \frac{i}{k}\right)}}. \tag{E.19}$$

Following similar method obtain the coefficient A as

$$A_n = \frac{(-1)^n q_n e^{-ik_n a}}{\sqrt{V(a + \frac{i}{k_n})}}. \tag{E.20}$$

Appendix F

Matlab code

In this section we present a code written in MATLAB for the determination of resonant states wave numbers in a double delta function potential implemented using Newton-Raphson method.

function RSs-NRM

clearvars

close all

V0=3;

kere = $-100 : 1 : 100$; guess value along the real k-plane

keim = $(-3 : 1 : 0)$*1i; guess value along the imaginary k-plane

tol = $1e - 9$; Tolerance

maxiter = 100; this determine the max. number of iteretions

ke = zeros(length(kere),length(keim)); ke - Maximum number of resonant states (RSs) wave numbers to be computed

iter = zeros(length(kere),length(keim));

This loop apply the Newton-Raphson method for finding

```
all the RSs wave numbers
for ii=1:length(kere)
for jj=1:length(keim)
ke(ii,jj) = kere(ii)+keim(jj);
        while(iter(ii,jj)< maxiter)||(abs(Newton-Raphson(ke(ii,jj),V0))>
tol)
        ke(ii,jj) = ke(ii,jj)-Newton-Raphson(ke(ii,jj),V0)/func-prime(ke(ii,jj),V0);
iter(ii,jj) = iter(ii,jj)+1; end
if iter(ii,jj)==maxiter
        ke(ii,jj)=0;
        end
        end
end
ke = ke(:);
kp = zeros(1,length(ke));
kp(1) = ke(1);
tol=1e − 6;
c=1;
for i = 2: length(ke);
        if all(abs(real(ke(i))-real(kp(1:c)))>tol)||all(abs(imag(ke(i))-
imag(kp(1:c)))>tol)
        c=c+1;
        kp(c) = ke(i);
        end
end
```

```
kp=kp(1:c);
```

This loop removes all repeated solutions and the ones that are zero at both real and imaginary axis

```
kp2 = zeros(1,length(kp));
tol = 1e − 6;
c =0;
for i = 1: length(kp);
        if(abs(kp(i))>tol)
        c = c+1;
        kp2(c) = kp(i);
        end
end
kp = kp2(1:c);
```

plot(kp,'+b'); Here we plot our RSs wave numbers in a complex k-plane.

```
M = [real(kp.'),imag(kp.')];
dlmwrite('output.dat',M,'t');
```

This is the function we solved

```
function[value] = Newton-Raphson(ke,V0)
value = exp(2*1i*ke)+1+2*1i*ke/V0;
end
function[value] = func-prime(ke,V0)
value = 2*1i*exp(2*1i*ke)+2*1i/V0;
end
```

```
end
```

Appendix G

Particle in a single delta-like potential

Consider a particle in a quantum well described by a delta-like potential $V(x) = -\alpha\delta(x)$, where α is a positive constant. Using the units in which $\hbar = 1$ and the particle mass $m = 1/2$, the Schrödinger equation takes the form

$$\left[-\frac{d^2}{dx^2} - \alpha\delta(x)\right]\psi(x) = E\psi(x). \tag{G.1}$$

For a bound state the energy $E = -\varkappa^2 < 0$, is negative where $\varkappa$ is a positive real number. The general form of the wave function follows from Eq.(G.1) for $x \neq 0$, i.e. where the delta function has no effect. Thus

$$\psi(x) = \begin{cases} Ae^{\varkappa x} + Be^{-\varkappa x} & \text{x} < 0, \\ Ce^{\varkappa x} + De^{-\varkappa x} & \text{x} > 0. \end{cases} \tag{G.2}$$

where A, B, C, and D are some constants.

Using the boundary conditions for localised states $\psi(x \to \pm\infty) = 0$ we find that $B = C = 0$, while the continuity of the wave function at $x = 0$ yields $A = D$. However, due to the delta-like potential, the wave function is not smooth at $x = 0$. It's derivative has a discontinuity. To take the effect of the delta-like potential into account and to calculate this discontinuity, let us integrate Eq.(G.1) over a small area surrounding the point $x = 0$

$$-\int_{-\epsilon}^{\epsilon} \frac{d^2\psi(x)}{dx^2}dx - \alpha\int_{-\epsilon}^{\epsilon} \delta(x)\psi(x)dx = E\int_{-\epsilon}^{\epsilon} \psi(x)dx \qquad \text{(G.3)}$$

and then take the limit $\epsilon \to 0_+$, where 0_+ is positive infinitesimal. The result is

$$-\psi'(0_+) + \psi'(0_-) - \alpha\psi(0) = 0. \qquad \text{(G.4)}$$

Differentiating the wave function, obtain

$$\psi'(x) = A\varkappa \begin{cases} e^{\varkappa x} & \text{x} < 0, \\ -e^{-\varkappa x} & \text{x} > 0. \end{cases} \qquad \text{(G.5)}$$

Substituting the derivatives into Eq.(G.4) gives

$$\varkappa = \frac{\alpha}{2} \qquad \text{(G.6)}$$

and therefore

$$E = -\varkappa^2 = -\frac{\alpha^2}{4}. \qquad \text{(G.7)}$$

Eq.(G.6) is a linear equation for $\varkappa$. Therefore, for any real positive constant α there is only one localised state in the potential $-\alpha\delta(x)$. This bound state has the energy given by Eq.(G.7). The wave function$\psi(x) = Ae^{-\alpha|x|/2}$ can be normalised by requiring

$$\int_{-\infty}^{\infty} \psi^2(x)dx = 2A^2 \int_0^{\infty} e^{-\alpha x} = \frac{2A^2}{\alpha} = 1, \qquad \text{(G.8)}$$

from what follows that $A = \sqrt{\frac{\alpha}{2}}$. The solution for the localised state (the energy and the wave function) obtained can be checked by double differentiation of the wave function

$$\psi''(x) = \sqrt{\frac{\alpha}{2}} \left[\frac{\alpha^2}{4} e^{-\alpha|x|/2} - \alpha\delta(x) \right] \qquad \text{(G.9)}$$

and substitution back into Eq.(G.1).

Appendix H

Calculation of the normalisation coefficients for RSs in a double well/barrier system

In this section we determine the normalisation coefficient for calculating the perturbation matrix. We consider the wavefunction within the the range $|x| \leqslant a$, in Eq. (3.4). Applying the normalisation condition

$$\int_{-a}^{a} \psi_n^2(x)dx - \frac{\psi_n^2(-a) + \psi_n^2(a)}{2ik_n} = 1. \tag{H.1}$$

to the wave function Eq. (3.4) and excluding exponentials with the help of the secular equation Eq. (3.10)

$$1 + \frac{2ik}{\gamma} = \mp e^{2ika}\,, \tag{H.2}$$

we can find the normalization constants A and C. Where the $+$ sign correspond to the even state and $-$ sign the odd state. From Eq. (3.4) we can write the wave function for $|x| \leqslant a$,

as

$$\psi_n(x) = C_n \left(e^{ik_n x} \pm e^{-ik_n x} \right) \tag{H.3}$$

Using equation Eq.(H.3) obtain

$$e^{ik_n x} = \cos k_n(x) + i \sin k_n(x) \tag{H.4}$$

and following from it

$$e^{-ikx} = \cos k_n(x) - i \sin k_n(x) \tag{H.5}$$

obtain

$$(e^{ik_n x} + e^{-ik_n x})^2 = 4 \cos^2 k_n(x) \tag{H.6}$$

Substituting Eq.(H.6) into Eq.(H.1) results in

$$4C_n^2 \int_{-a}^{a} \cos^2 k_n(x) dx - \frac{8C_n^2 \cos^2 k_n(a)}{2ik_n} = 1. \tag{H.7}$$

Performing integration

$$4C_n^2 \int_{-a}^{a} \frac{1}{2} \left(1 + \cos(2k_n(x))\right) dx - \frac{8C_n^2 \cos^2 k_n(a)}{2ik_n} = 1 \tag{H.8}$$

$$2C_n^2 \left[\int_{-a}^{a} dx + \int_{-a}^{a} \cos(2k_n(x)) dx \right] + \frac{8C_n^2 \cos^2 k_n(a)}{2ik_n} = 1 \tag{H.9}$$

integrating Eq.(H.9) we get

$$C_n^2\left[4a+\frac{\sin(2k_n(a))-\sin(2k_n(-a))}{k_n}\right]+\frac{8C_n^2\cos^2 k_n(a)}{2ik_n}=1 \tag{H.10}$$

$$C_n^2\left[4a+\frac{2}{k_n}\sin(2k_n(a))-\frac{4}{ik_n}\cos^2 k_n(a)\right]=1. \tag{H.11}$$

Let from Eq.(H.11) write

$$\sin(2k_na)=\frac{e^{2ik_na}-e^{-2ik_na}}{2i} \tag{H.12}$$

and

$$\cos^2(k_na)=\left(\frac{e^{2ik_na}+e^{-2ik_na}}{2}\right)^2=\frac{e^{2ik_na}+e^{-2ik_na}+2}{4}. \tag{H.13}$$

Using Eq.(H.2) and putting Eq.(H.12) and Eq.(H.13) into Eq.(H.11) and rearranging obtain the normalisation coefficient for even state as

$$C=\frac{1}{2\sqrt{[a-(\gamma+2ik)^{-1}]}}. \tag{H.14}$$

Similar method were applied and obtain the coefficient for odd state as

$$C=\frac{1}{2\sqrt{[-a+(\gamma+2ik)^{-1}]}} \tag{H.15}$$

and also the normalisation coefficient A as

$$A=C\left(1+\frac{\gamma}{2ik}\right)^{-1}. \tag{H.16}$$

Appendix I

Symmetry in a double delta-function potential

In this section we prove the symmetry of a wave function for both even and odd states in a double delta-function potential in Chap. 3. The solutions to the time-independent Schrödinger equation with a double delta function potential Eq.(3.1) come in two forms :

1. Even parity: $\psi_e(-x) = \psi_e(x)$ symmetric states

2. Odd parity: $-\psi_o(-x) = \psi_o(x)$ anti-symmetric states

Let's first consider the symmetric solution for an even-parity wavefunction

$$\psi_e(x) = \begin{cases} Ae^{-ik_n x}, & \text{if } x < -a \\ C_1 e^{ik_n x} + C_2 e^{-ik_n x}, & \text{if } |x| \leq a \\ Be^{ik_n x}, & \text{if } x > a \end{cases} \tag{I.1}$$

Then

$$\psi_e(-x) = \begin{cases} Ae^{ik_n x}, & \text{if } x < -a \\ C_1 e^{-ik_n x} + C_2 e^{ik_n x}, & \text{if } |x| \leq a \\ Be^{-ik_n x}, & \text{if } x > a \end{cases} \tag{I.2}$$

Now require that the wavefunction is symmetric $\psi_e(-x) = \psi_e(x)$.

Let's consider first the region for $x < -a$:

$$Ae^{ik_n x} = Be^{ik_n x} \tag{I.3}$$

valid for any $x < -a$. Therefore

$$A = B. \tag{I.4}$$

Lets now consider the region for $-a < x < a$

$$C_1 e^{ik_n x} + C_2 e^{-ik_n x} = C_1 e^{-ik_n x} + C_2 e^{ik_n x}. \tag{I.5}$$

Rearranging Eq.(I.5), we obtain

$$(C_1 - C_2)\, e^{ik_n x} - (C_1 - C_2)\, e^{-ik_n x} = 0. \tag{I.6}$$

Factorizing Eq.(I.6) we have

$$(C_1 - C_2)\left(e^{ik_n x} - e^{-ik_n x}\right) = 0 \tag{I.7}$$

which holds only for any $-a < x < a$. Therefore,

$$C_1 = C_2 = C. \tag{I.8}$$

Using Eq.(I.4) and Eq.(I.8) into Eq.(I.1), we can write the even-parity wavefunction as

$$\psi_e(x) = \begin{cases} Be^{ik_n x}, & \text{if } x < -a \\ C\left(e^{ik_n x} + e^{-ik_n x}\right), & \text{if } |x| \leq a \\ Be^{-ik_n x}, & \text{if } x > a \end{cases} \tag{I.9}$$

which clearly shows the symmetry of the wave function about the origin. This is also applicable to the rectangular well in Chap. 2. For the odd-parity wavefunction we start with the same form of the solution

$$\psi_o(x) = \begin{cases} Ae^{-ik_n x}, & \text{if } x < -a \\ C_1 e^{-ik_n x} + C_2 e^{ik_n x}, & \text{if } |x| \leq a \\ Be^{ik_n x}, & \text{if } x > a \end{cases} \tag{I.10}$$

Then

$$\psi_o(-x) = \begin{cases} Ae^{ik_n x}, & \text{if } x < -a \\ C_1 e^{-ik_n x} - C_2 e^{ik_n x}, & \text{if } |x| \leq a \\ Be^{-ik_n x}, & \text{if } x > a \end{cases} \tag{I.11}$$

For the wavefunction to be odd-parity $\psi_o(-x) = \psi_o(x)$.

Let's first consider the region for $x > a$

$$Be^{-ik_n x} = -Ae^{-ik_n x} \tag{I.12}$$

valid only for $x > a$. Therefore,

$$B = -A \tag{I.13}$$

or

$$A = -B. \tag{I.14}$$

Let's now consider the region for $a < x < -a$

$$C_1 e^{ik_n x} + C_2 e^{-ik_n x} = -C_1 e^{-ik_n x} - C_2 e^{ik_n x}. \tag{I.15}$$

Rearranging Eq.(I.15) we obtain

$$(C_1 + C_2)\, e^{ik_n x} = -\,(C_1 + C_2)\, e^{-ik_n x} \tag{I.16}$$

Factorising Eq.(I.16) we obtain

$$(C_1 + C_2)\left(e^{ik_n x} + e^{-ik_n x}\right) = 0 \tag{I.17}$$

which holds only if $a < x < -a$. Therefore

$$C_1 = -C_2 \tag{I.18}$$

or

$$C_2 = -C_1. \tag{I.19}$$

We now let's from Eq.(I.18) and Eq.(I.19) respectively as

$$C_1 = C \tag{I.20}$$

and

$$C_2 = -C. \tag{I.21}$$

Substitute equations Eq.(I.14), Eq.(I.20) and Eq.(I.21) into Eq.(I.10) gets

$$\psi_o(x) = \begin{cases} -Be^{ik_n x}, & \text{if } x < -a \\ C\left(e^{ik_n x} - e^{-ik_n x}\right), & \text{if } |x| \leq a \\ Be^{-ik_n x}, & \text{if } x > a \end{cases} \tag{I.22}$$

This clearly shows the anti-symmetric wavefunction, $\psi_o(-x) = \psi_o(x)$.

Appendix J

Derivation of the exact solution for an asymetric triple quantum well

In this section we derive the exact solution for an asymetric triple quantum well in Chap. 3. The model of this potential for a one-dimensional time independendent Schrödinger equation is given by

$$V(x) = -\gamma\delta(x-a) - \gamma\delta(x+a) - \beta\delta(x-b) \qquad \text{(J.1)}$$

The wave function satisfying the outgoing boundary conditions has the form

$$\psi(x) = \begin{cases} Ae^{\varkappa x}, & \text{if } \varkappa < -a \\ Be^{\varkappa x} + Ce^{-\varkappa x}, & \text{if } -a < x < b \\ De^{-\varkappa x} + Ee^{\varkappa x}, & \text{if } b < x < a \\ Fe^{-\varkappa x}, & \text{if } x > a \end{cases} \tag{J.2}$$

The wavefunction $\psi(x)$ is continuos at $x = \pm a$ and at $x = b$ and its first derivative $\psi'(x)$ has a discontinuity. The continuity relations at $x = \pm a$ and at $x = b$ are repectively given by

$$\psi(\pm a + 0_+) = \psi(\pm a - 0_+) \tag{J.3}$$

and

$$\psi(b + 0) = \psi(b - 0) \tag{J.4}$$

The discontinuity at $x = \pm a$ and at $x = b$ is given, respectively, by the following relations

$$\psi'(\pm a + 0_+) - \psi'(\pm a - 0_+) = -\gamma\psi(\pm a) \tag{J.5}$$

and

$$\psi'(b + 0) - \psi'(b - 0) = -\beta\psi(b). \tag{J.6}$$

Using the above relations we obtain the following set of six simultaneous equations for the constant coefficients in the wave function Eq.(J.2

$$Ae^{-\varkappa a} = Be^{-\varkappa a} + Ce^{\varkappa a}, \tag{J.7}$$

$$Be^{\varkappa b} + Ce^{-\varkappa b} = De^{-\varkappa b} + Ee^{\varkappa b}, \tag{J.8}$$

$$Fe^{-\varkappa a} = De^{-\varkappa a} + Ee^{\varkappa a}, \tag{J.9}$$

$$\varkappa Be^{-\varkappa a} - \varkappa Ce^{\varkappa a} = -\gamma Ae^{\varkappa a} + \varkappa Ae^{-\varkappa a}, \tag{J.10}$$

$$\varkappa De^{-\varkappa a} - \varkappa Ee^{\varkappa a} = -\gamma Fe^{\varkappa a} + \varkappa Fe^{-\varkappa a}, \tag{J.11}$$

$$-\varkappa De^{-\varkappa b}+\varkappa Ee^{\varkappa b}-\varkappa Be^{\varkappa b}+\varkappa Ce^{-\varkappa b} = -\beta Be^{\varkappa b}-\beta Ce^{-\varkappa b}. \tag{J.12}$$

We multiply Eq.(J.7) by $\varkappa$ and get

$$\varkappa Ae^{\varkappa a} = \varkappa Be^{-\varkappa a} + \varkappa Ce^{\varkappa a}. \tag{J.13}$$

Subtracting Eq.(J.10) from Eq.(J.13) we get the coefficient B in terms of A,

$$B = \frac{A}{2\varkappa}(2\varkappa - \gamma), \tag{J.14}$$

and adding Eq.(J.10) to Eq.(J.13) we get the coefficient C in terms of A,

$$C = \frac{\gamma}{2\varkappa} e^{-2\varkappa a} A. \tag{J.15}$$

We multiply Eq.(J.9) by $\varkappa$ and obtain

$$\varkappa F e^{-\varkappa a} = \varkappa D e^{-\varkappa a} + \varkappa E e^{\varkappa a}. \tag{J.16}$$

Adding Eq.(J.11) to Eq.(J.16) we get the coefficient D in terms of F:

$$D = \frac{F}{2\varkappa}(2\varkappa - \gamma). \tag{J.17}$$

Subtracting Eq.(J.16) from Eq.(J.11) we get the coefficient E in terms of F:

$$E = \frac{\gamma}{2\varkappa} e^{-2\varkappa a} F. \tag{J.18}$$

We now substitute the expressed coefficients B, C, D, E into Eq.(J.8) to get the following equation

$$\frac{A}{2\varkappa}(2\varkappa-\gamma)e^{\varkappa b}+\frac{\gamma}{2\varkappa}e^{-2\varkappa a}Ae^{-\varkappa b} = \frac{F}{2\varkappa}(2\varkappa-\gamma)e^{-\varkappa b}+\frac{\gamma}{2\varkappa}e^{-2\varkappa a}Fe^{\varkappa b} \tag{J.19}$$

which can be simplified to

$$A\left[(2\varkappa-\gamma)e^{\varkappa b}+\gamma e^{-2\varkappa a}e^{-\varkappa b}\right]-F\left[(2\varkappa-\gamma)e^{-\varkappa b}+\gamma e^{-2\varkappa a}e^{\varkappa b}\right]=0 \tag{J.20}$$

Substituting the coefficients B, C, D, E into Eq.(J.12) we obtain

$$\begin{aligned}-\varkappa\frac{F}{2\varkappa}(2\varkappa-\gamma)e^{-\varkappa b}+\varkappa\frac{\gamma}{2\varkappa}e^{-2\varkappa a}Fe^{\varkappa b}\\ -\varkappa\frac{A}{2\varkappa}(2\varkappa-\gamma)e^{\varkappa b}+\varkappa\frac{\gamma}{2\varkappa}e^{-2\varkappa a}Ae^{-\varkappa b}=\\ -\beta\frac{A}{2\varkappa}(2\varkappa-\gamma)e^{\varkappa b}-\beta\frac{\gamma}{2\varkappa}e^{-2\varkappa a}Ae^{-\varkappa b}.\end{aligned} \tag{J.21}$$

We collect the like terms of Eq.(J.21) and get the expression of the form

$$\begin{aligned}A\left[\frac{\gamma}{2}e^{-2\varkappa a}e^{-\varkappa b}\left(1+\frac{\beta}{\varkappa}\right)-\frac{1}{2}(2\varkappa-\gamma)e^{\varkappa b}\left(1-\frac{\beta}{\varkappa}\right)\right]=\\ F\left[\frac{1}{2}(2\varkappa-\gamma)e^{-\varkappa b}-\frac{\gamma}{2}e^{-2\varkappa a}e^{\varkappa b}\right].\end{aligned} \tag{J.22}$$

Simplifying Eq.(J.22) we obtain

$$\begin{aligned}A\left[\gamma e^{-2\varkappa a}e^{-\varkappa b}\left(1+\frac{\beta}{\varkappa}\right)-(2\varkappa-\gamma)\left(1-\frac{\beta}{\varkappa}\right)e^{\varkappa b}\right]-\\ F\left[(2\varkappa-\gamma)e^{-\varkappa b}-\gamma e^{-2\varkappa a}e^{\varkappa b}\right]=0\end{aligned} \tag{J.23}$$

Now combining Eq.(J.20) and Eq.(J.23) we obtain the secular equation for $\varkappa$:

$$\frac{\gamma e^{-2\varkappa a}e^{-\varkappa b}\left[(2\varkappa-\gamma)e^{-\varkappa b}+\gamma e^{-2\varkappa a}e^{\varkappa b}\right]\left(1+\frac{\beta}{\varkappa}\right)}{\left[(2\varkappa-\gamma)e^{\varkappa b}+\gamma e^{-2\varkappa a}e^{-\varkappa b}\right]}$$
$$-\frac{\left[(2\varkappa-\gamma)e^{-\varkappa b}+\gamma e^{-2\varkappa a}e^{\varkappa b}\right](2\varkappa-\gamma)\left(1-\frac{\beta}{\varkappa}\right)e^{\varkappa b}}{\left[(2\varkappa-\gamma)e^{\varkappa b}+\gamma e^{-2\varkappa a}e^{-\varkappa b}\right]}$$
$$-(2\varkappa-\gamma)e^{-\varkappa b}+\gamma e^{-2\varkappa a}e^{\varkappa b}=0 \qquad \text{(J.24)}$$

which can be simplified to the following:

$$\left((2\varkappa-\gamma)e^{-\varkappa b}+\gamma e^{-2\varkappa a}e^{\varkappa b}\right)\left[\gamma e^{-2\varkappa a}e^{-\varkappa b}\left(1+\frac{\beta}{\varkappa}\right)-(2\varkappa-\gamma)\left(1-\frac{\beta}{\varkappa}\right)e^{\varkappa b}\right]$$
$$-\left((2\varkappa-\gamma)e^{-\varkappa b}-\gamma e^{-2\varkappa a}e^{\varkappa b}\right)\left((2\varkappa-\gamma)e^{\varkappa b}+e^{-2\varkappa a}e^{-\varkappa b}\right)=0 \qquad \text{(J.25)}$$

Eq.(J.25) can be reduced to

$$\xi^2(1-\eta)-2\xi\cos(2i\varkappa b)+1+\eta=0\,, \qquad \text{(J.26)}$$

where

$$\xi=\frac{e^{-2\varkappa a}}{1+-2\varkappa/\gamma} \quad \text{and} \quad \eta=\frac{-2\varkappa}{\beta}\,. \qquad \text{(J.27)}$$

By replacing $\varkappa=-ik$, one obtains Eq.(3.40).

Appendix K

Derivation of transmission amplitude for a double delta function potential

In this section we derive Eq.(3.48) for the transmission amplitude for the double delta potential $V(x)$ given by

$$V(x) = -\gamma\delta(x-a) - \gamma\delta(x+a) \tag{K.1}$$

where γ is the strength of the potential well. There is a general method for finding the transmission from piecewise potentials: transfer matrix method [56]. Here we find this transmission in a similar way, by using the homogenous solutions, and finding the constant coefficients applying the boundary conditions.

Consider a free particle incoming from left to the right and and having a probability to be reflected back and transmitted througth the double quantum well structure. This correspond to

the following form of the wave function.

$$\psi(x) = \begin{cases} Ae^{ikx} + Be^{-ikx}, & \text{if } x < -a \\ Ce^{ikx} + De^{-ikx}, & \text{if } |x| \leq a \\ Fe^{ikx}, & \text{if } x > a \end{cases} \tag{K.2}$$

The continuity relations across the delta function satisfies the following boundary conditions at $x = \pm a$

$$\psi(\pm a + 0_+) = \psi(\pm a - 0_+), \tag{K.3}$$

$$\psi'(\pm a + 0_+) - \psi'(\pm a - 0_+) = -\gamma\psi(\pm a). \tag{K.4}$$

This results in the following simultaneous algebraic equations :

$$Ae^{-ika} + Be^{ika} = Ce^{-ika} + De^{ika}, \tag{K.5}$$

$$Ce^{ika} + De^{-ika} = Fe^{ika}, \tag{K.6}$$

$$ik\left[Ce^{-ika} - De^{ika} - Ae^{-ika} + Be^{ika}\right] = -\gamma(Ae^{-ika} + Be^{ika}), \tag{K.7}$$

$$ik\left[Fe^{ika} - Ce^{ika} + De^{-ika}\right] = -\gamma Fe^{ika}. \tag{K.8}$$

We multiply Eq.(K.5) by ik and get

$$ikAe^{-ika} + ikBe^{ika} = ikCe^{-ika} + ikDe^{ika}. \tag{K.9}$$

Adding Eq.(K.5) and Eq.(K.9) we get the coefficient C in terms of A and B :

$$C = \frac{A(2ik - \gamma)e^{-ika} - \gamma Be^{ika}}{2ike^{-ika}} \tag{K.10}$$

Subtracting Eq.(K.9) from Eq.(K.5) we get the coefficient D in terms of A and B :

$$D = \frac{\gamma Ae^{-ika} + B(2ik + \gamma)e^{ika}}{2ike^{ika}}. \tag{K.11}$$

Then we multiply Eq.(K.6) by ik and get

$$ikCe^{ika} + ikDe^{-ika} = ikFe^{ika}. \tag{K.12}$$

Adding and subtracting Eq.(K.12) from Eq.(K.17) we get the coefficients C and D, respectively, in terms of F :

$$C = \frac{F(2ik + \gamma)}{2ik}, \tag{K.13}$$

$$D = \frac{-\gamma Fe^{2ika}}{2ik}. \tag{K.14}$$

Combining Eq.(K.10) with Eq.(K.13) and Eq.(K.11) with Eq.(K.14), we get two espressions for B in terms of A and F :

$$B = \frac{A(2ik-\gamma)e^{-ika} - F(2ik+\gamma)e^{-ika}}{\gamma e^{ika}} \tag{K.15}$$

and

$$B = \frac{-\gamma F e^{3ika} - \gamma A e^{-ika}}{(2ik+\gamma)e^{ika}}. \tag{K.16}$$

Excluding B from Eq.(K.15) and Eq.(K.16), we obtain

$$\frac{A(2ik-\gamma)e^{-ika} - F(2ik+\gamma)e^{-ika}}{\gamma e^{ika}} = \frac{-\gamma F e^{3ika} - \gamma A e^{-ika}}{(2ik+\gamma)e^{ika}} \tag{K.17}$$

After some algebra Eq.(K.17) yields

$$t(k) = \frac{F}{A} = \frac{(2ik-\gamma)(2ik+\gamma)+\gamma^2}{(2ik+\gamma)(2ik+\gamma) - \gamma^2 e^{4ika}} \tag{K.18}$$

which determines the transmission amplitude $t(k)$. Simplifying Eq.(K.18) further, we obtain Eq.(3.48)

$$t_a(k) = \frac{F}{A} = \frac{4k^2}{4k(k-i\gamma) - \gamma^2(1-e^{4ika})}. \tag{K.19}$$

Bibliography

[1] A. Muljarov, W. Langbein, and R. Zimmermann, "Brillouin-wigner perturbation theory in open electromagnetic systems," *Europhys Lett.*, vol. 92, p. 50010, 2010.

[2] A. Mekis, S. Fan, and J. D. Joannopoulos, "Bound states in photonic crystal waveguides and waveguide bends," *Phys. Rev. B*, vol. 58, 1998.

[3] K. R. Brownstein, "Criterion for existence of a bound state in one dimension," *Am. J. Phys*, vol. 68, p. 160, 2000.

[4] G. Gamow, "Zur quantentheorie des atomkernes," *Zeitschrift für Physik*, vol. 51, no. 3, pp. 204–212, 1928.

[5] A. J. Siegert, "On the derivation of the dispersion formula for nuclear reactions," *Phys. Rev.*, vol. 56, p. 750, 1939.

[6] G. García-Calderón and R. Peierls, "Resonant states and their uses," *Nucl. Phys. A*, vol. 265, no. 3, pp. 443 – 460, 1976.

[7] N. Moiseyev *Phys. Rep.*, vol. 302, p. 212, 1998.

[8] A. Baz', Y. Zel'dovich, and A. Perelomov, *Scattering, Reactions and Decay in Nonrelativistic Quantum Mechanics*. U. S. Department of Commerce, Washington, D. C., 1969.

[9] R. Newton, "Analytic properties of radial wave functions," *J. Math. Phys.*, vol. 1, p. 319, 1960.

[10] R. M. More, "Theory of decaying states," *Phys. Rev. A*, vol. 4, pp. 1782–1790, Nov 1971.

[11] M. B. Doost, W. Langbein, and E. A. Muljarov, "Resonant-state expansion applied to planar open optical systems," *Phys. Rev. A*, vol. 85, p. 023835, 2012.

[12] M. B. Doost, W. Langbein, and E. A. Muljarov, "Resonant state expansion applied to two-dimensional open optical systems," *Phys. Rev. A*, vol. 87, p. 043827, 2013.

[13] M. B. Doost, W. Langbein, and E. A. Muljarov, "Resonant-state expansion applied to three-dimensional open optical systems," *Phys. Rev. A*, vol. 90, p. 013834, Jul 2014.

[14] L. J. Armitage, M. B. Doost, W. Langbein, and E. A. Muljarov, "Resonant-state expansion applied to planar waveguides," *Phys. Rev. A*, vol. 89, p. 053832, May 2014.

[15] E. A. Muljarov and W. Langbein, "Resonant-state expansion of dispersive open optical systems: Creating gold from sand," *Phys. Rev. B*, vol. 93, p. 075417, Feb 2016.

[16] E. A. Muljarov and T. Weiss, "Resonant-state expansion for open optical systems: Generalization to magnetic, chiral, and bi-anisotropic," *Optics Letters*, vol. 43, pp. 1978–1981, 2018.

[17] H. S. Sehmi, W. Langbein, and E. A. Muljarov, "Optimizing the drude-lorentz model for material permittivity: Method, program, and examples for gold, silver, and copper," *Phys. Rev. B*, vol. 95, p. 115444, 2017.

[18] J. Bang, F. Gareev, M. Gizzatkulov, and S. Goncharov, "Expansion of continuum functions on resonance wave functions and amplitudes," *Nuclear Physics A*, vol. 309, pp. 381–421, oct 1978.

[19] P. Lind, "Completeness relations and resonant state expansions," *Phys. Rev. C*, vol. 47, pp. 1903–1920, May 1993.

[20] K. S. Yee *IEEE Trans. Anten. Prop.*, vol. 14, p. 302, 1966.

[21] K. S. Kunz and R. J. Luebbers, *The finite difference time domain method for electromagnetics*. Boca Raton: CRC Press, 1993.

[22] G. T. G. Dhatt and E. Lefrancois, "Finite element method," *ISTE Ltd*, 2012.

[23] P. Lalanne and E. Silberstein, "Fourier-modal methods applied to waveguide computational problems," *Opt. Lett.*, vol. 25, no. 15, pp. 1092–1094, 2000.

[24] M. Pisarenco, J. Maubach, I. Setija, and R. Matteij *J. Opt. Soc. Am. A*, vol. 27, p. 2423, 2010.

[25] R. de L. Kronig and W. G. Penney, "Quantum mechanics of electrons in crystal lattices," *Proceedings of the Royal Society of London A: Math. Phys. Eng. Sci.*, vol. 130, no. 814, p. 499, 1931.

[26] N. Hatano, K. Sasada, H. Nakamura, and T. Petrosky, "Some properties of the resonant state in quantum mechanics and its computation," *Progress of Theoretical Physics*, vol. 119, no. 2, pp. 187–222, 2008.

[27] F. Mandle, *Quantum Mechanics*. Manchester, UK: Wiley, 1st edition ed., 1992.

[28] R. Zavin and N. Moiseyev, "One-dimensional symmetric rectangular well: from bound to resonance via self-orthogonal virtual state," *J. Phys. A: Math. Gen.*, vol. 37, p. 4619, 2004.

[29] R. Dingle and C. H. Henry *Phys. Rev. Lett.*, vol. 33, p. 827, 1974.

[30] G. M. Smith and J. J. Coleman, *Heterostructures and Quantum Devices*, vol. A volume of VLSI Electronics: Microstructure Science. Academic Press, San Diego,.

[31] C. H. Johansson and J. O. Linde, "The x-ray determination

of the atomic arrangement in the mixed-crystal series gold-copper and palladiumcopper," *Annalen der Physik*, vol. 78, p. 439, 1925.

[32] L. Esaki and R. Tsu, "Superlattice and negative dierential conductivity in semiconductors," *IBM J. Res. Develop*, vol. 14, p. 6165, 1970.

[33] A. J. Bradley, "The formation of superlattices in alloys of iron and aluminium," *Proc. Royal. Soc. A*, vol. 136, p. 210232, 1932.

[34] W. L. Bragg and E. J. Williams, "The effect of thermal agitation on atomic arrangement in alloys," *Proc. Royal. Soc. A*, vol. 145, p. 699730, 1934.

[35] H. A. Bethe, "Statistical theory of superlattices," *Proc. Royal. Soc. A*, vol. 150, p. 552575, 1935.

[36] F. Bloch, "ber die quantenmechanik der elektronen in kristallgittern," *Z. Phys.*, vol. vol. 52, pp. 555–600,, 1928.

[37] G. W. Hill, "On the part of the motion of the lunar perigee which is a function of the mean motions of the sun and moon," *Acta Math*, vol. 8, pp. 1–36, 1886.

[38] G. Floquet, "Sur les quations direntielles linaires coecients priodiques," *Annales scientiques de l'cole Normale Suprieure*, vol. 12, pp. 47–88, 1883.

[39] N. W. Ashcroft and N. D. Mermin, *Solid state physics*. Sunders College, 1976.

[40] G. Allen, "Band structures of one-dimensional crystals with square-well potentials," *Phys. Rev.*, vol. 91, p. 531, 1953.

[41] H. M. NUSSENZVEIG, "The poles of the s-matrix of rectangular potential well or barrier," *Nuclear Physics*, vol. 11, pp. 499–521, 1959.

[42] D. Sprung, H. Wu, and J. Martorell, "Poles, bound states, and resonances illustrated by the square well potential," *Am. J. Phys.*, vol. 64, p. 136, 1996.

[43] B. Belchev, S. Neale, and M. A. Walton, "Flow of s-matrix poles for elementary quantum poentials," *arxiv:1110.4902v1*, 2017.

[44] N. Hatano, T. Kawamoto, and J. Feinberg, "Probabilistic interpretation of resonant states," *Journal of Physics*, vol. 73, no. 3, pp. 553–564, 2009.

[45] A. U. Mashewari and P. Prema *Am. J. Phys.*, vol. 78, p. 412, 2010.

[46] K. Ziock, *Basic Quantum Mechanics*. 1969.

[47] D. Griffiths, *Introduction to Quantum Mechanics*. Pearson international edition, Pearson Prentice Hall, 2005.

[48] E. E. Shnol, "Remarks on the theory of quasistationary states," *Theor. Math. Phys.*, vol. 8, p. 729.

[49] R. M. More and E. Gerjuoy, "Properties of resonance wave functions," *phys. Rev. A*, vol. 7, p. 1288, 1973.

[50] D. K. Watson, "Partial widths and resonance normalization," *Phys. Rev. A*, vol. 34, p. 1016, 1986.

[51] E. L. Ivchenko and M. Willander, "Exciton polaritons in periodic nanos tructures," *Phys. Status Solidi B*, vol. 215, p. 199, 1999.

[52] J. von Neumann and E. Wigner, "On the von neumann and wigner potentials," *Phys. Z*, vol. 30, p. 465, 1929.

[53] B. V. Zeghbroeck, *Principles of Semiconductor Devices*. Prentice Hall, 2011.

[54] S. L. Chuang, *Physics of Optoelectronic Devices*. New York: John Wiley and sons,, first edition ed., 1995.

[55] P. B. Nilesh, D. P. Sandeep, M. K. Pravin, and P. B. Pranav, "Deriving time dependent schrdinger equation from wave-mechanics, schrdinger time independent equation, classical and hamilton-jacobi equations," *Leonardo Electronic Journal of Practices and Technologies*, pp. 31–48, 2015.

[56] D. W. L. Sprung, H. Wu, and J. Martorell, "Scattering by a finite periodic potential," *Am. J. Phys.*, 1993.